$7

QEX

July/August 2018

www.arrl.org

A Forum for Communications Experimenters

Issue No. 309

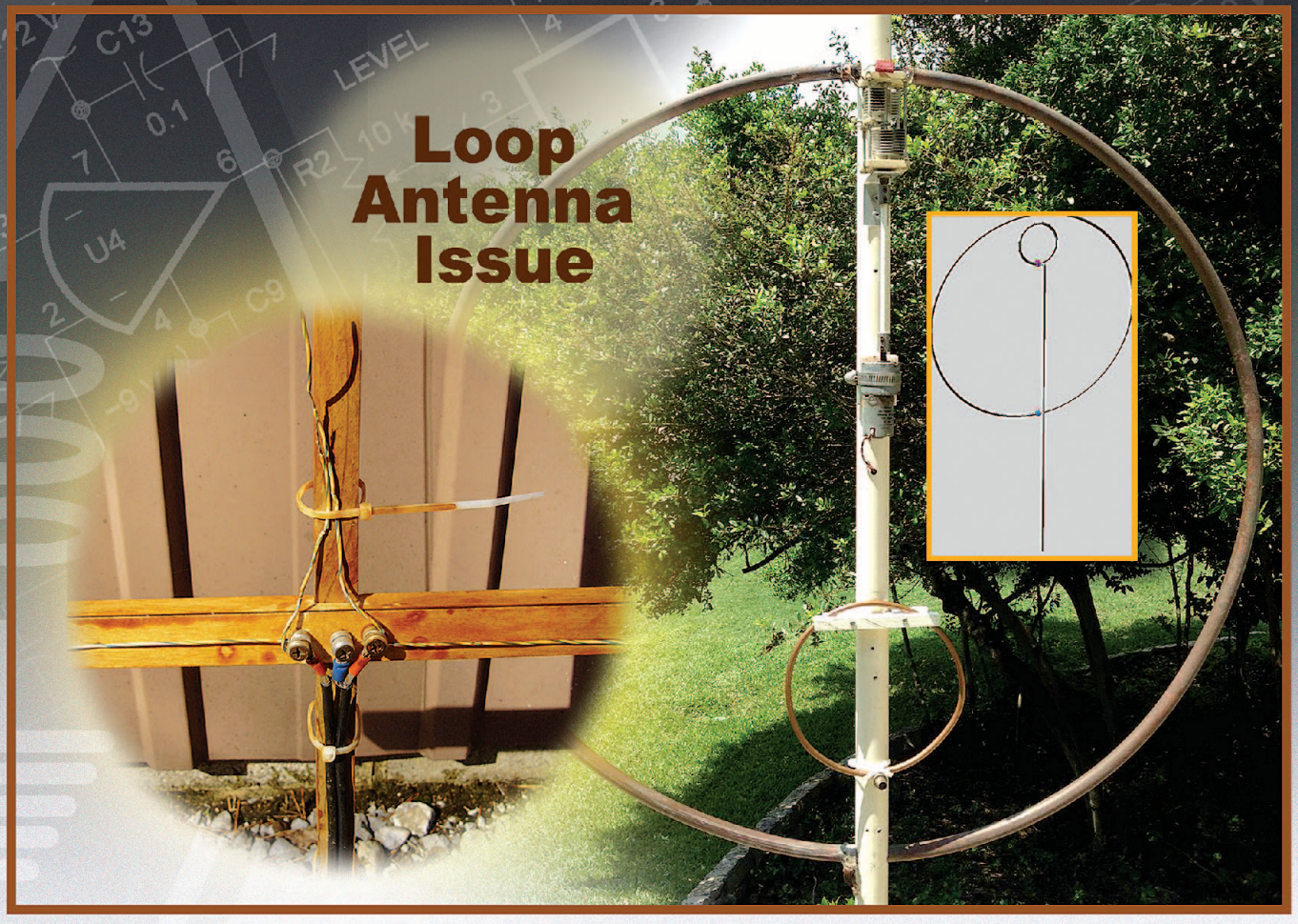

HF, VHF, and UHF Loop Antennas

ARRL The national association for AMATEUR RADIO™
225 Main Street
Newington, CT USA 06111-1494

Back To Space

Amateur Radio on the International Space Station (ARISS) is a global group supported by NASA and the space agencies of other countries and groups such as the ARRL, AMSAT-NA, IARU, and (CASIS) Center for the Advancement of Science in space.

The ARISS mission is to provide and operate Amateur Radio systems in space aboard the International Space Station, helping inspire, educate and engage youth and communities worldwide in science, technology, engineering and mathematics.

Kenwood has a proud heritage of space flight beginning with the TM-V7A, TM-D700A, TM-D710E and upcoming TM-D710GA. We at Kenwood are happy to donate our engineering time and energies to provide customized firmware and radios to the ARISS mission.

Join Kenwood in helping ARISS to reach more potential Hams by sending your donations to:

AMSAT-NA - Attn: ARISS Donation
10605 Concord St #304 • Kensington MD 20895

Donations to ARISS are tax deductible and go directly toward reaching out to the next generation of Hams. Additional donations may be made online at http://www.amsat.org/ (select the "ARISS Donate" button)

KENWOOD

Customer Support/Distribution
(310) 639-4200 Fax: (310) 537-8235

www.kenwood.com/usa

ADS#14818

QEX

July/August 2018

About the Cover

This theme issue of *QEX* features loop antenna articles from several authors who investigate the patterns and efficiency of both the small HF gap-resonated loops, and full-wavelength loops for VHF and UHF. Authors explain the importance of the current variation and *Q*-factor of small loops; use of a Smith chart for easily matching and tuning; how coupling to earth ground affects the impedance, pattern, gain, and RF exposure compliance distance; and the effects of various loop shapes and stacks of loops having one-wavelength perimeter elements.

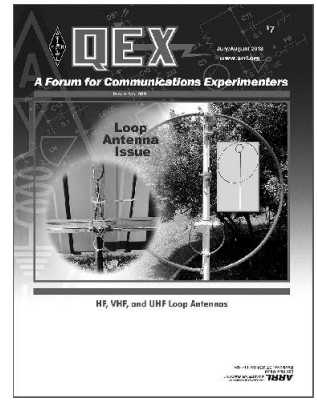

QEX (ISSN: 0886-8093) is published bimonthly in January, March, May, July, September, and November by the American Radio Relay League, 225 Main Street, Newington, CT 06111-1494. Periodicals postage paid at Hartford, CT and at additional mailing offices.

POSTMASTER: Send address changes to: QEX, 225 Main St, Newington, CT 06111-1494
Issue No 309

Publisher
American Radio Relay League

Kazimierz "Kai" Siwiak, KE4PT
Editor

Lori Weinberg, KB1EIB
Assistant Editor

Zack Lau, W1VT
Ray Mack, W5IFS
Contributing Editors

Production Department

Steve Ford, WB8IMY
Publications Manager

Michelle Bloom, WB1ENT
Production Supervisor

Sue Fagan, KB1OKW
Graphic Design Supervisor

David Pingree, N1NAS
Senior Technical Illustrator

Brian Washing
Technical Illustrator

Advertising Information Contact:

Janet L. Rocco, W1JLR
Business Services
860-594-0203 – Direct
800-243-7768 – ARRL
860-594-4285 – Fax

Circulation Department

Cathy Stepina, *QEX Circulation*

Offices

225 Main St, Newington, CT 06111-1494 USA
Telephone: 860-594-0200
Fax: 860-594-0259 (24 hour direct line)
e-mail: **qex@arrl.org**

Subscription rate for 6 issues:

In the US: $29;

US by First Class Mail: $40;

International and Canada by Airmail: $35

Members are asked to include their membership control number or a label from their QST when applying.

In order to ensure prompt delivery, we ask that you periodically check the address information on your mailing label. If you find any inaccuracies, please contact the Circulation Department immediately. Thank you for your assistance.

In This Issue

Features

2 **Perspectives**
Kazimierz "Kai" Siwiak, KE4PT

3 **Small Transmitting Loops: A Different Perspective on Tuning and Determining *Q* and Efficiency**
Milton E. Cram, W8NUE

9 **Effects Due to Ground For Small Transmitting Loop Antennas**
Peter DeNeef, AE7PD

12 **Small Gap-resonated HF Loop Antenna Fed by a Secondary Loop**
Kai Siwiak, KE4PT and Richard Quick, W4RQ

18 **Adapt Your Equipment to Operate at Millimeter Waves up to 32 GHz**
Euclides Lourenço Chuma, PY2EAJ

22 **An Arduino-based DDS for the Heathkit SB-104 Transceiver**
Tom Sowden, W6KAN

26 **Conductivity of Trees at HF**
Rudy Severns, N6LF

28 **Satellite Distance and Velocity**
Andrzej (Andy) Przedpelski, KØABP

31 **Some Additional Geometrics for Loop Antennas**
John Stanley, K4ERO

37 **PiGate Emergency E-mail System**
Mark Griffith, KDØQYN

40 **Tech Notes**

42 **Letters**

43 **Upcoming Conferences**

Index of Advertisers

ARRL.....44, Cover III
DX Engineering: 25
Kenwood Communications:.....Cover II
SteppIR Communication Systems.....Cover IV
Tucson Amateur Packet Radio: 21

The American Radio Relay League

The American Radio Relay League, Inc, is a noncommercial association of radio amateurs, organized for the promotion of interest in Amateur Radio communication and experimentation, for the establishment of networks to provide communications in the event of disasters or other emergencies, for the advancement of the radio art and of the public welfare, for the representation of the radio amateur in legislative matters, and for the maintenance of fraternalism and a high standard of conduct.

ARRL is an incorporated association without capital stock chartered under the laws of the state of Connecticut, and is an exempt organization under Section 501(c)(3) of the Internal Revenue Code of 1986. Its affairs are governed by a Board of Directors, whose voting members are elected every three years by the general membership. The officers are elected or appointed by the Directors. The League is noncommercial, and no one who could gain financially from the shaping of its affairs is eligible for membership on its Board.

"Of, by, and for the radio amateur," ARRL numbers within its ranks the vast majority of active amateurs in the nation and has a proud history of achievement as the standard-bearer in amateur affairs.

A *bona fide* interest in Amateur Radio is the only essential qualification of membership; an Amateur Radio license is not a prerequisite, although full voting membership is granted only to licensed amateurs in the US.

Membership inquiries and general correspondence should be addressed to the administrative headquarters:

ARRL
225 Main Street
Newington, CT 06111 USA
Telephone: 860-594-0200
FAX: 860-594-0259 (24-hour direct line)

Officers

President: Rick Roderick, K5UR
PO Box 1463, Little Rock, AR 72203

Chief Executive Officer: Barry Shelly, N1VXY

The purpose of *QEX* is to:

1) provide a medium for the exchange of ideas and information among Amateur Radio experimenters,

2) document advanced technical work in the Amateur Radio field, and

3) support efforts to advance the state of the Amateur Radio art.

All correspondence concerning *QEX* should be addressed to the American Radio Relay League, 225 Main Street, Newington, CT 06111 USA. Envelopes containing manuscripts and letters for publication in *QEX* should be marked Editor, *QEX*.

Both theoretical and practical technical articles are welcomed. Manuscripts should be submitted in word-processor format, if possible. We can redraw any figures as long as their content is clear. Photos should be glossy, color or black-and-white prints of at least the size they are to appear in *QEX* or high-resolution digital images (300 dots per inch or higher at the printed size). Further information for authors can be found on the Web at **www.arrl.org/qex/** or by e-mail to **qex@arrl.org**.

Kazimierz "Kai" Siwiak, KE4PT

Perspectives

Themes and Mentors

In the previous *Perspectives*, I should have identified Rod Newkirk, W9BRD [the call sign now belongs to his son David], who personified Elmers in 1971. Thanks to Carl Luetzelschwab, K9LA, for pointing that out!

We previously raised awareness about the aging of our *QEX* readership, as well as of the Amateur Radio population. We've heard from several of you sages, elders and mentors of Amateur Radio who are reaching across to younger generations. We'd like to hear from more of you (**qex@arrl.org**). Let's keep ham radio awareness among the younger crowds alive.

In This Issue

We feature Loop Antennas in this *QEX* theme issue, and cover other topics across the HF to millimeter wave spectrum as well.

Milton E. Cram, W8NUE, shows a simple way to tune and match the HF loop antenna using the Smith chart, and estimates *Q* from the complex impedance.

Peter DeNeef, AE7PD, investigates how the location of the resonating capacitor and coupling to earth ground affect the small HF loop pattern and gain.

Kai Siwiak, KE4PT, and Richard Quick, W4RQ, introduce improved formulas for the current and impedance of the small HF loop, leading to an accurate determination of close-near-fields, and far-field null depths.

John Stanley, K4ERO, compares the performance of stacks of rectangular, hour-glass, and diamond shaped loops having one-wavelength perimeter elements.

Peter DeNeef, AE7PD, reports on the effects of the ground on RF exposure compliance distances of a small HF loop antenna.

Kai Siwiak, KE4PT, lists several equivalent *Q*-factor formulas and their uses.

Rudy Severns, N6LF, measures live-tree dielectric parameters.

Andy Przedpelski, KØABP, uses missile miss distance indicator scoring techniques to determine a satellite's distance and velocity.

Euclides Lourenço Chuma, PY2EAJ, presents construction details for a millimeter wave prescaler and doubler.

Mark Griffith, KDØQYN, describes the PiGate system that with Winlink2000 global email system provides a robust platform that can be deployed in a disaster scenario.

Tom Sowden, W6KAN, stabilizes the frequency of his vintage transceiver with an Arduino based DDS.

Keep the full-length *QEX* articles flowing in, but if brevity is your forte, share a **Technical Note** of several hundred words in length plus a figure or two. Expand on another author's work and add to the Amateur Radio institutional memory with your technical observation. Let us know that your submission is intended as a **Note**.

QEX is edited by Kazimierz "Kai" Siwiak, KE4PT, (**ksiwiak@arrl.org**) and is published bimonthly. *QEX* is a forum for the free exchange of ideas among communications experimenters. The content is driven by you, the reader and prospective author. The subscription rate (6 issues per year in the United States is $29. First Class delivery in the US is available at an annual rate of $40. For international subscribers, including those in Canada and Mexico, *QEX* can be delivered by airmail for $35 annually. Subscribe today at **www.arrl.org/qex**.

Would you like to write for *QEX*? We pay $50 per published page for articles and Technical Notes. Get more information and an Author Guide at **www.arrl.org/qex-author-guide**. If you prefer postal mail, send a business-size self-addressed, stamped (US postage) envelope to: *QEX* Author Guide, c/o Maty Weinberg, ARRL, 225 Main St, Newington, CT 06111.

Very best regards,

Kazimierz "Kai" Siwiak, KE4PT

Milton E. Cram, W8NUE
9807 Vista View, Austin, TX 78750; **w8nue@arrl.net**

Small Transmitting Loops: A Different Perspective on Tuning and Determining *Q* and Efficiency

The simplest way to tune and match the loop antenna is by using the Smith chart, and Q can be estimated using the complex impedance.

Over the past several decades numerous articles have been published[1-7] that describe the construction and testing of small transmitting loop antennas. "Small" in this context refers to an antenna that has a circumference that is less than about a tenth of a wavelength. In this article I focus more on evaluation of the performance of the antenna and less so on the construction aspects. I rely on both models and measurements on a simple loop antenna. To my knowledge, there have been no articles that describe the method of matching a loop or of determining the *Q* of the antenna as presented herein. I do not attempt to cover electromagnetic theory, or modeling using such tools as NEC. The notes describe construction methods, NEC models, and so on. This is a *phenomenological* approach, where it is assumed that the current distribution in the loop is constant and the behavior is adequately described using a simple RLC circuit.

My purpose is to:

- describe the electrical behavior of a small transmitting loop antenna near the tuned frequency using an electrical circuit analog;
- provide guidance in tuning the antenna for an impedance match to a coaxial transmission line;
- describe a measurement method for determining the *Q* of the antenna system;
- estimate the efficiency of the antenna based on measured *Q*;
- compare model data with data obtained from measurements.

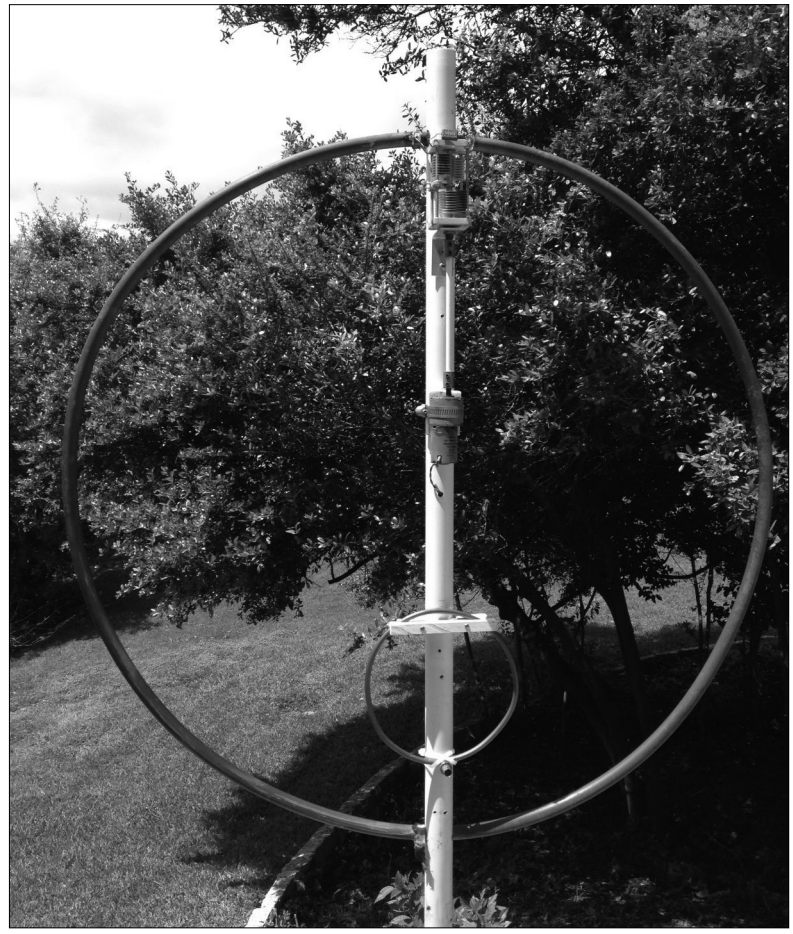

Figure 1 — The small transmitting loop antenna includes the main loop with the resonating capacitor on top, and the feeding loop near the bottom. [Milton Cram, W8NUE, photo.]

Assumptions

The circumference of the loop is assumed small compared to wavelength, that is, current is essentially constant around the loop. For a more accurate current distribution, see reference[8-10] by Siwiak, Findling and Quick. The coax cable is connected to a small coupling loop that is inductively coupled to the main loop. This analysis should also apply to "delta" and "gamma" matching systems.

The loop antenna (Figure 1) to be examined is one that I built several years ago for PSK31 operation on 20 meters. The main loop is approximately 32 inches in diameter, and is constructed from 5/8 inch OD copper tubing. A butterfly capacitor is connected across the gap formed where the length of copper tubing is shaped into a loop. This capacitor resonates the loop at 14.1 MHz. A small 7.75 inch diameter feeding loop, formed from 0.25 inch OD copper tubing, transfers power into and out of the main loop. A 50 Ω coax cable connects across the gap that is formed when the tubing is shaped into the smaller feeding circular loop.

The position of the small coupling loop is used to alter the mutual inductance, or coupling coefficient, between the two loops, and this provides a means to adjust the matching between the coax and the antenna for a 1:1 VSWR.

Although the butterfly capacitor may not have losses as low as a vacuum variable capacitor, it is what I had available. Likewise, losses in the loop would be lower with a larger diameter main loop conductor. Improvements would be possible if more attention were paid to reducing losses in the system.

While the purpose of his article is not to describe the design and construction of small transmitting loop antennas, my description and Figure 1 should enable anyone to replicate the evaluation that I have done. There are numerous articles available from the internet, and other sources, to guide one in building such an antenna. Be warned that there are many misleading claims about such antennas — such as claims of "efficiency greater than 90% on 80 and 40 meters", and there are errors in some of the formulas.

Circuit Model

I assume that the loop antenna can be modeled using a simple first-order system electronic circuit analog. That is, the antenna is equivalent to a transformer with a series RC circuit across the secondary of the transformer. Such a model (Figure 2) has also been suggested by others[11]. A detailed analysis of this circuit model can provide very useful information for both the adjustment of the antenna for proper match to the feed line, and in estimating the efficiency of the antenna.

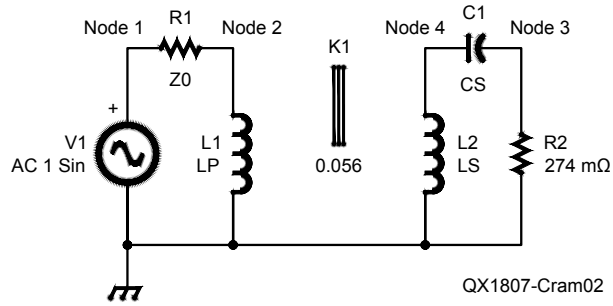

Figure 2 — A TopSpice model of the small transmitting loop antenna. Spice parameters are: Z0 = 50 Ω; LP = 0.434 μH; LS = 2.05 μH, CS = 62.55 pF; W0 = {1/SQRT(LS*CS)}; XLP = {W0*LP/Z0}; R2 = 274 mΩ.

The *primary* of the transformer is the *small coupling loop* to which the transmission line is connected. The *main loop* of the antenna is the *secondary* of the transformer, loaded with a resistor and capacitor. The inductance L (henry) of a single turn loop is,

$$L = \mu_0 b \ln\left(\frac{8b}{a} - 2\right) \tag{1}$$

where μ_0 is the permeability of free space, b is the radius of the loop in meters, and a is the radius of the conductor in meters.

In my model the primary inductance is 0.434 μH, and the secondary inductance is 2.05 μH. The resonating capacitance at 14.1 MHz is 62.5 pF. The secondary resistance includes the radiation resistance of the antenna *and* the effect of all losses in the antenna system, such as the resistive losses in the antenna materials, ground and other nearby lossy materials. I set the value for the total resistance to 0.27 Ω based on measured data (explained later). With these values of resistance and the inductances the simulations are in close agreement with measurements.

I analyzed the circuit in Figure 2, with the free demo Version 8 of *TopSpice* (**www.penzar.com**). I chose this application because of its ability to generate Smith charts. The demo version is limited in the number of components and nodes, but suffices for this simple model.

To gain further insight into the model, I also derived the equations that apply to the circuit. The input impedance to the antenna, at the point the coax is connected to the coupling loop is,

$$Z_{in}(\omega) = j\omega L_p + \frac{(\omega M)^2}{Z_s(\omega)} \tag{2}$$

where the series impedance of the secondary is,

$$Z_s(\omega) = R_s + j\omega L_s + \frac{1}{j\omega C_s} \tag{3}$$

L_p is the inductance of the coupling loop, L_s is the inductance of the main loop, C_s is the resonating capacitance, and includes any stray capacitance. Resistance R_s accounts for all power loss in the antenna system, including radiation loss. To more easily understand the behavior of the antenna near resonance, I have used a change of variables in the equation for the input impedance. I have also employed the commonly used expression for the Q of the tuned circuit.

The mutual inductance between the primary and secondary will be represented by the coupling coefficient k using the formula,

$$M^2 = k^2 L_p L_s \cdot \tag{4}$$

The resonant frequency of a series tuned circuit is,

$$f_0 = \frac{1}{2\pi\sqrt{L_s C_s}}$$

and Q is,

$$Q = \frac{2\pi f_0 L_s}{R_s}$$

Since we are interested in the behavior of the antenna near its resonant frequency, we make the substitution $f = f_0(1+\delta)$, where $|\delta| << 1$. Without going into the detailed manipulation, the input impedance is,

$$Z_{in}(\delta) = j\omega_0 L_p(1+\delta) + \frac{\omega_0^2 M^2 (1+\delta)^2}{Z_s(\delta)} \tag{5}$$

where the series impedance of the secondary is,

$$Z_s(\delta) = R_s + j\omega_0 L_s(1+\delta) + \frac{1}{j\omega_0 C_s(1+\delta)} \tag{6}$$

Using the common definition of Q, the equation for the input impedance can be simplified to,

$$Z_{in}(\delta) = j\omega_0 L_p(1+\delta) + (1+2\delta)k^2 Q(1+2\delta Q) \quad (7)$$

Because $|\delta| << 1$, we made the substitution $(1+\delta)^2 = 1+2\delta$, and $1/(1+\delta) = 1-\delta$. This introduces negligible error. As you will see later, the calculated impedance matches measured data very closely. These approximations imply that we have a high Q system.

Eqn. (7) is used to examine the real and imaginary parts of the input impedance as a function of the deviation of the frequency from the self-resonant frequency of the loop. The frequency deviation is δf_0.

The real part of $Z_{in}(\delta)$ is,

$$\mathrm{Re}\{Z_{in}(\delta)\} = \frac{\omega_0 L_p(1+2\delta)k^2 Q}{(1+4\delta^2 Q^2)} \quad (8)$$

and the imaginary part of $Z_{in}(\delta)$ is,

$$\mathrm{Im}\{Z_{in}(\delta)\} = \omega_0 L_p\left((1+\delta) - \frac{(1+2\delta)2\delta k^2 Q^2}{(1+4\delta^2 Q^2)}\right) \quad (9)$$

At resonance, we satisfy two conditions,

$$\mathrm{Re}\{Z_{in}(\delta)\} = Z_0 \quad (10)$$

$$\mathrm{Im}\{Z_{in}(\delta)\} = 0 \quad (11)$$

where Z_0 is the characteristic impedance of the coax transmission line, nominally 50 Ω. From the condition on the real part we have

$$\frac{\omega_0 L_p(1+2\delta)k^2 Q}{(1+4\delta^2 Q^2)} = Z_0 \quad (12)$$

re-written as,

$$\frac{(1+2\delta)k^2 Q}{(1+4\delta^2 Q^2)} = \frac{Z_0}{\omega_0 L_p}. \quad (13)$$

If we now insert expression (13) into (9) for the imaginary part of $Z_{in}(\delta)$ we obtain

$$\mathrm{Im}\{Z_{in}(\delta)\} = \omega_0 L_p\left((1+\delta) - \frac{2\delta Q Z_0}{\omega_0 L_p}\right) \quad (14)$$

Setting this expression to 0, as required for resonance,

$$\delta_{res} = \frac{1}{\frac{2QZ_0}{\omega_0 L_p} - 1} \quad (15)$$

When the frequency f is $f_0(1+\delta_{res})$, the real part of the impedance is Z_0 and the imaginary part is 0. That is, *resonance occurs at a frequency different from that where the reactance of the main loop is zero.*

We now return to the Eqn. (8) for the real part of the impedance to determine what coupling coefficient is needed to achieve Z_0 ohms for the real part. After some manipulation we obtain,

$$k^2 = \frac{Z_0\left(1+4\delta_{res}^2 Q^2\right)}{\omega_0 L_p\left(1+2\delta_{res}\right)Q} \quad (16)$$

In practice, we do not have to solve this equation for the coupling coefficient as we usually adjust the coupling to achieve the desired resonance condition using either an impedance analyzer, or a VSWR bridge. However, it may be enlightening to make the calculation once we have an estimate of the Q.

Determination of the antenna Q

The Q of the antenna is of interest for two main reasons. First, the usable bandwidth (without the need for retuning) is determined by the Q and second, the efficiency of the antenna is dependent on Q.

It has been proposed[12] that the Q of an RLC circuit can be determined from VSWR measurements. I have confirmed mathematically, using this circuit model, that VSWR measurements can indeed be used to estimate the Q. However, for the method to work, the VSWR must be very close to 1:1 at the operating frequency. When this condition is met, if one determines frequencies on either side of resonance where the VSWR reaches a specific level, the difference in frequencies at the specified VSWR level, divided into the frequency at 1:1 VSWR provides a number that is proportional to the Q of the antenna. For a target VSWR of 2.618, the proportionality constant is 1.

Since using the VSWR method to determine Q requires a good match, I decided to look at an alternative method. Using plots (Figure 3) of the real and imaginary part of Z_{in} obtained from the *TopSpice* model, it is obvious that changes in the coupling coefficient between the small and large loops have a very small effect on the frequencies at which the imaginary part of Z has its

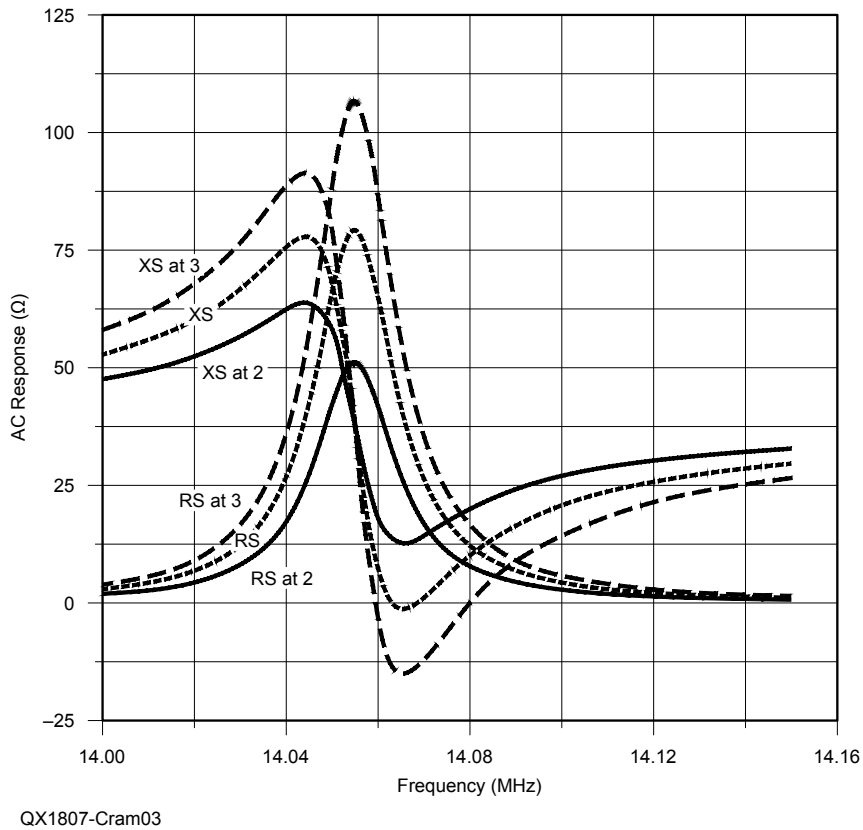

Figure 3 — R and X plots for the small transmitting loop tuned to approximately 14.07 MHz.

maximum and minimum values (close to the resonant frequency f_0). This led me to further analyze the expression for the imaginary part of Z_{in} in the vicinity of f_0.

Recall Eqn. (9) for the imaginary part of $Z_{in}(\delta)$. Since δ is very small, we can approximate $\mathrm{Im}\{Z_{in}(\delta)\}$ with,

$$\mathrm{Im}\left\{Z_{in}(\delta)\right\} = \omega_0 L_p \left(1 - \frac{2\delta k^2 Q^2}{(1+4\delta^2 Q^2)}\right) \tag{17}$$

We then differentiate this expression with respect to δ and set the derivative to zero to locate the maximum and minimum values as a function of δ. This yields the result that when $\delta = \pm 1/2Q$, the imaginary part of the input impedance will have either a maximum or minimum value. Pursuing this further, we focus on the *TopSpice* model results.

Figure 3 is an output from the *TopSpice* program showing the behavior of the real and imaginary parts of the input impedance close to the resonant frequency f_0. The three sets of plots in the above figure correspond to three different values of coupling coefficient. It is particularly interesting that the location in frequency of the maximum and minimum values of the imaginary (X) part of the impedance do not appear to move as the coupling coefficient is changed, as suggested earlier. This tends to confirm that the previous analysis is a valid means to calculate the Q. That is, we can use the expression

$$Q = \frac{f_0}{|f_{\max} - f_{\min}|} \tag{18}$$

where

$$f_{\max} = f_0\left(1 + \frac{1}{2Q}\right) \text{ and } f_{\min} = f_0\left(1 - \frac{1}{2Q}\right)$$

If we further examine the plots, we find that on the middle (R, X) set, X is zero very close to 14.07 MHz and R is very close to 50 Ω. When the coupling coefficient is reduced, X never passes through zero, so there can be no resonance. When the coupling coefficient is increased, we again have two frequencies for which X is zero, but now the R value is either too high, or too low. Consequently, there is only one value of coupling coefficient that achieves perfect match. VSWR is not a good way to determine if coupling needs to be increased or decreased since VSWR can be too high because the transformed impedance is either too high or too low.

To further demonstrate the effect of coupling coefficient changes on the input impedance, I used the *TopSpice* model to generate Smith Chart plots seen in Figure 4. Only the center curve passes through the center of the Smith chart where $R = 50\ \Omega$ and $X = 0$. This corresponds to a VSWR of 1:1, or a reflection coefficient of zero.

This figure demonstrates that if one uses an impedance analyzer that is capable of plotting a Smith chart, it is easy to determine which way the coupling must be changed to achieve a perfect match. The upper curve (solid line) requires an increase in coupling, while the lowest curve (large dashes) requires a decrease in coupling. Such a conclusion is not obvious when using the impedance or VSWR plot.

Note the point labeled ZLS at the top of the Smith chart. This point represents the normalized impedance $j\omega_0 L_p$ of the primary (feeding) loop at f_0. Each of the circular plotted curves appear to be tangent to the outer circle of the Smith chart at ZLS.

Efficiency

Low-power operators are especially interested in the efficiency of their antenna systems. In this section, I will provide some estimates of antenna efficiency based on measurements using a Vector Impedance Analyzer (VIA).

The rationale for my determination of efficiency is that the effective series resistance R_{eff} of the loop antenna adequately accounts for all power losses, including the radiated power. Ideal inductors and capacitors can store energy, but over a complete cycle of the RF, dissipate no power. In this analysis, the losses in the inductor and capacitor are lumped into the single resistance R_{eff}. Furthermore, this effective resistance is related to the Q as noted earlier. It is also generally accepted that the radiation resistance, which is part of the effective resistance, represents power that is radiated by the structure.

The radiation resistance[13] is about,

$$R_{rad} = 197 C_\lambda^4 \tag{19}$$

where C_λ is the circumference of the loop in wavelengths. Siwiak and Quick discuss an improved formula[14] for radiation resistance that includes the effects of non-uniform

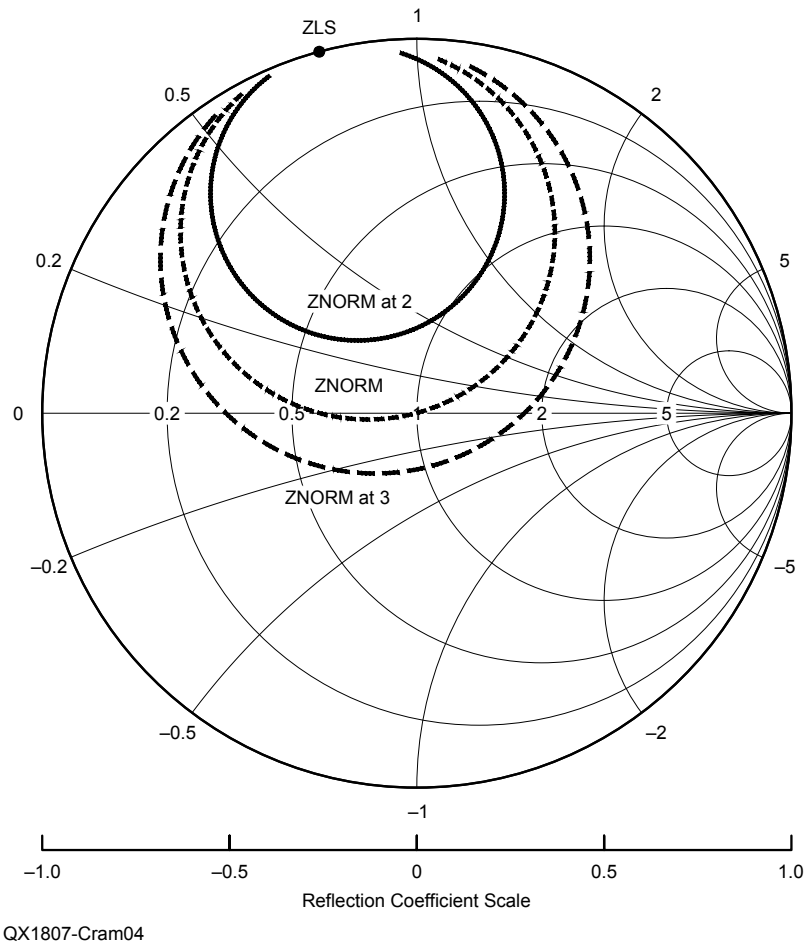

Figure 4 — Smith chart plots for three different coupling coefficient values.

current in the loop.

Allow I_{rf} to represent the rms RF current that flows in the loop. The total power that is dissipated in the loop is,

$$P_{total} = I_{rf}^2 R_{eff} \tag{20}$$

and the power radiated is,

$$P_{rad} = I_{rf}^2 R_{rad} \ , \tag{21}$$

the radiation efficiency is therefore,

$$efficiency = 100\% \frac{P_{rad}}{P_{total}} = 100\% \frac{R_{rad}}{R_{total}} \tag{22}$$

The Q of the antenna is,

$$Q = \frac{\omega L_s}{R_{eff}} \tag{23}$$

where R_{eff} is the same as R_s in the *TopSpice* model. We can also express efficiency as

$$efficiency = 100\% \frac{R_{rad} Q}{\omega L_s} \tag{24}$$

This shows that the only options we have for increasing efficiency is to increase R_{rad} or Q. R_{rad} can be increased by making the loop larger, and Q may be increased by using lower-loss materials.

Measurements on Small Loop Antenna

Next we discuss measurements using a Vector Impedance Analyzer (VIA), like the one offered by the Austin Texas QRP group (**www.qsl.net/k5bcq/Kits/Kits.html**). The VIA is first calibrated using a short piece of 50 Ω coax between the VIA and the open, short, and calibration resistor. This makes the measurement point at the end of the coax, away from the VIA.

The antenna is initially set with the plane of the small loop parallel to the plane of the main loop. The small coupling loop is positioned so that no point on its circumference is closer to the main loop than about 1 inch. Also, see Figure 1, the coupling loop is mounted diametrically opposite from the tuning capacitor.

A VSWR scan is then run over a wide frequency range (Figure 5) to determine the approximate tuned frequency. The tuning capacitor is then adjusted to set the operating frequency of the antenna as close to 14.1 MHz as possible. The scan range of the VIA is reduced to a few hundred kilohertz, as in Figure 6. We then scan the new range and use the Smith chart plot option (Figure 7) on the VIA. Note the similarity to the traces of Figure 4. This plot reveals whether the coupling between the small and large loops is too little or too much. If the plot does not encircle the center of the chart, then the coupling is too small. If the plot encircles the chart center, then the coupling is too much. The movable cursor in the VIA plot has been placed at the VSWR minimum, to allow readout of the corresponding frequency.

Since the magnetic field due to the main loop current is strongest immediately adjacent to the conductor and weakens towards the center of the loop, moving the small coupling loop closer to the main loop will increase the coupling coefficient. Likewise, moving the small coupling loop closer to the center of the main loop will reduce the coupling coefficient. The coupling coefficient can also be reduced by rotating the plane of the small loop so that it is no longer parallel to the plane of the main loop.

In Figures 8 and 9 the display cursor has been placed over the maximum and minimum points on the reactance curves (upper traces). The corresponding frequencies are 14,078,996 and 14,100,313 Hz. The difference between these two values is 21,300 Hz. Since the tuned frequency is (Figure 6) about 14,098,000 kHz, the calculated Q is 14,098,000/21,300, or 662.

We now calculate R_{rad} and L_s using Eqns. (19) and (1), respectively, and use the measured Q as described above to provide an estimate of the efficiency of the antenna. For the 32 inch loop, $R_{rad} = 0.04\ \Omega$. The $Q = 660$, and $L_s = 2.05\ \mu H$. At 14.1 MHz, this value of Q gives $R_{eff} = 0.274\ \Omega$ yielding an efficiency of about 14.5% (or -8.4 dB). This is the value of R_{eff} that I used in the circuit model.

Note in Figure 7 the point where the circular loop is tangent to the outer circle of the Smith chart is very close to the corresponding point in Figure 4. This indicates that the calculated and measured coupling loop inductances are in very close agreement. Finally, Figure 10 shows the measured reflection coefficient (V-shaped trace, left side scale) and its phase (trace starts on the left just above 90°using the right side scale).

Closing Comments.

The effective loss resistance R_{eff} of the loop can be found from the measurement of Q, which is assumed to include *all* power losses, including radiation loss. The calculated radiation resistance R_{rad} is based on an ideal determination of the loss due to radiated power. Consequently, calculation of efficiency using R_{eff} and R_{rad} will produce a value for efficiency subject to how accurately R_{rad} represents the radiation resistance. Q must be relatively high for the approximation $\delta << 1$ to hold true, hence this analysis may

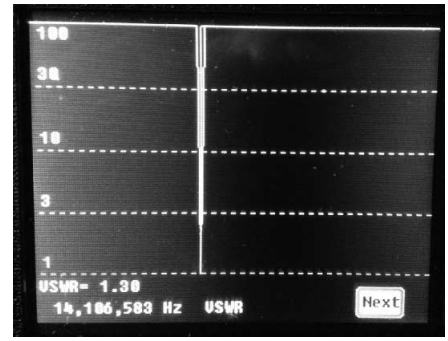

Figure 5 — Broad band VSWR Scan (10 to 20 MHz) to locate resonance.

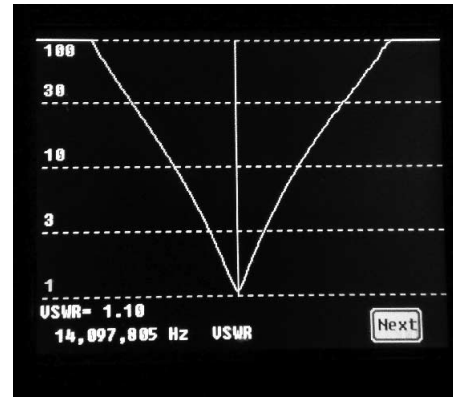

Figure 6 — Narrow band, 14.0 to 14.2 MHz, measured VSWR scan.

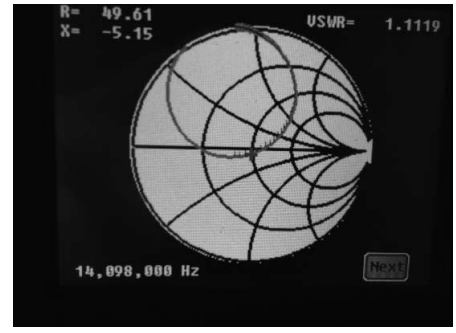

Figure 7 — The narrow band, 14.0 to 14.2 MHz, scan presented as a Smith chart. The cursor is shown at 14,098,000 kHz, the point of minimum VSWR.

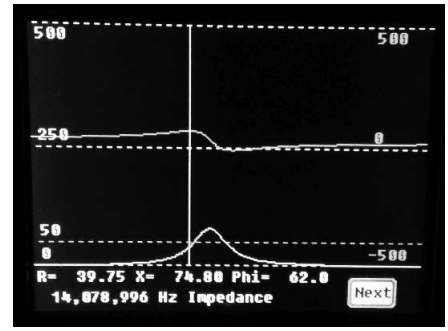

Figure 8 — Impedance plot showing maximum reactance on the upper trace. Lower trace is resistance.

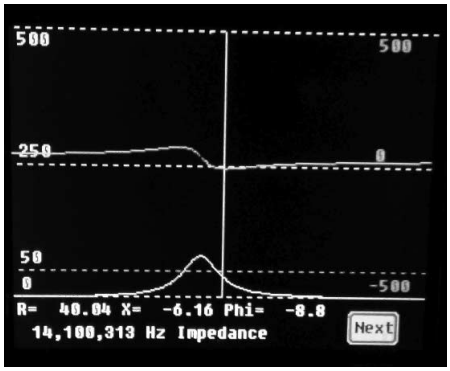

Figure 9 — Impedance plot showing minimum reactance, upper trace. Lower trace is resistance.

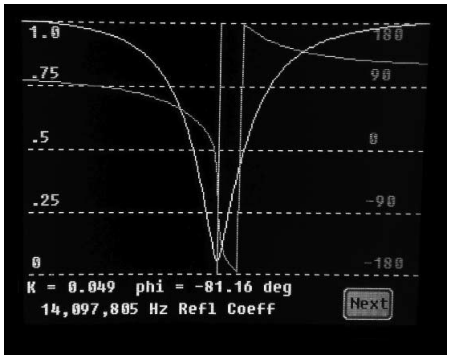

Figure 10 — Measured reflection coefficient magnitude (V-shaped trace, left-edge scale) and its phase (trace starts and ends near 90 on the right-edge scale).

$\delta << 1$ to hold true, hence this analysis may not produce accurate results when the Q is low (<100).

Regarding radiation resistance, I used the simplified Eqn. (19), which ignores the effects of non-uniform current in the loop, or any effects from the *E*-field present in the gap where the tuning capacitor is located. Only the far *electric* and *magnetic* fields due to a perfectly constant loop current are involved in deriving Eqn. (19). Some radiated power might couple to objects close to the antenna. The effect of such power loss is included in R_{eff}.

Conclusions

We have shown that the simple circuit model, with an appropriate choice of parameters, produces results that closely match measured data from a test loop antenna. Using a VIA we have obtained measured data from a small-diameter copper-tubing loop ($C_\lambda = 0.12$), that are in very good agreement with *TopSpice* circuit analysis simulations.

I have presented a method for using the plotting features of a VIA to facilitate adjustments to the antenna for correct impedance matching. In addition to VSWR and impedance plots, the Smith chart presentation of the measurements is a straightforward method for adjusting the coupling to the antenna. There is no guessing as to which way to adjust coupling for impedance matching.

VIA plots of the complex input impedance allow a simple means to determine the Q of the antenna. From this Q, and the calculated inductance of the loop, and the operating frequency, one can easily estimate an upper limit on the efficiency of the antenna. As shown in this example the efficiency is slightly less than 15%.

Milton E. (Milt) Cram, W8NUE, was first licensed in 1953 and holds an Amateur Extra Class license, and is a member of ARRL and QRP ARCI. He earned the BS, MS, and PhD degrees in Electrical Engineering from Georgia Tech. He has many years of experience in the automotive, oil and gas service industry, nuclear power instrumentation, and military electromagnetics applications, and holds patents in each of those areas. Milt is active in the Austin TX QRP Club and has contributed to several projects that have been offered by the club — most recently, the Vector Impedance Analyzer kit. He has published articles in QST and QEX on touch paddle keys, and the NUE-PSK digital modem. He is currently retired and living in Austin TX, where he continues to design projects for the ham community.

Notes

[1]Steve Yates, AA5TB, small loop calculator, **www.aa5tb.com/loop.html**.
[2]Glen E. Gardner, Jr., AA8C, Loop antenna, **gridtoys.com/glen/loop/loop3.html**.
[3]Small transmitting loop, **owenduffy.net/blog/?p=4888**.
[4]Carol F. Milazzo, KP4MD, "14-30 MHz Magnetic Loop, Antenna", **www.qsl.net/kp4md/magloophf.htm**.
[5]Small transmitting loop, **https://www.nonstopsystems.com/radio/frank_radio_antenna_magloop.htm**.
[6]John S. Belrose, "Performance of Electrically Small Tuned Transmitting Loop Antennas" *Radcom, Radio Society of Great Britain*, London, UK, June/July, 2004.
[7]Mike Underhill, "Small Loop Antenna Efficiency" Presented in Kempton UK, May 2006,
[8]A. Findling, K9CHP and K. Siwiak, KE4PT, "How Efficient is Your QRP Small Loop Antenna?", *QRP Quarterly*, Summer 2012.
[9]K. Siwiak, "Loop Antennas," in John G. Proakis (Ed.), **Wiley Encyclopedia of Telecommunications**, New York, NY: John Wiley & Sons, 2002, pp. 1290-1299.
[10]K. Siwiak and R. Quick, "Small Gap-resonated HF Loop Antenna Fed by a Secondary Loop", *QEX*, Jul./Aug., 2018, elsewhere in this issue.
[11]Alan Boswell, Andrew J. Tyler, and Adam White, "Performance of a Small Loop Antenna in the 3-10 MHz Band", *IEEE Transactions on Antennas and Propagation*, Vol. 47, No. 2Apr., 2005, pp. 51-56.
[12]A. D. Yaghjian and S. R. Best, "Impedance, Bandwidth and Q of Antennas," *IEEE International Symposium on Antennas and Propagation Digest*, 1, Columbus, Ohio, June 2003, pp. 501-504.
[13]J. Kraus, Chapter 6, **Antennas**, McGraw Hill, 1950.
[14]K. Siwiak and R. Quick, op. cit., Note 10.

Peter DeNeef, AE7PD
2033 Abby Gate Dr., Roseville, CA 95747; **hamradioandvision@gmail.com**

Effects Due to Ground For Small Transmitting Loop Antennas

The location of the resonating capacitor and coupling to earth ground affect the loop pattern and gain.

Amateurs often place small transmitting loop antennas close to the ground for convenient tuning, for portability, or because of local antenna restrictions. I used computer simulations of a typical Amateur Radio HF loop to learn the effects of height above ground on the gain and antenna patterns.

Early in the development of the Numerical Electromagnetics Code (NEC), G.J. Burke noted unstable results with models of electrically small loops. When there is little variation in the standing wave current on a loop, a small change in frequency can change the calculated admittance by orders of magnitude. He concluded[1], "For a loop over a finitely conducting ground the solution fails when the loop size is somewhat less than resonant. Hence small loops over ground cannot presently be modeled". In a 2015 e-mail Dr. Burke wrote to me that improvements in the NEC over the years do not resolve this issue for modeling small loops.

At 7 MHz a 1 meter loop is electrically small ($C_\lambda = 0.07$), where C_λ is the circumference in wavelengths. The variation in the current distribution[2, 3] around the loop is just 2% at 7 MHz, so results from NEC simulations are open to question. Until recently, testing NEC simulations for electrically small loops over lossy media has been problematic. In 2014, Austin, *et al.*, demonstrated a technique[4] for comparing NEC results to theoretical predictions of the input impedance. As described in "Accuracy Tests" below, NEC simulations for a 1 meter diameter loop at 7 MHz agree with this theory, validating the calculations.

Antenna Patterns

I used an NEC-2 model in EZNEC[5] for a vertical 1 m diameter loop of 10 mm (3/8 inch) diameter copper tubing located above "good" ground[6] (conductivity σ = 7 mS/m and relative permittivity ε_r = 17). A voltage source is at the bottom of the loop, and a lossless tuning capacitor is across the gap at the top.

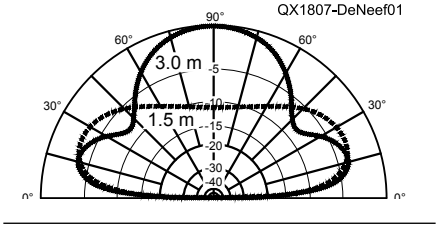

Figure 1 — Elevation plots for loops 1.5 m and 3.0 m above ground at 29 MHz. The resonating capacitor is at the top of the loop. Outer circle is 4.5 dBi.

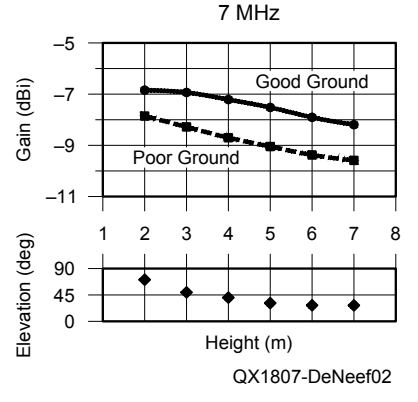

Figure 2 — For 7 MHz, maximum gain and elevation angles vs. height.

Figure 1 shows elevation plots at 29 MHz for two loops — one with a center-height of 1.5 m, and the other at 3.0 m. The plots are in the plane of the loop, where the gain is highest. The loop mounted closer to the ground has a different radiation pattern and less gain. For the loop at h = 1.5 m the maximum gain is 1.4 dBi at 24° elevation, and at h = 3.0 m it is 4.5 dBi at 90°.

The type of ground has a relatively small effect on the gain of this loop. Figures 2 – 5 show the maximum gain *vs.* height for 7, 14, 21, and 29 MHz, respectively. The solid lines show the gain with good ground as specified above, and the dashed lines are with very "poor" ground (σ = 1 mS/m, ε_r = 5). A chart under each graph shows the elevation angle at maximum gain for the "good" ground. The elevation plots represented by Figures 2 – 5 are available from the **www.arrl.org/QEXfiles** web page.

7 MHz

Figure 2 shows gain decreasing slowly as the height increases. The elevation at maximum gain also decreases, but the patterns are so wide (large 3 dB beamwidth) that for practical purposes the plots are similar from 2 m to 5 m. The figure does not show data for heights below 2 m because, as discussed below, NEC simulations for 7 MHz are less accurate for loops below this height. Theoretical predictions for the impedance at this frequency show that the resistance effect of ground increases rapidly below 2 m.

14 MHz

Figure 3 shows gain increasing slowly with height between 1 m and 2 m, and the wide elevation patterns are all similar in this range. For h from 3 m to 5 m, radiation is restricted to lower elevations. At $h = 6$ m the elevation plot has two lobes: at 90° and 18°.

21 MHz

Figure 4 shows that, unlike the previous two bands, gain increases rapidly as the height increases. At 4 m and above, the radiation pattern shifts upward as a new lobe develops at 90° elevation.

29 MHz

Figure 5 shows gain increasing with height up to 4 m. Compared with the plots for 21 MHz, the low-angle lobe at 1 m to 2 m is narrower, and the transition to upward radiation occurs at $h = 3$ m.

Capacitor Location

Kai Siwiak, KE4PT, analyzed (see Siwiak, KE4PT) the electric field that surrounds the loop, and especially around the tuning gap, of a small loop and he observes that the location of the capacitor can affect the pattern of radiation. Figure 6 shows an elevation plot at 29 MHz for two loops at a height of 3 m. With the capacitor at the bottom of the loop the radiation pattern is different from the loop with the capacitor at the top seen in Figure 1. At this frequency the pattern with the capacitor at the bottom is more like that of a loop at $h = 1.5$ m with the capacitor at the top (Figure 1). The elevation plots on the **/QEXfiles** web page are shown for both configurations.

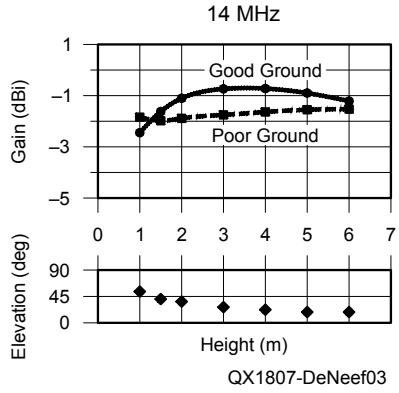

Figure 3 — For 14 MHz, maximum gain and elevation angles vs. height.

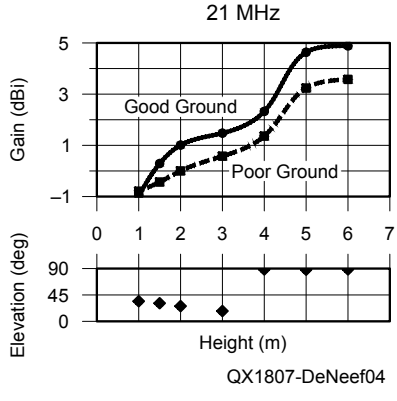

Figure 4 — For 21 MHz, maximum gain and elevation angles vs. height.

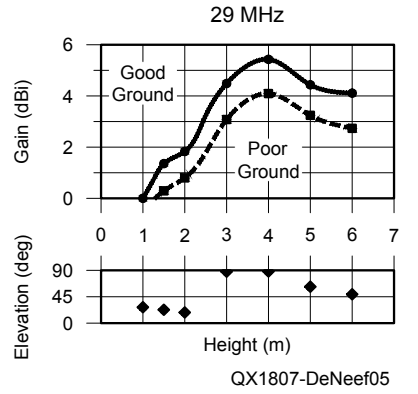

Figure 5 — For 29 MHz, maximum gain and elevation angles vs. height.

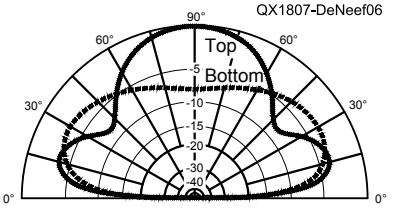

Figure 6 — Elevation plots with the capacitor at the top or bottom of a loop at h = 3 m at 29 MHz. Outer circle is 4.5 dBi.

Accuracy Tests

In addition to the standard accuracy tests for NEC calculations — Average Lossless Gain and Convergence — I used these tests:

1. Comparisons with the Theory Used by Austin et al.

The input resistance of the loop (see Austin *et al.*, and Vogler *et al.*) is $R = R_f + R_g$, where R_f is the radiation resistance of the loop in free space, and R_g is ground-loss resistance. The loop conductor and capacitor are assumed lossless. Nomograms in Vogler, *et al.*, enable you to find R_g/R_f. I calculated R_f using a lossless NEC model of the loop in free space with no capacitor. The nomograms for vertical loops are labeled "HMD" (horizontal magnetic dipole) because the dipole moment lies along the axis perpendicular to the loop and is horizontal.

Figure 7 shows comparisons between theory (solid curves) and NEC-2D simulations (data points) for loops at 7, 14, and 21 MHz. The results shown at 7 MHz for a one-meter diameter loop are recalculations for the example in Austin, *et al*. As they noted, the NEC simulations show reasonable agreement with theory when the height is greater than λ/20.

This theory is for electrically small loops, so I used a 0.5 m diameter loop ($C_\lambda = 0.07$) for the comparisons at 14 MHz, and a 0.25 m diameter loop ($C_\lambda = 0.06$) at 21 MHz. Agreement is poor when $C_\lambda > 0.1$ because the theory does not account for ground coupling by non-uniform components of current on

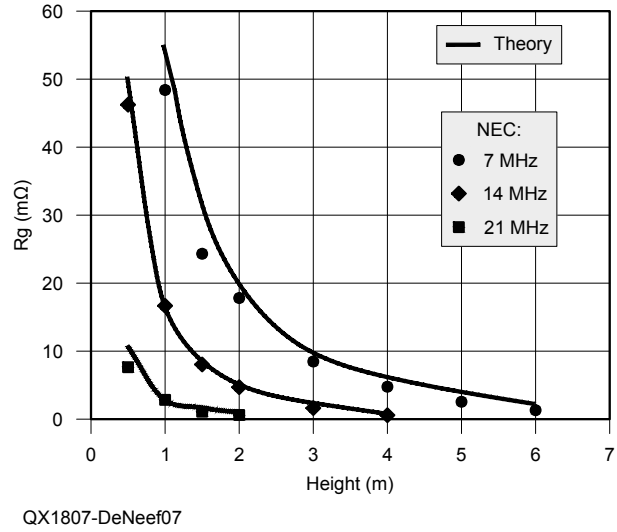

Figure 7 — Comparison of theory and NEC simulations of R_g *vs.* height for three different electrically small loops.

the loop; the dipole component of current increases as ($2C_\lambda^2$). I selected realistic ground properties that minimize interpolation error with the nomograms. In each case the index of refraction is $n = 5$, as in Austin *et al*.

NEC simulations of R_g for a 1 m loop show that the effect of ground increases rapidly below $h = 2$ m at 14, 21, and 29 MHz. For 7 MHz the impedance theory predicts a rapid increase in Rg close to the ground ($h < 2$ in Fig. 6).

The calculations also show that R_g ($R - R_f$) can be negative. R_g is different from the usual definition for ground resistance, which specifically distinguishes the power dissipated in the ground[7].

2. Double-precision (NEC-2D) vs. single-precision (NEC-2)

The unstable NEC results mentioned in the introduction are caused by an ill-conditioned matrix. Small differences between large numbers can cause inaccuracies. With double-precision computation the problem shifts to a lower frequency (see Burke). There is no significant difference between my NEC-2D and NEC-2 simulations of the antenna patterns. I used NEC-2D for the comparisons of R_g with theory in Figure 7.

3. NEC Admittance

There are no sudden changes in the loop admittance at frequencies around 7, 14, 21, and 29 MHz.

4. Wave Impedance Inside the Loop

At the center of a small loop in free space the magnitude of the ratio of the electric field to the magnetic field is $\eta_0 C_\lambda$, where $\eta_0 = 376.73\ \Omega$ (see Siwiak, KE4PT). I used this relationship to validate NEC calculations when $C_\lambda < 0.2$.

Conclusions

NEC-2 calculations for an HF loop antenna at heights from 1 m to 6 m show that coupling to earth ground affects the antenna pattern and the gain. The effects of good ground and very poor ground are similar in magnitude.

For the range 7 – 29 MHz the gains and elevation patterns for the 7 MHz band are the least affected by the height of a loop. At 21 and 29 MHz the gain and elevation angles increase significantly for heights above 3 or 4 m. The location of the capacitor can make a difference in the loop performance, especially at higher frequencies.

My thanks to Kai, Siwiak, KE4PT, for very helpful answers to my questions about small loops.

Peter DeNeef, AE7PD, received his first license as KF7FPX in 2009. He has written about RF exposure safety for QEX (Nov/Dec, 2017), as well as articles about international RF safety guidelines of the International Commission on Non-Ionizing Radiation Protection (ICNIRP). More of his articles can be found on his popular web site for vision-impaired hams, ***www.HamRadioAndVision.com****.*

Notes

[1]G. J. Burke, "Recent Advances to NEC: Applications and Validation," UCRL Preprint 100651, Mar. 3, 1989, pp. 3 – 4 to 3-8, see: **https://e-reports-ext.llnl.gov/pdf/210389.pdf**.

[2]K. Siwiak and Y. Bahreini, **Radiowave Propagation and Antennas for Personal Communications, 3rd Ed.**, Artech House, Norwood, MA, 2007.

[3]K. Siwiak, KE4PT, "Effect of Small HF Loop Near Fields on Direction Finding," *QST*, July 2015, pp. 63 – 64.

[4]B. A. Austin, A. Boswell, and Michael A. Perks, "Loss Mechanisms in the Electrically Small Loop Antenna", *IEEE Antennas and Propagation Magazine*, Vol. 56, No. 4, Aug. 2014, pp. 142 – 147.

[5]Several versions of *EZNEC* antenna modeling software are available from developer Roy Lewallen, W7EL, at **www.eznec.com**.

[6]L. E. Vogler and J. L. Noble, "Curves of Input Impedance Change Due to Ground for Dipole Antennas," NBS Monograph 72, Jan. 31, 1964, see: **nvlpubs.nist.gov/nistpubs/Legacy/MONO/nbsmonograph72.pdf**.

[7]Robert J. Zavrel, Jr, W7SX, Appendix B in, **Antenna Physics: An Introduction**. Available from your ARRL dealer or the ARRL Bookstore, ARRL item no. 0499. Telephone 860-594-0355, or toll-free in the US 888-277-5289; **www.arrl.org/shop**; **pubsales@arrl.org**.

Kai Siwiak, KE4PT and **Richard Quick, W4RQ**
10988 NW 14th St., Coral Springs, FL 33071; **k.siwiak@ieee.org** 695 Fairway Dr., Plantation, FL 33317; **w4rq@arrl.net**

Small Gap-resonated HF Loop Antenna Fed by a Secondary Loop

Improved formulas for the loop current and loop impedance lead to an accurate determination of close-near-fields, and far field null depths.

The small gap-resonated high frequency circular loop antenna has received much attention in Amateur Radio since John H. Dunlavy, Jr. patented[1] his efficient small loop that can be tuned over wide bandwidths. The now-expired patent spawned a multitude of homebrew loops and several commercial products aimed at hams.

Loop analysis dates back to the earliest days of radio with Pocklington's 1897 paper[2] on the thin wire loop. Later Hallén[3] expanded on the receiving qualities of loops, and Storer[4] studied the impedance of thin wire loops. Loop analysis was generalized[5] by Q. Balzano and one of us, Kai Siwiak, KE4PT, to fat wires giving, among other results, the details of current density along the circumference as well as the cross-section of the loop wire. The results here are derived from the Balzano-Siwiak work, and specialized[6] to electrically small loops. We relied on the Neumann formula[7] to find the mutual coupling between the primary and the secondary feeding loops. We also report on the effects of common mode currents (CMCs) coupling to the feeding coax cable, as well as mutual coupling of the loop to the ground. We verified our analytical results by simulations using Numerical Electromagnetic Code (NEC) models in 4*nec*2 software[8]. Our NEC model includes the primary loop, the secondary feeding loop, a resonating capacitor, and a conductor representing the shield of the coaxial feed line.

We present results rather than lengthy derivations that can be gleaned from the referenced notes. In Section (1) we show the loop current density along the loop circumference and in the cross section, revealing current bunching. In Section (2) we present the loop impedance, including effects of loop wire thickness, and non-uniform loop current. In Section (3) we show the effect of the secondary feeding loop. In Section (4) we provide details about the loop near fields and far-field null filling that are a direct result of considering the non-uniform loop current. In Section (5) we show the effects of loop currents coupling to a coaxial feed line shield. In Section (6) we calculate coupling of the loop to the ground. In Section (7) we determine the loop efficiency. We conclude with a summary in Section (8).

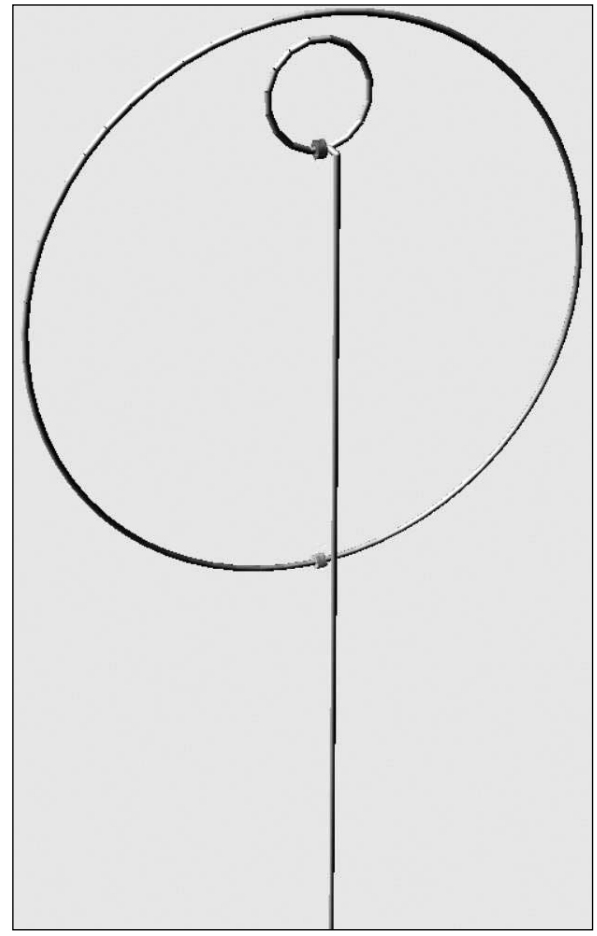

Figure 1 — The electrically small HF loop includes a primary loop and a secondary feeding loop, both in the same *zx*-plane, and a coaxial cable feed line also in the *zx*-plane, but slightly displaced in the *y*-axis, so that the cable does not touch the bottom of the primary loop. A resonating capacitor connects across a gap at the bottom of the primary loop.

1 — Small Loop Currents and Fields

The circular loop geometry for our study is shown in Figure 1, rendered in 4*nec*2 software. The primary loop diameter is 2*b*, the loop

wire diameter is $2a$, the angular extent along the loop circumferences is ϕ, with the loop gap located at $\phi = 0°$. The resonating capacitor is connected across the gap at the bottom of the primary loop. The secondary feeding loop is $2b_2$ in diameter and with $2a_2$ conductor diameter. A coaxial cable feed connects across a gap at the bottom of the smaller secondary loop. We studied the effect of currents coupling to the coax cable shield by varying the length of that coax.

The variation around the loop wire cross-sectional circumference is angle ψ with $\psi = 0°$ pointing to the outside of the loop. We examine a specific loop with $a = 0.00406$ m, $b = 0.4534$ m (loop circumference is 2.85 m), $a_2 = 0.002$ m, and $b_2 = 0.077$ m. The loop centers were displace by 0.343 m. We varied the length of the coax feed line for the common mode current coupling portion of the study. Our loop dimensions closely match those of the *AlexLoop*[9] by Alex Grimberg, PY1AHD.

1.1 — The Dunlavy Loop

John Dunlavy discovered that a loop antenna comprising a one turn primary loop having a circumference of less than three-eighths of a wavelength and interrupted along its length by a gap, with a tuning capacitor connected across the gap, can be tuned by up to a 10:1 tuning range. A single-turn secondary loop, much smaller than the primary loop, is inductively coupled to the primary loop. Both loops are in the same plane. The secondary loop diameter is selected to bear an optimum relationship to the diameter of the primary loop so that variation in feed impedance is minimized over the band of operation. A low impedance transmission line (50 Ω) connects to the terminals of the secondary loop.

Dunlavy used relatively thick conductors of copper or aluminum, and a construction that minimized excessive resistive losses.

1.2 — Loop Current Density

The loop current density $J(\phi, \psi)$ is a Fourier series in terms of $\cos(n\phi)$ along the loop circumference and $\cos(m\psi)$ along the cross-sectional circumference. We initially retained just the $m = n = 0$ and 1 terms. The $m = 1$ term reveals current bunching on the inner surface of the loop conductor. The $n = 1$ term accounts for the first order variation of the circumferential loop current. Including that term reveals details about the close-near fields, and about the far-field peak-to-null ratio. The current density is,

$$J(\phi,\psi) = \frac{I_0}{2\pi a}\left\{1 - 2(kb)^2\cos(\phi)\right\}\left\{1 + Y(a,b)\cos(\psi)\right\} \quad (1)$$

The first curly brackets contain the circumferential variation of the current in ϕ. The second curly brackets include the function $Y(a, b)\cos(\psi)$, which describes current bunching in the cross-sectional circumference of the loop conductor. These curly-bracket terms are ignored in most previous formulas for loop current density. From Note 6 a curve-fit approximation for Y is,

$$Y(a,b) = -\left(\frac{2a}{10a+b}\right)^{0.75} \quad (2)$$

which when multiplied by $\cos(\psi)$ integrates to zero in the ψ-directed cross sectional circumference of the loop conductor. In our example values of a and b, $Y = -0.046$, indicating less than 5% current bunching on the inner surface of the loop conductor. Since our loops have an a to b ratio of less than 0.009, we will not consider the current bunching in the ψ direction any further.

Integrating the current density over the loop conductor cross section in ψ, and noticing that the circumference in wavelengths $kb = 2\pi b/\lambda = C_\lambda$, we see that the loop current is,

$$I(\phi) = I_0\left\{1 - 2C_\lambda{}^2\cos(\phi)\right\} \quad (3)$$

which instantly reveals that the first order current amplitude variation term depends solely on the loop circumference in wavelengths. The loop current Eqn. (3) is valid for $C_\lambda < 0.3$, and is used to solve for the loop fields in classic fashion.

Figure 2 shows the loop current for the 2.85 m circumference loop at 7, 14, and 30 MHz, where C_λ is 0.067, 0.133, and 0.285 respectively. The variation increases with frequency.

1.3— General Form of the Loop Fields

With reference to the details in Note 5, the electric and magnetic fields are obtained from the vector **A** and scalar V potentials in classical fashion,

$$\mathbf{E} = -\nabla V - j\omega\mathbf{A} \quad (4)$$

$$\mathbf{H} = \frac{1}{\mu_0}\nabla\times\mathbf{A} \quad (5)$$

The boundary conditions require that tangential electric fields are zero on the loop surface everywhere except at the loop gap. The components of the vector potential in cylindrical coordinates are,

$$A_\phi = \frac{1}{4\pi}\iint_{S'} J_\phi\cos(\phi-\phi')GdS' \quad (6)$$

$$A_\rho = \frac{1}{4\pi}\iint_{S'} J_\phi\sin(\phi-\phi')GdS' \quad (7)$$

and the scalar potential is,

$$V = \frac{j\eta_0}{4\pi\varepsilon_0 k}\iint_{S'}\frac{1}{\rho'}\frac{\partial J_\phi}{\partial\phi'}GdS' \quad (8)$$

The integrals are over the surface S' of the loop wire. The intrinsic impedance of free space is $\eta_0\,\Omega$, and $k = 2\pi/\lambda$ m^{-1} is the wave number, and ε_0 F/m is the free space permittivity. The Green's function is,

$$G = \frac{e^{-jk|\mathbf{r}-\mathbf{r}'|}}{|\mathbf{r}-\mathbf{r}'|} \quad (9)$$

where $|\mathbf{r}-\mathbf{r}'|$ is the distance between the field point and the current density point on the wire. We solved these equations in a *Mathcad* spread sheet, and the details are available on the **www.arrl.org/qexfiles** web page. The results are valid from the surface of the loop conductor to everywhere in space. We also validated these analytical results with simulations using an NEC model rendered in 4*nec*2 software, see Table 1, also on the **/qexfiles** web page. The NEC model includes the primary loop, the secondary feeding loop, a length of wire representing the shield of the coax cable feed line, and a resonating capacitor.

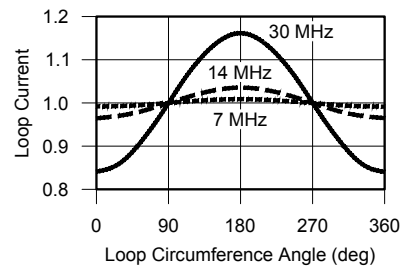

Figure 2 — Loop currents at 7, 14, and 30 MHz along the loop circumference vary in amplitude due to the inclusion of a Fourier series expansion term.

Table 1.

Numerical Electromagnetic Code (4nec2) model includes the primary loop, a secondary feeding loop and segment of wire representing the shield of the coax cable feed line, and a resonating capacitor.

```
CM                                      Frequency - frq MHz
CM                                      Includes feed stub; (1+j0)V source
CM                                      RG-213/U primary loop, Rloss aluminum
CM                                      RG-58/U coupling loop
CM                                      No Ground
CE
SY frq=14.10                            'frequency MHz
SY b=0.45339                            'primary loop radius, m
SY a=0.004064                           'Primary loop wire radius, m
SY b2=0.077                             'Feed loop radius, m
SY a2=0.002                             'Feed loop wire radius, m
CM
SY C=43.40e-12                          'INPUT RESONATING CAPACITOR, Farad
CM
SY Qc=2400                              'Input resonating capacitor Q
SY Rp=Qc/(2*3.1415926535*frq*1e6*C)     'Parallel equivalent capacitor resistance
SY cond=34000000                        'aluminum, RC-213/U shield conductivity
SY n=64                                  'Input n-polygon primary loop
SY n2=16                                'Input n-polygon coupling loop
SY ang1b=-90-360/(2*n)                  'start of arc angle of primary loop
SY ang2b=ang1b+360                      'end of arc of primary loop
SY ang1b2=-90-360/(2*n2)                'start of arc angle of feed loop
SY ang2b2=ang1b2+360                    'end of arc angle of feed loop
SY zb=1.5                               'elevation in Z of center of loop
SY loopgap=4.5*(a+a2)                   'gap between primary and feed loop
SY zb2=zb+0.343038                      'elevation in Z of center of feed loop
CM
SY nstub=1                              'CHOOSE number of stub segments
CM                                      nstub=34 for 1.5 m cable; 74 for AlexLoop 129 inch coax length
SY stublength=0.0445*nstub              'compute stub 'SEGMENT LENGTH FIXED AT 0.0445 m
SY stubZ=1.7675                         'stub start coordinate
SY sEnd=stubZ-stublength                'stub end coordinate
CM                                      primary loop arc, GA, shifted in Z
GA  1  n      b                -0.0150219548  ang1b  ang2b  a
GM  0  0      0                0              0      0      0
GA  2  n2     b2               -0.0150219548  ang1b2 ang2b2 a2
GM  0  0      0                0              0      0      0
CM
GW  3  1      -0.0150219548    0              stubZ  -0.0150219548  0.03  stubZ  a2
GW  4  nstub  -0.0150219548    0.03           stubZ  -0.0150219548  0.03  sEnd   a2
GE  0
LD  1  1      1                1              Rp     0              C
LD  5  0      0                0              cond
GN  -1
EK
EX  0  2      1                0              1.     0.0
FR  0  0      0                0              frq    0
EN
```

2 — Small Loop Impedance

The general form of the loop impedance with just radiation loss is,

$$Z_{loop} = \eta_0 \frac{\pi}{6}(kb)^4\left[1+8(kb)^2\right]\left[1-\frac{a^2}{b^2}\right]+\cdots$$
$$+j\omega\left[\mu_0 b\left[\ln\left(\frac{8b}{a}\right)-2+\frac{2}{3}(kb)^2\right]+M_{12}\right]\left[1+2(kb)^2\right] \quad (10)$$

including terms due to conductor thickness, and to the first-order current variation. The radian frequency is ω, and μ_0 is the free space permeability. M_{12} is the mutual coupling inductance between the primary and secondary loops obtained using the Neumann formula.

The *loaded* radiation Q of the antenna is,

$$Q_{rad} = \frac{1}{2}\frac{\mathrm{Im}\{Z_{loop}\}}{\mathrm{Re}\{Z_{loop}\}} \quad (11)$$

The primary loop loss resistance is,

$$R_{loss} = \frac{b}{a\delta\sigma} \quad (12)$$

where the σ is the loop conductivity in S/m, and the skin depth for good conductors is,

$$\delta = \sqrt{\frac{2}{\omega\mu_0\sigma}} \quad (13)$$

The Q_c of the resonating capacitor also contributes to losses in the form of parallel resistance across the capacitor, so that the net loaded Q_L of the antenna is,

$$Q_L = \frac{0.5}{\frac{1}{Q_C} + \frac{\mathrm{Re}\left\{Z_{loop}\right\} + R_{loss}}{\mathrm{Im}\left\{Z_{loop}\right\}}} \tag{14}$$

from which we can determine the loop current amplitude term I_0 for a given transmitter-supplied RF power P,

$$I_0 = \sqrt{\left(\frac{P}{R_{rad}}\right)\left(\frac{Q_L}{Q_{rad}}\right)} \tag{15}$$

The efficiency *eff* of the loop antenna follows as,

$$eff = \frac{I_0^{\,2} R_{rad}}{P} = \frac{Q_L}{Q_{rad}} \tag{16}$$

The value of Q_L can be obtained from Eqn. (14) or from direct measurements.

3 — The Secondary Feeding Loop

The secondary feeding loop has two main effects on the system. First, the total loop inductance increases by the mutual coupling inductance, M_{12}, between the primary loop and the secondary feeding loop. The result is that less capacitance is needed to resonate the antenna than if just the primary loop inductance were considered. Second, the relative diameters of the secondary feeding loop and the primary loop step up the primary loop resonant radiation plus loss resistance to the feed point value needed to match the feeding coax cable.

We used the Jordan and Balmain[10] high frequency extension to the Neumann formula, specialized to circular loops with constant current, to find the mutual coupling M_{12} between the primary loop and the secondary feeding loop.

$$M_{12} = \int_0^{2\pi}\int_0^{2\pi} \frac{b_2 b D_{12} \exp(-jkR_g)}{R_g} d\theta_1 d\theta_2 \tag{17}$$

and D_{12} and R_g are function of θ_1 and θ_2, the angles around the circumferences of the two loops,

$$D_{12} = \cos(\theta_1)\cos(\theta_2) + \sin(\theta_1)\sin(\theta_2) \tag{18}$$

and R_g further depends on the relative displacements of the two loops,

$$R_g = \sqrt{\left[b_2 \sin\theta_2 - b\sin\theta_1 + X\right]^2 + \cdots \\ + \left[b_2 \cos\theta_2 - b\cos\theta_1 + Z\right]^2 + Y^2} \tag{19}$$

where X, Y, and Z are the center-to-center displacement distances of the two loops that are in the zx plane. We solved Eqn. (17) using direct numerical integration in *Mathcad* software and include that solution on the **/qex-files** web page. For our loop dimensions, $(L_{self}+M_{12})/L_{self}$ is 1.02. M_{11} is the self-inductance of the primary loop. M_{12} is 57.3 nH for our example, and the loop centers are displace in the loop plane by 0.343 m.

Eqn. (17) can also be used to compute the complex self inductance L_{self} of the primary loop. Then, $j\omega L_{self}$ provides another way to compute the primary loop radiation impedance and reactance for a constant loop current.

4 — Fields at the Loop Center and in the Far Field Null

The electric field perpendicular to the surface of the wire is proportional to the rate of change (differentiation) of the current in the circumferential ϕ direction around the loop. Since we've included a loop term that varies with $\cos(\phi)$, thus survives differentiation in ϕ, we can derive a expression for the electric field in the center of the loop plane. Likewise, we can analyze the far field of the loop in the far-field null direction. In both cases the solution originates with the $2(C_\lambda)^2\cos(\phi)$ term of the loop current.

4.1— Fields at the Loop Center

The electric field at the center of the loop in the zx plane is found from the derivative with respect to ϕ of the loop current. Stated at the loop center $(x, y, z) = (0, 0, 0)$,

$$E_\phi(0,0,0) = -j\frac{\eta_0 k I_0}{2} \tag{20}$$

and the magnetic field can be approximated from the single-turn solenoid equation,

$$H_z(0,0,0) = \frac{I_0}{2b}\ . \tag{21}$$

The electric field depends on wavelength (via k) but does not depend on any loop dimension. The magnetic field, however, depends on the loop radius b. The wave impedance Z_W at the loop center is a measure of how well the loop discriminates between the electric and magnetic fields. That wave impedance is,

$$Z_W = \frac{E_\phi}{H_z} = -j\eta_0 kb = -j\eta_0 C_\lambda \tag{22}$$

clearly revealing the dependence of Z_W on the loop circumference. Also, because the electric field at (0, 0, 0) depends on the *variation* in the loop current, we would not be able to formulate an expression for the wave impedance from just a constant current term.

4.2— The Far-field Null

We evaluated the fields very far from the antenna using the exact analytical expressions in *Mathcad* to determine the loop peak-to-null ratio, and validated the results by NEC simulations. The far-field peak-to-null ratio depends on the current variation term in a simple manner for $C_\lambda < 0.3$. Stated in decibels the peak-to-null ratio of the small loop is,

$$N_{dB} = -20\log(2C_\lambda) \tag{23}$$

Table 2 shows the null depth across the 7 to 30 MHz operating range of our example loop. We compared the null depth using the simple formula of Eqn. (23), a detailed loop near-field calculation in *Mathcad*, and the null calculated from the 4*nec*2 model. The null becomes monotonically and smoothly shallower as the frequency increases for a fixed-size loop. This is normal and expected; recall that at $C_\lambda = 1$ we have the popular full-wavelength loop that exhibits gain of about +4 dBi in the broadside direction. Omitting the current variation term results in an erroneous prediction of an infinitely deep null.

The formula and analysis rely on the first term of the current variation, while the NEC result calculates the exact loop current. The single additional Fourier term loop current approximation becomes less reliable as frequency increases, but is still viable up to 30 MHz. As a result, we estimate that our loop current including a single variation term is reasonably accurate up to at least $C_\lambda = 0.3$.

5 — Loop Coupling to the Coax Feed Line

The secondary loop is fed directly with unbalanced coaxial cable, so there is opportunity to generate common mode currents on the coax feed line. We modeled the primary loop, secondary loop and coax outer shield in 4*nec*2, as rendered in Figure 1. We then varied the length of the

Table 2.
The null depth becomes progressively shallower as the frequency increases.

f, MHz	*Null [Eq. (23)], dB*	*Null [analysis], dB*	*Null [4nec2], dB*
7	17.52	17.52	17.50
10	14.42	14.57	14.50
14	11.50	11.41	11.47
18	9.32	9.29	9.12
21	7.98	7.94	7.83
24	6.82	6.77	6.76
30	4.88	4.79	4.13

coax and searched for the maximum current on the coax cable shield, just like on a previous study involving common mode currents (CMC) on the feed line to a dipole[11] that lacked a current choke.

5.1 — Common Mode Currents on the Feed Line

In this loop antenna, the CMCs are generated at the connection of the coax feed directly to the secondary loop. The CMCs appear to end-feed the shield of the coax feed line. We would expect a maximum coupling to a half-wavelength long feed line. Indeed, Figure 3 shows that the maximum CMC occurs for a coaxial feed line length of 0.45 λ.

We considered a loop that had a fixed coaxial cable length of about 3.3 m — or 0.08 λ at 7 MHz and 0.33 λ at 30 MHz — so if a common mode choke were to be used, it should be located on the coax cable at least a loop diameter away from the loop antenna, perhaps somewhere between 0 and 1.5 m from the transmitter end of the 3.3 m long coax cable.

5.2 — Measuring Loop Currents

We attempted to measure the loop currents and the feed line CMC at 14 and 28 MHz for the loop with its 3.28 m coaxial feed cable, and for an extended cable 9.61 m in length, as close as we could get to 0.452 wavelengths at 14 MHz, the length corresponding to a peak current in Figure 3. One of us, (W4RQ) constructed a 2.5 cm diameter current probe for the task.

We were able to measure in the 20 m band that the primary loop current was stronger than the feed loop current, and that the primary loop current varies along the circumference with the upper half of the loop (near the secondary feeding loop, 180º in Figure 2) having a slightly greater value than the lower half.

Due to the relative insensitivity of our homebrew *H*-field probe, we found no discernible CMCs on the feed-line, either for a long (9.61 m) or short (3.28 m) coaxial cable. With the long (nearly $\lambda/2$) feed line length, the loop tuning was exceptionally "touchy" and unstable.

6 — Vertical Loop Coupling to the Ground

We used the Neumann formula, Eqn. (17) with b_2 set to b, and a displacement between the loops to resemble a loop center-to-center distance to its image in the ground. We estimated the loop coupling to the ground by calculating the mutual inductance between the primary loop and its image in the ground, normalized to the loop self inductance and expressed in percent. That coupling affects the impedance of the loop antenna system. There is also a ground reflection, quite apart from the mutual coupling to ground, that affects the radiation pattern in the elevation plane. Here we are concerned only with the mutual coupling term that affects impedance.

Placing the loop above a perfect electric conducting (PEC) ground results in the strongest coupling. We also estimated the coupling for the "average" ground (σ = 0.005 S/m, ε_r = 13), and to a "poor" ground (σ = 0.001 S/m, ε_r = 5), by reducing the PEC coupling by the magnitude of the refection coefficient for normal incidence on the ground. The reflection coefficient magnitude is 1.0 for the PEC ground, 0.593 for the "average" ground and 0.393 for "poor" ground dielectric parameters at 14.1 MHz. Figure 4 shows the ratio of the mutual coupling to the self inductance in percent, a measure of ground coupling analogous to the ratio of mutual impedance to self impedance for a vertical dipole above ground.

Even for a PEC ground the coupling is less than 0.5% for a loop with its center more than one loop diameter above ground — where the bottom of the loop is a loop radius above ground. Using parameters for "real" ground further reduces that apparent mutual coupling. A loop with its center more than one loop diameter above ground is essentially independent of ground coupling as far as the effect on impedance and loop tuning is concerned. Note that ground reflections, quite apart from ground coupling, do have a significant effect on the loop antenna patterns.

7 — Efficiency of the Small Loop

We compared three methods to estimate the radiation efficiency of the small loop. In one *calculated* method we analytically determined the total loaded Q_L using Eqn. (14) and compared that to the loaded Q_{rad} of Eqn. (11), and then applied Eqn. (16) for the efficiency.

In a second method we measure *loaded* Q_L using a matched transmitter, and the classic bandwidth formula,

$$Q_L = \frac{\sqrt{F_H F_L}}{F_H - F_L} = \frac{\text{Frequency}}{\text{Bandwidth}} \tag{24}$$

where, given the antenna impedance, $Z = R + jX$ then F_H is the

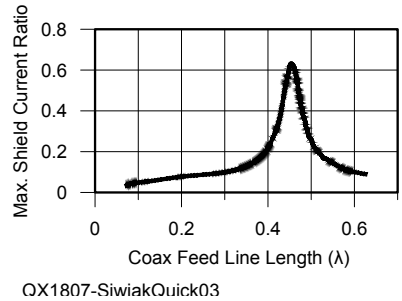

Figure 3 — Simulations using an NEC model of the loop antenna system of Figure 1 show that the maximum common mode current on the feeding cable has a strong but narrow peak for cable lengths that are near the half-wave resonant length.

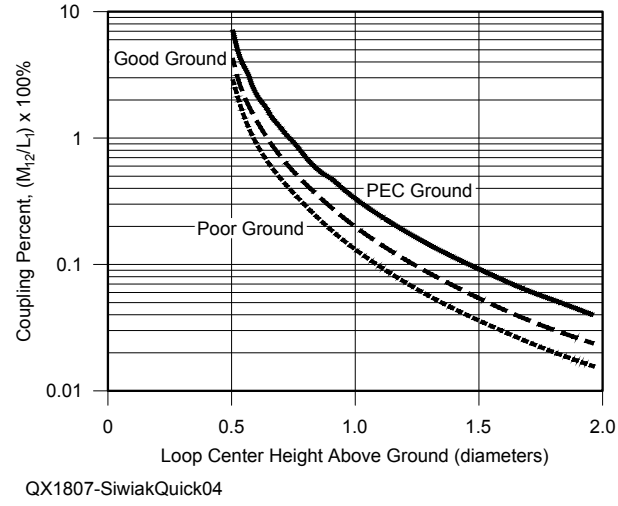

Figure 4 — The percent coupling to ground for this small HF loop is insignificant when the loop center is at least one loop diameter above the ground. Coupling is strongest for a PEC ground, and decreases significantly for realistic ground parameters.

frequency where $R = X$, and F_L is where $R = -X$, so that $F_H - F_L$ is the 3 dB bandwidth. F_H and F_L correspond to the 2.236:1 VSWR and the 7 dB return loss points. When the reactance does not cross zero, we can apply the incremental impedance formula,

$$Q = \frac{f}{2}\frac{|\Delta Z/\Delta f|}{R} \tag{25}$$

where for a small antenna, $|\Delta Z/\Delta f|$ is the magnitude of the incremental change in impedance Z divided by the incremental change in frequency f; and R is the resistance, or $\mathrm{Re}\{Z\}$ at frequency f. We then applied Eqn. (16) for the efficiency. These two approaches are the Q-method[12] for measuring efficiency.

Finally, we used the NEC model to simulate the efficiency. Figure 5 shows that all three methods of determining efficiency are within 0.5 dB of each other across 7 to 29 MHz, inspiring confidence in the analysis and in the NEC model.

The loop loss and radiation resistances increase with frequency. When resonated by the tuning capacitor, and transformed by mutual coupling to the feeding loop, the result is nearly constant input impedance across the operating frequencies. This is one of the key characteristics taught by Dunlavy in his 1971 patent. The secondary loop diameter and location bear an optimum relationship to the diameter of the primary loop so that variation in feed impedance is minimized over the band of operation.

8 — Conclusions

We introduced new improved formulas for the small HF loop current, and for the loop impedance by including one additional term of the Fourier series expansion for the loop current. That term is needed to adequately describe the current for loops up to 0.3 wavelengths in circumference. Including the additional Fourier term results in simple and accurate expressions for (1) the ratio of the electric-to-magnetic fields (field impedance Z_W) at the exact center of the loop, and (2) the far-field null depth.

CMCs on the feed line are small (negligible) as long as the feeding coax cable is not longer than the 3.3 m (less than 0.33 λ at the upper frequency extreme) length supplied with our example loop. CMC chokes, if used, could be attached between the transmitter end of the coax and up to 1.5 m from the transmitter end of the 3.3 m long cable.

Coupling of the vertical loop to a PEC ground is small, and decreases for realistic ground parameters, especially if the loop center is at least a loop diameter above ground. The loop coupling to ground, distinct from ground reflections that affect the elevation patterns, affects only the impedance match, which then requires a very small retuning of the loop.

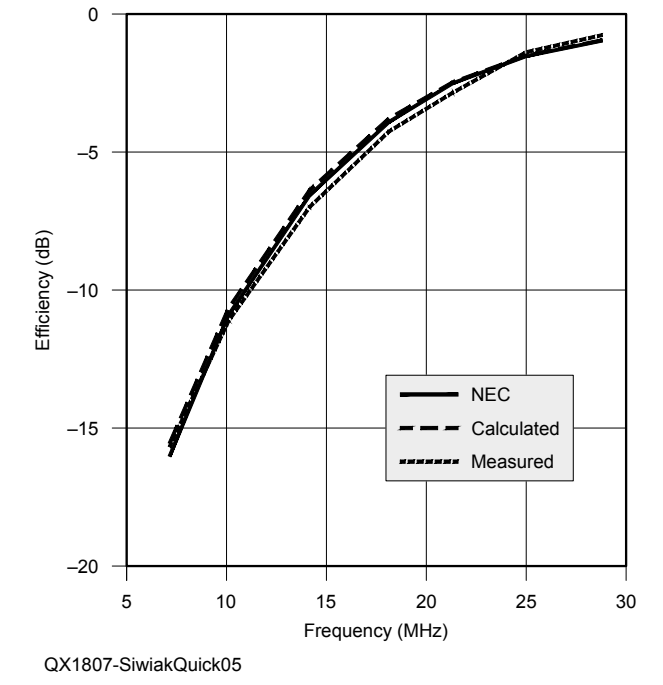

Figure 5 — Small loop efficiency simulated in NEC (solid), calculated from loop equations (long dashes), and measured using the Q method (short dashes). The close agreement among three methods validates the analysis, the Q measurements, and the completely independent NEC model.

Kazimierz (Kai) Siwiak, KE4PT, earned his PhD from Florida Atlantic University, Boca Raton, FL, specializing in antennas and propagation. He is a registered Professional Engineer and Life Senior Member of IEEE. Dr. Siwiak holds 41 US patents, has authored many peer-reviewed papers, several textbooks, and has contributed chapters to other books. Kai holds an Amateur Extra class license, is a life member of AMSAT, and member of ARRL where he serves on the RF Safety Committee and as Technical Advisor. He is a QST Contributing Editor, and Editor of QEX. Kai is a dedicated DXer and enjoys portable operating. His interests include flying (instrument and multiengine commercial pilot), hiking, and camping.

Richard Quick, W4RQ, is a retired Electronics and Metrology Engineering Technician. He was first licensed in 1977, and now holds the Amateur Extra class license. Richard is a member of the ARRL. He has built and tested several small loop transmitting antennas, studying the effects of using various materials and components, and has modeled them using Numerical Electromagnetic Code. Richard has co-authored the articles, "Does Your Antenna Need a Choke or Balun?" (QST, March 2017) and "Live Trees Affect Antenna Performance" (QST, February 2018). Richard enjoys operating at low power levels and from portable locations. He is an avid CW operator.

Notes

[1]John H. Dunlavy, Jr., "Wide Range Tunable Transmitting Loop Antenna", *US Patent 3,388,905*, issued June 28, 1971.
[2]H. C. Pocklington, "Electrical oscillations in wires," *Proc. Cambridge Phil. Soc.*, vol. 9, pp. 324-333, 1897.
[3]E. Hallén, "Theoretical investigation into transmitting and receiving qualities of antennae," *Nova Acta Regiae Soc. Ser. Upps.*, vol. II, pp. 1-4 , Nov. 4, 1938.
[4]J. E. Storer, "Impedance of thin-wire loop antennas," *Trans. AIEE*, vol. 75, pp. 606-619, Nov. 1956.
[5]Q. Balzano and K. Siwiak, "The Near Field of Annular Antennas," *IEEE Trans. Veh. Tech.*, Vol. VT-36, Nov. 1987, pp. 173-184.
[6]K. Siwiak, "Loop Antennas," in John G. Proakis (Ed.), **Wiley Encyclopedia of Telecommunications**, New York, NY: John Wiley & Sons, 2002, pp. 1290-1299.
[7]F. E. Neumann, "Allgemeine Gesetze der inducirten elektrischen Ströme [General laws of electrically induced currents]", *Treatises of the Royal Academy of Sciences in Berlin*, *Annalen der Physik*, 1846, vol. 143, issue 1, pp. 31-44.
[8]The *4nec2* NEC based antenna modeler and optimizer, by Arie Voors, **www.qsl.net/4nec2**.
[9] P. Salas, AD5X, Short Takes: The AlexLoop Walkham Portable Antenna, *QST*, Nov., 2013, p. 67.
[10]E.C. Jordan and K. G. Balmain, Section 14.16, p. 598, **Electromagnetic Waves and Radiating Systems, Second Edition**, Prentice–Hall, Inc., Englewood Cliffs, NJ.
[11]R. Quick, W4RQ, and K. Siwiak, KE4PT, "Does Your Antenna Need a Choke or a Balun?", *QST*, Mar, 2017, pp. 30-33.
[12]A. Findling, K9CHP and K. Siwiak, KE4PT, "How Efficient is Your QRP Small Loop Antenna?", *QRP Quarterly*, Summer 2012.
[13]K. Siwiak, KE4PT, "Q and the Energy Stored Around Antennas", *QST*, Feb., 2013, pp 37-38.

Euclides Lourenço Chuma, PY2EAJ
Rua Cel Manuel de Moraes 204, Campinas, SP 13073-02, Brazil; **codigocerto@yahoo.com.br**

Adapt Your Equipment to Operate at Millimeter Waves up to 32 GHz

Start exploring millimeter waves on a modest budget by adding a prescaler and doubler to your test equipment.

The use of millimeter waves in wireless communications has a long history, evolving from over more than a century ago, when Guglielmo Marconi developed the first wireless telegraph communication systems in 1896 and when Father Roberto Landell de Moura publicly demonstrated a wireless broadcast of the human voice in 1900.

Today, research in radio communications is focused at frequencies above 10 GHz, mainly in SHF and EHF bands or millimeter-wave bands where the wavelength λ is between 1 and 30 mm. Amateur Radio frequency allocations in that range include 8 bands between 10 GHz and 241 GHz, and all above 275 GHz. I present two projects here. The first is a divide-by-4 prescaler circuit that operates in the 10 to 28 GHz range and can extend the upper frequency range of a frequency counter. The second is a frequency doubler with an output frequency range of 24 to 32 GHz. It extends the frequency range of an RF signal generator and has an output power of +21 dBm. Figure 1 shows the divide-by-4 prescaler (left) and the frequency doubler (right).

Figure 1 — Prescaler (left) and multiplier (right).

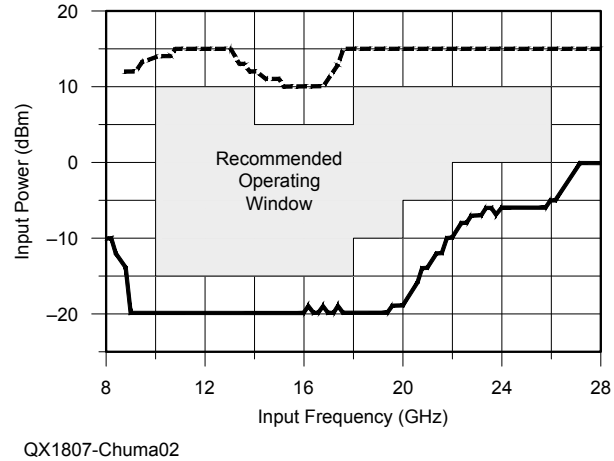

Figure 2 — Input sensitivity window of the HMC447LC3.

The Prescaler

The heart of the divide-by-4 prescaler is the HMC447LC3 MMIC[1] from Analog Devices. The HMC447LC3 is a regenerative divider implemented in InGaP GaAs HBT (heterojunction bipolar transistor) technology that improves the noise and the ability to work in high frequencies. The HMC447LC3 is housed in a 3 mm by 3 mm leadless SMT package, and consumes just 96 mA from a single positive 5 V supply. It delivers a very flat output power across the rated bandwidth. Figure 2 shows the input

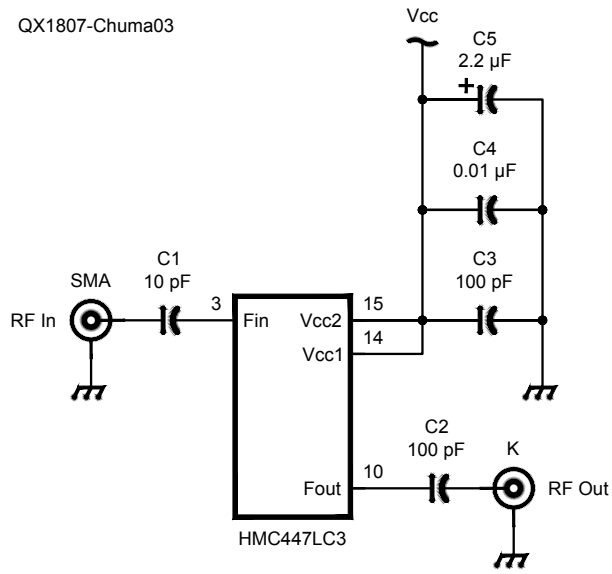

Figure 3 — Schematic circuit of the prescaler using the HMC447LC3. The package base is ground.

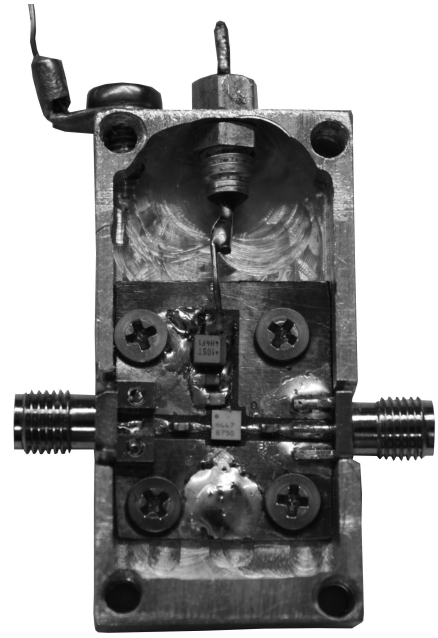

Figure 6 — Assembled prescaler in a machined aluminum housing.

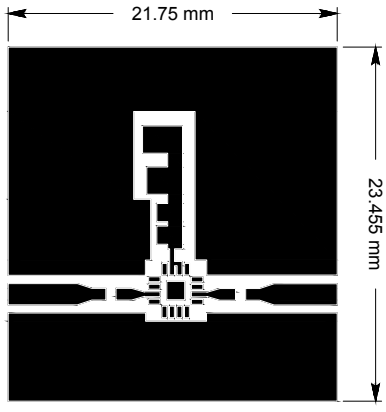

Figure 4 — PCB layout of the prescaler.

Figure 5 — This 2.92 mm connector can be used at higher frequencies (up to 40 GHz) than an SMA connector.

sensitivity window of the HMC447LC3.

Figure 3 shows the very simple schematic circuit needed to use the HMC447LC3. This apparent simplicity hides the physical difficulties in the assembly of the project. Special attention is needed with the PCB, which must have a very low loss dielectric material able to operate at these extremely high frequencies. I used[2] Rogers RT/duroid® 5870 with a thickness of 0.020 inches and 1/2 oz copper on both sides. It is very important to use proper microstrip line to connect the HMC447LC3 to the connectors. The PCB layout is shown in the Figure 4, note that the package base is ground.

Special attention also is necessary for the connectors on input and output of the circuit at these frequencies. I used a 2.92 mm (Figure 5) edge mount type connector, Hirose model[3] HK-LR-SR2. The 2.92 mm connector works up to 40 GHz. That is important because the input frequency of the prescaler operates up to 28 GHz. I used a common SMA edge mount connector at the output. It must operate up to 7 GHz.

I made the aluminum housings using a bench drill machine with end mill cutter, and exercised plenty of patience! I used a

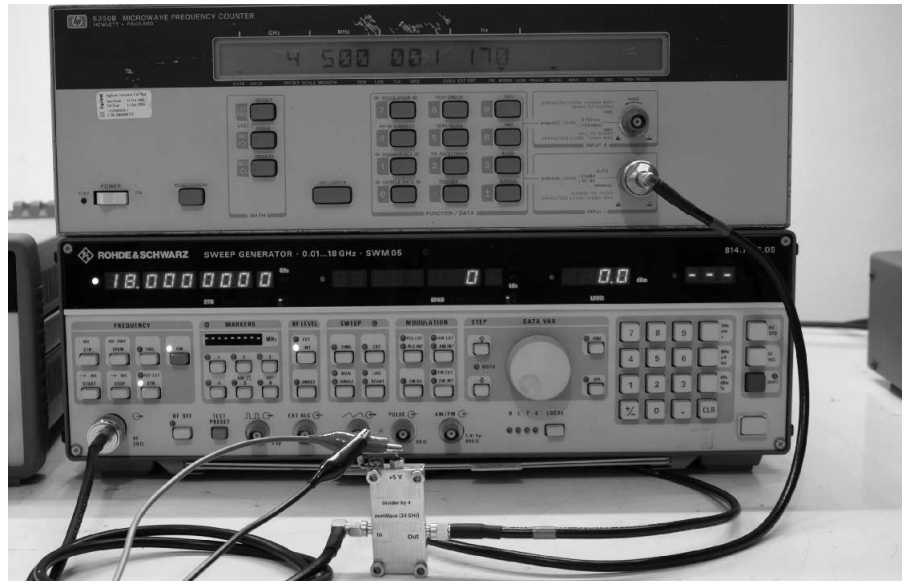

Figure 7 — Testing the prescaler with 18 GHz input and 4.5 GHz output signals.

feed-through by-pass capacitor in the V_{CC} supply to control interference. Figure 6 shows the prescaler assembled in the aluminum housing. Figure 7 shows the prescaler being tested with an 18 GHz input signal (lower sweep generator display) and an output signal of 4.5 GHz (upper frequency counter display).

The Multiplier/Doubler

I based the multiplier/doubler circuit on the HMC942LP4E from Analog Devices[4]. This device uses GaAs pHEMT technology. When driven by a +4 dBm signal, it provides output power of between +13 dBm and +20 dBm from 24 to 32 GHz. Figure 8 shows the output power, with +4 dBm drive level, *vs*. frequency at three temperatures.

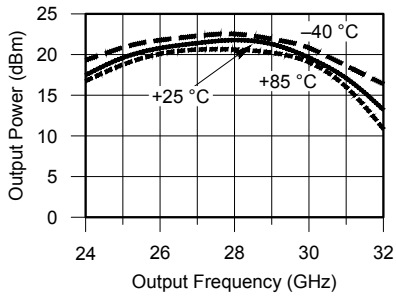

Figure 8 — Output power *vs.* frequency and temperature with +4 dBm drive level to the HMC942LP4E.

The HMC942LP4E is housed in a 4 mm by 4 mm leadless SMT package. Figure 9 shows the schematic circuit to use the HMC942LP4E. Figure 10 shows the PCB layout including the microstrip lines to connect the HMC942LP4E to the connectors.

The multiplier/doubler is very similar to prescaler in the construction details. This PCB also uses the Rogers RT/duroid 5870 with a thickness of 0.020 inches and 1/2 oz copper on both sides. The input connector is a common edge mount SMA and the output connector is the 2.92 mm edge mount connector HK-LR-SR2 from Hirose. The assembled multiplier in its milled aluminum housing can be seen in Figure 11. Figure 12 shows the multiplier with an input signal of 13 GHz (lower display) and an output signal of 26 GHz (upper display).

Next Steps

I now have the capability to generate and measure signals up to 32 GHz, so my next steps are to develop high pass filters to pass only signals above 18 GHz, and finally develop a harmonic mixer capable of operating above 18 GHz to couple to the spectrum analyzer. I've reached 32 GHz, and my next challenges are at 40 GHz, 50 GHz, 60 GHz and beyond.

Euclides Lourenço Chuma, PY2EAJ, earned a degree in mathematics from UNICAMP in 2003, a graduate degree in Network and Telecommunication Systems from INATEL in 2015, and MSc in Electrical

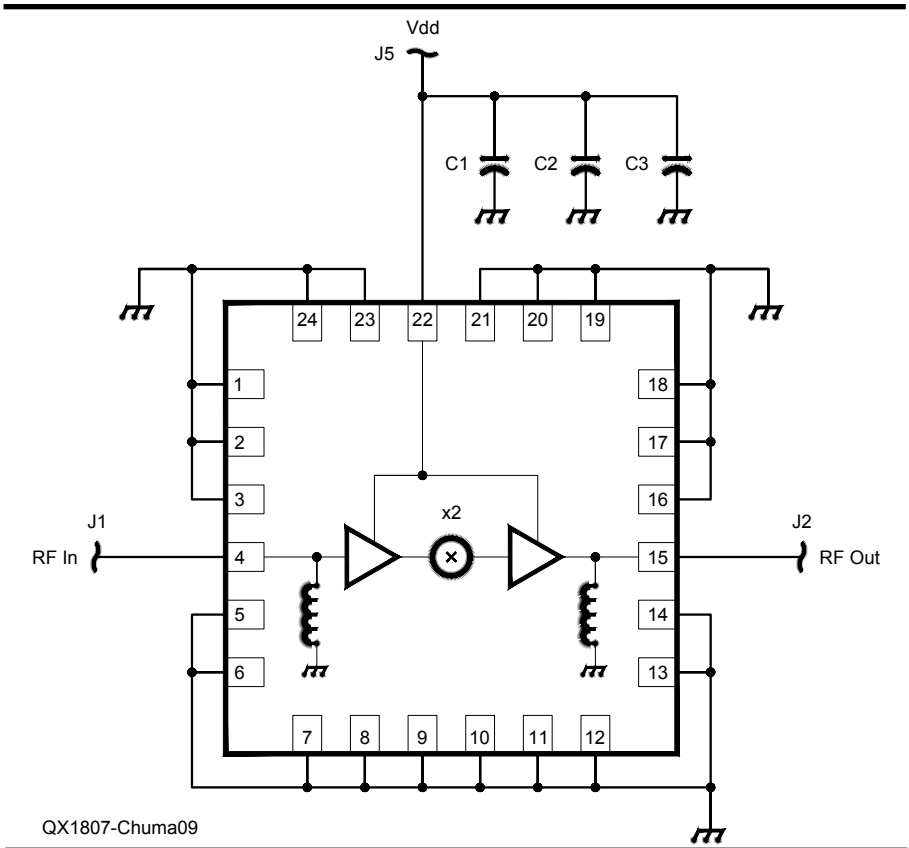

Figure 9 — Schematic circuit of the multiplier using the HMC942LP4E. C1 is 100 pF, C2 is 1000 pF and C3 is 4.7 µF

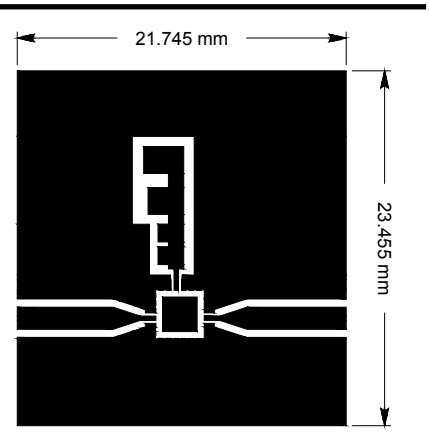

Figure 10 — PCB layout of the multiplier.

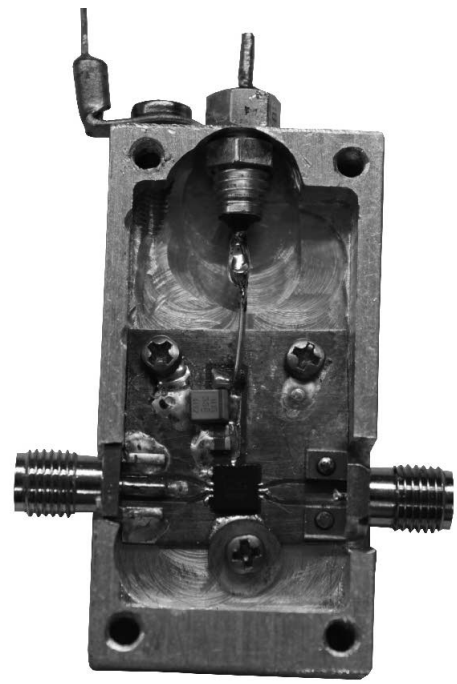

Figure 11 — Assembled multiplier/doubler in a machined aluminum housing.

Engineering from UNICAMP in 2017. He is currently a PhD Candidate in Electrical Engineering at UNICAMP, SP-Brazil. His research interests are antennas, microwave, millimeter-waves, wireless power transfer, software defined radio and cognitive radio.

Notes

[1]Analog Devices HMC447LC3 datasheet, **www.analog.com/media/en/technical-documentation/data-sheets/hmc447.pdf**.
[2]Rogers RT/duroid 5870 datasheet, **https://www.rogerscorp.com/documents/606/acm/RT-duroid-5870-5880-Data-Sheet.pdf**.
[3]Hirose HK-LR-SR2 datasheet, **https://www.hirose.com/product/en/products/2.92mm/HK-LR-SR2**.
[4]Analog Devices HMC942LP4E datasheet, **www.analog.com/media/en/technical-documentation/data-sheets/hmc942.pdf**.

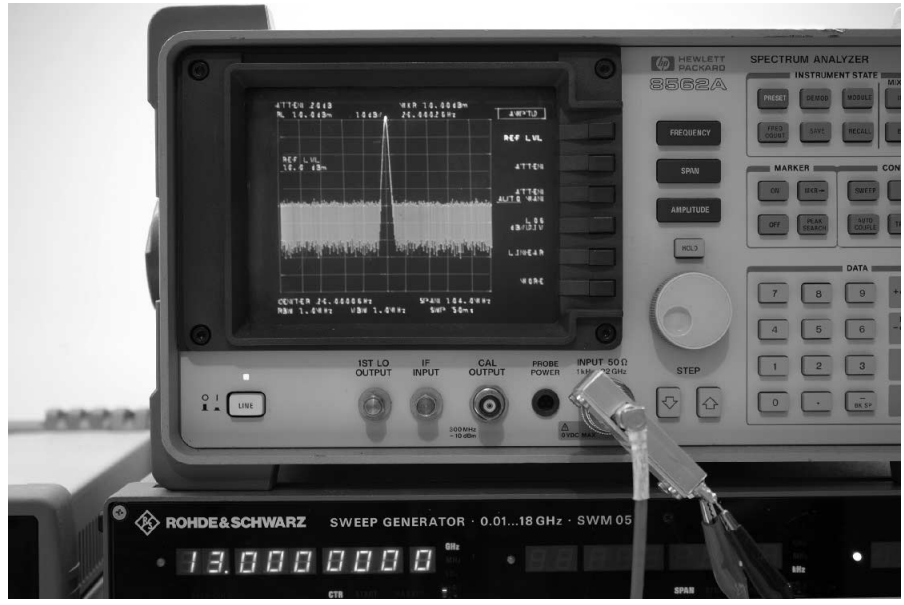

Figure 12 — Testing the multiplier shows13 GHz input and 26 GHz output signals.

Tom Sowden, W6KAN
27253 Mountain Meadow Road, Escondido, CA 92026; **w6kan@arrl.net**

An Arduino-based DDS for the Heathkit SB-104 Transceiver

Stabilize the frequency of your vintage transceiver with this external VFO.

I updated my Heathkit SB-104 into the 21st century by stabilizing the internal VFO drift with this external VFO. This vintage radio is not that far removed from today's sophisticated transceivers. I found the Richard Visokey, AD7C, Arduino DDS project[1] in an internet search. Combining an Arduino Uno board (Figure 1), a DDS-60 synthesizer board (Figure 2), with an LCD looked like a doable project. Sourcing the boards on the internet was easy and inexpensive.

Arduino Uno and Sketches

The UNO is a small computer that can be programmed to do amazing things. A good starting point to get familiar with the platform and the code (called sketches in Arduino vernacular) is the set of tutorials available at **www.arduino.cc**. The ARRL also has a good book[2] that is helpful for beginners. One does not have to be code proficient since there are thousands of Arduino libraries on the internet that cover a vast range of projects. After you get comfortable with it, you can easily change a sketch to fit your projects. Sketches are *open source* so there are no costs or proprietary issues. Most designs I have dealt with are variations of some basic sketch that someone with a higher skill level wrote and published.

The DDS

My goal was to develop a Direct Digital Synthesizer (DDS) software and hardware — a digital VFO — that would hold the SB-104 on frequency without any frequency drift. Like so many older radios, the Heathkit uses a standard VFO frequency in the 5 MHz

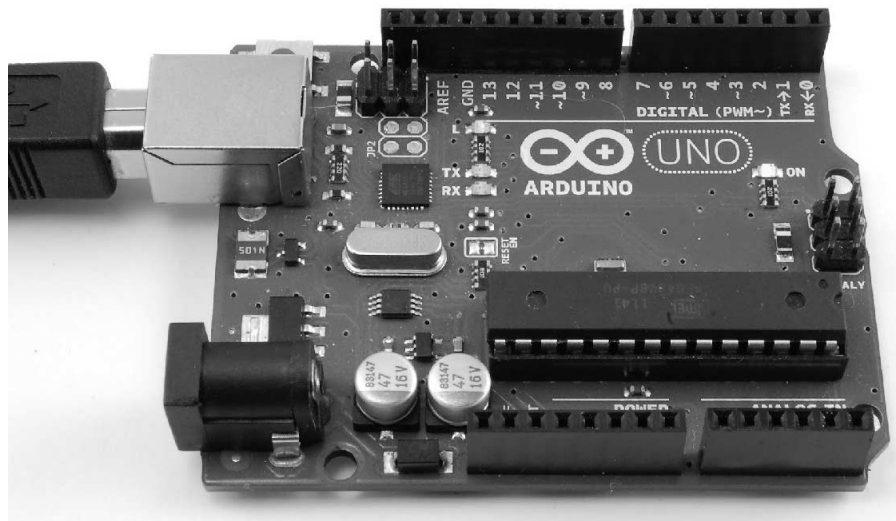

Figure 1 — The Arduino UNO is the processor for this project. [Source: www.ad7c.com/projects/ad9850-dds-vfo/.]

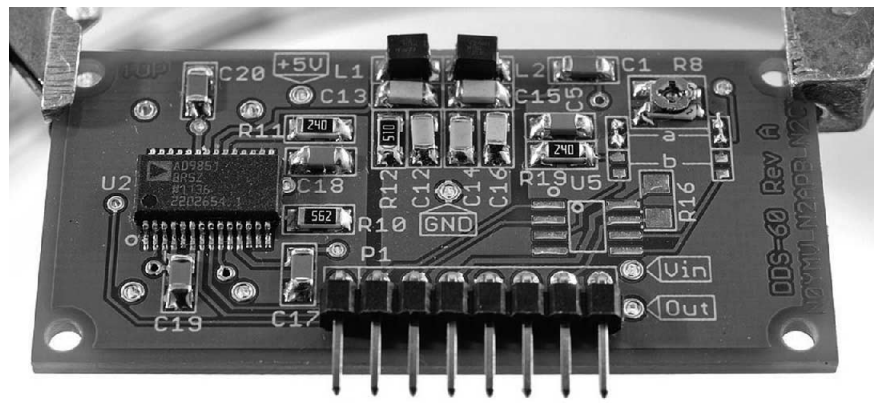

Figure 2 — The DDS-60 direct digital synthesizer board is the heart of the project. [Source: midnightdesignsolutions.com/dds60/.]

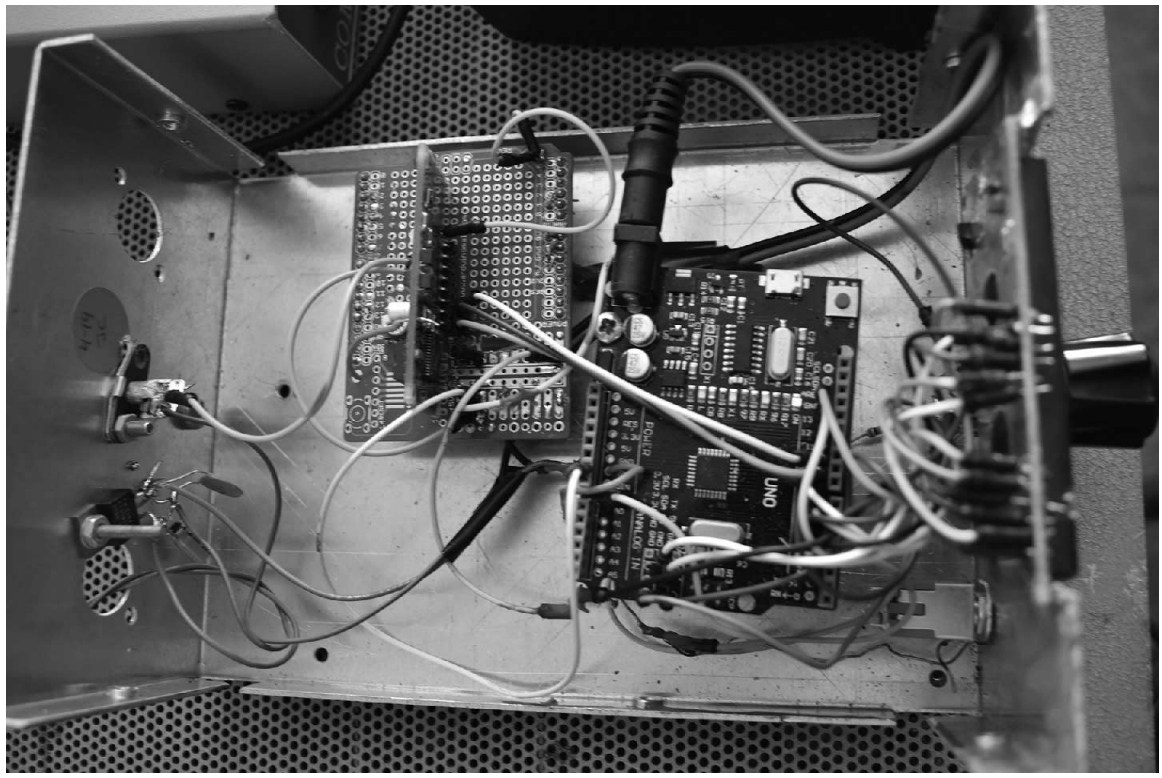

Figure 3 — Internal view of the DDS shows, from right to left, the LCD, the Arduino board, and the DDS 60 board. The voltage regulator chip is mounted on the back panel (left). [Tom Sowden, W6KAN, photo.]

range. The output is mixed with crystal oscillators to generated needed frequencies for each band.

I use my SB-104 exclusively on 40 meters, and I wanted my readout on the LCD to show the 40 meter frequency, not the actual 5 MHz VFO output. This required a few changes to the sketch.

One problem was the very low output level of the AD9850 board recommended by AD7C. The SB-104 needs an injection voltage in the 3 to 5 V peak-to-peak range and the AD9850 board fell far short of that. An internet search revealed a DDS 60 board, complete with a built-in buffer amplifier preceded by a low pass filter. The filter suppresses spurs from the output. My friend Marsh Parker, NC7V, offered to give me one that he had in is junk box. The DDS-60 is available as a kit or wired and tested, and its schematic diagram is available on the Midnight Design Solutions web page **midnightdesignsolutions.com/dds60/**.

Figure 4 — The Arduino-based external VFO is on top of the Heathkit SB-104 transceiver. [Tom Sowden, W6KAN, photo.]

The 9851 chip in the DDS-60 looked to be compatible with the Arduino to output a sine wave at the desired frequency. Its clock speed is 30 MHz, confirmed by an e-mail to George Heron, N2APB, the board designer. My sketch (available on the **www.arrl.org/QEXfiles** web page) uses that clock speed.

Figure 3 shows an internal view of the DDS that includes the DDS 60 board, the Arduino UNO board, and the LCD. The voltage regulator IC is mounted on the back panel. The 11 V dc voltage from the Heathkit was not stable enough, especially during SSB transmission voice peaks. To correct this I installed an LM340T-12 voltage regulator wired it to the primary 13.5 V Heathkit supply. The regulator needs a 20 µF 50 V capacitor across its input, and 0.001 µF across its regulated output. The parts needed for this project are:

- Arduino Uno R3 board, USB cable, and jumper wires kit.[3]
- DDS 60 Midnight Design Solutions.
- LCD Blue Module for Arduino Backlight Screen 5 V Display[4]
- Rotary KY040 encoder.
- LM340T 12 V dc voltage regulator.

- Capacitor, 20 µF, 50 V dc.
- Capacitor, ceramic, 0.001 µF.
- RCA female jack.
- RG-8x hookup coax with RCA male plugs.
- Potentiometer, 25 kΩ, miniature for LCD.
- Push button switch.

Wiring schematic[5] for the DDS VFO shows the AD9850 connections, which should be modified as follows to accommodate the DDS-60 board. Change the label "DDS AD9850" to DDS-60; then delete the connection from "RST" on the DDS-60 to "D11" on the Nano board.

Both the Arduino and DDS-60 boards have built-in voltage regulators to provide the 5 Vdc needed for some of the components. On most Uno boards there are a number of regulated 5 Vdc output pins. Four of these are connected to: the 25 kΩ contrast potentiometer, pin 2 of the LCD, pin 15 of the LCD, and the VCC input pin on the DDS 60.

I used the jumper wires provided with my Uno kit for all of the connections. These are supplied in various lengths, and pins on each end fit nicely in the different boards. Once I double checked each connection I soldered the wires in place to keep them from coming out.

Displaying Frequency

The challenge now was to adjust the LCD readout to show the 40 meter frequency and not the 5 MHz VFO frequency. The crystal used in the SB-104 for 40 meters is 12,500 kHz. Getting the readout on the Arduino was not necessary since the Heathkit SB-104 has a built-in counter that shows the mixed frequency. However that display has a resolution of just 100 Hz. I found a way to change the sketch to show the frequency as I want it. The complete sketch is on the **/QEXfiles** web page.

First, download the Arduino IDE editor/compiler at from the Arduino web page **https://www.arduino.cc/en/Main/Software**. Also download Richard Visokey's code from the AD7C web page. Once the files are in your directory you can load them into the Arduino IDE. Paste the full code from my sketch over Visokey's sketch, compile it and load it into your Arduino. Of course you can make any changes you want for your project.

Make the following changes for this project. Revise the frequency calculation to 30 MHz from 120 MHz. Find the following line in the sketch:

```
// frequency calc from datasheet page 8 = <sys clock> * <frequency tuning word>/2^32
void sendFrequency(double frequency) {
 int32_t freq = frequency * 4294967295 / 30000000;
// note the 30 MHz or clock rate of the DDS 60 – the original 9850 board ran at 120MHz.
```

I wanted a slight delay in the print out that would momentarily show (for about a half second) the VFO frequency. The 40 meter IF crystal in the SB-104 was cut for 12,500 kHz, it has likely changed over the years. It also drifts a bit until the radio warms up. By experimenting with this number I finally got the readout to be "on the money with WWV" using 12,506,290 Hz. Your frequency will differ! Note the "rx" in the sketch is the actual DDS output (5 MHz+). The code calculates the difference and prints out the 40 meter frequency to within one hertz. Underneath this figure the LCD shows the "step" frequency — noted as 10 Hz, 50 Hz, 100 Hz — all the way up to one megahertz. Push in the encoder button to change the value to your preference. The sketch changes are:

```
delay (500); // half second pause to see the VFO frequency.
lcd.clear(); // clears the LCD display of previous inputs
lcd.setCursor (7,0); // sets the cursor on line one in the center
lcd.print (12506290 - rx); // my solution to see the 40 m frequency
lcd.setCursor (7,1);// puts the step frequency in the middle on line 2
lcd.print(hertz);
```

Since I use the radio only on 40 meters I did not worry about how to correct for the other bands. You can revise the sketch with your solution. Experiment with different changes and see what happens after you compile each iteration. Make sure that you save a copy of a known good sketch so you have a way to recover from mistakes. There is no downside to experimenting. Lots of help is out there so you are never alone.

Figure 4 shows my external DDS VFO on top of my SB-104 transceiver. The Heathkit in the lower part of the picture can display only in 100 Hz increments, while the Arduino solution, shown here at a 100 Hz step, can be set to display to one hertz.

Try something with the Arduino — you will surprise yourself with what you can accomplish.

Tom Sowden, W6KAN, was raised in a small Kansas town where he received his General class license at age 15. He has always enjoyed building equipment. During his teenage years Tom built Heathkit equipment to be able to get first-class gear at an affordable price. He graduated from Northwestern University in Evanston, Illinois with a degree in investment management and worked as a trainee for Standard & Poor's Corporation. He then joined the Navy and served on a minesweeper off the coast of Vietnam. He has had several careers including 20 years in the flour milling business and 20 years in the bag business. Ten years ago he and his wife of over 31 years moved to California, and his call sign changed to W6KAN, like the old postal code "KAN" for Kansas. Tom continues to enjoy the hobby that opened up the world to him as a small-town Kansas kid. Tom has three children and five grandchildren.

Notes

[1]Richard Visokey, AD7C, **www.ad7c.com/projects/ad9850-dds-vfo/**.

[2]Glen Popiel, KW5GP, *Arduino for Ham Radio*. Available from your ARRL dealer or the ARRL Bookstore, ARRL item no. 0161. Telephone 860-594-0355, or toll-free in the US 888-277-5289; **www.arrl.org/shop/**; **pubsales@arrl.org**.

[3]Smarza starter kit, **https://www.ebay.com/itm/Smraza-Starter-Kit-for-Arduino-with-Uno-R3-Breadboard-Jumper-Wires-USB-Cable-Le/222447846556?hash=item33caecc49c:g:-1sAAOSwhQhY0f6~**.

[4]**https://www.ebay.com/itm/Blue-Module-With-For-Arduino-2016-Backlight-Screen-5V-Display-LCD-1602-1602A/331886474138?epid=566317856&hash=item4d45f9b39a:g:EtwAAOSwc1FXZ6fA)**.

[5]Schematic, **www.ad7c.com/downloads/AD980_DDS_VFO_Schematic.gif**.

Showroom Staffing Hours:
9 am to 5 pm ET, Monday-Saturday

Ordering (via phone):
8:30 am to midnight ET, Monday-Friday
8:30 am to 5 pm ET, Weekends

Phone or e-mail Tech Support: 330-572-3200
8:30 am to 7 pm ET, Monday-Friday
9:00 am to 5 pm ET, Saturday
All Times Eastern I Country Code: +1
DXEngineering@DXEngineering.com

800-777-0703 | DXEngineering.com

Get the Gear to Boost Station Performance for Less!

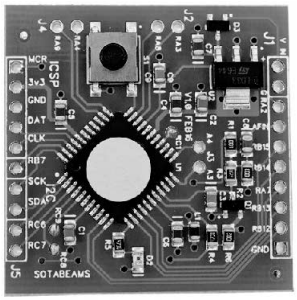

SOTAbeams

DX Engineering offers a great selection of trusted performance-enhancing gear from SOTAbeams, including its self-contained WSPRlite Propagation and Antenna Tester. This specialized WSPR test beacon transmits to a worldwide network of receiving stations and works with proprietary software to display a transmit signal's geographical range as well as received power on an easy-to-read propagation map. Also available is the WSPR Add-on Kit for 160, 80 and 40M; LASERBEAM DSP Filter Modules; and the new 3-Band Low Pass Filter PCB Kit, a convenient way to enjoy three selectable low pass filters on a single PCB. Enter "Sotabeams" at DXEngineering.com to see the full lineup of testers, filters and accessories.

REU-AA-30ZERO

New!

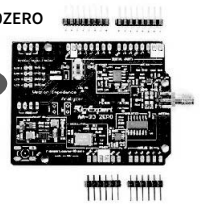

REU-AA-55ZOOM

RigExpert®

Antenna Analyzers and Project Board

Professional broadcasters, telecommunications engineers and serious Amateur Operators all over the planet trust antenna analyzers from RigExpert. They combine functionality, accuracy, durability, and ease-of-use. Maximize your frequency range coverage with the best RigExpert has to offer: the REU-AA-600 (0.1 - 600 MHz), REU-AA-1000 (0.1 - 1,000 MHz), and REU-AA-1,400 (0.1 - 1,400 MHz). For experimenters, RigExpert's 0.06 - 30 MHz Antenna Analyzer Project Board (REU-AA-30ZERO) can be incorporated into a range of products, from making your own automatic antenna tuner to pairing it with the ESP8266 Wi-Fi SoM to remotely perform RF-circuit or antenna analysis. Enter "REU Board Only" at DXEngineering for more details.

Advanced Design Thrust Bearings and Tower Accessory Shelves

The Advanced Design 2 Inch (DXE-TB-300) and 3 Inch (DXE-TB-400) Thrust Bearings from DX Engineering feature ball bearings that ride on an all-metal surface to promote a longer service life. They can also handle much greater static loads, which reduces stress on the rotator, and makes rotator service possible without removing your antenna—saving you tons of hassle, time and money! The unique multi-piece design of DX Engineering's new Tower Accessory Shelves make them easier to install in the midpoint of a tower. They feature a thicker, stainless steel plate for greater stability when mounting a rotator and/or thrust bearing on Rohn and Amerite 25 (DXE-AS25G) and 45/55 (DXE-AS455G) towers.

DXE-TB-300 $169.99 **DXE-TB-400 $239.99**
DXE-AS25G $79.99 **DXE-AS455G $124.99**

Coaxial Cable Assemblies

These low-loss cable assemblies are available in standard lengths with DX Engineering's revolutionary patented PL-259 connector, featuring the best qualities of both crimp-on and solder-on connectors. Use the online Custom Cable Builder at DXEngineering.com to build assemblies made to your exact specs. DX Engineering's coaxial cable is also available by the foot or in bulk spools.

YAESU ICOM KENWOOD ALINCO

Free Standard Shipping for Orders Over $99* If your order, before tax, is over 99 bucks, then you won't spend a dime on shipping. (Additional special handling fees may be incurred for Hazardous Materials, Truck Freight, International Orders, Next Day Air, Oversize Shipments, etc.).

FAST FREE SHIPPING over $99*

Email Support 24/7/365 at DXEngineering@DXEngineering.com ***Stay connected:*** YouTube

Rudy Severns, N6LF

PO Box 589, Cottage Grove, OR 97424; **n6lf@arrl.net**

Conductivity of Trees at HF

N6LF publishes his measurements of tree dielectric parameters.

The effect of trees on HF antennas has been a very long running discussion in the amateur community with little resolution or hard data. During the 1960s and 1970s much work was done for the military on propagation through jungle forests, but much of this work was for frequencies above 50 MHz, so it didn't really answer the questions. In the February 2018 edition[1] of *QST* Kai Siwiak, KE4PT, and Richard Quick, W4RQ, took a serious look at this using NEC modeling [as well as infinite cylinder analytical modeling — *Ed.*] to quantify the impact of trees on vertical radiators, which it turns out can be significant. The article is a real step forward.

Electrical Parameters of Trees

A critical part of the analysis is a determination of the electrical characteristics of trees, that is, their conductivity (S/m) and relative permittivity ε_r. After reading their article I realized that I had already performed measurements on both coniferous (Douglas fir) and deciduous (big leaf western maple) trees, which might help. In 2007 I had a 3-element vertical array[2] on 160 m located in a dense fir forest where the trees were conveniently approximately $\lambda/4$ high and close to the antenna, within 50 ft, well within the near-field. While the array seemed to work okay I wondered just how much I was losing to the forest so I made some measurements on actual trees.

I assumed that the primary loss would be from the longitudinal E-field, that is, the vertical polarization, and that a tree could be viewed as a cylindrical vertical impedance which could be measured experimentally. For the experiments I drove a series of nails approximately 2 inches long, connected with a wire to form two rings about one foot apart as shown in Figure 1. The impedance between the two rings was measured using a vector network analyzer (an N2PK VNA). Measurements were made on Douglas fir — diameter at the inner bark of 10 inches — and big leaf maple — 8 inch diameter — trees in late March when the sap was up.

One problem when using a VNA is the need to properly calibrate out the effect of the cable and leads to the two rings, to isolate the impedance of the tree between the two rings. For the open-circuit, short-circuit, load calibration procedure I used a plastic trash can as shown in Figure 2.

The trash can diameter was about the same as the trees being measured. The interconnected nails in each ring were inserted into holes. The open-circuit calibration is shown in Figure 2, for the short-circuit calibration I used 6 parallel wires distributed symmetrically around the trash can each end

Figure 1 — Impedance measurement on a Douglas fir tree.

Figure 2 — Calibration test fixture shows the AIM4170 as the VNA, but the same fixture was used to calibrate the N2PK vector network analyzer that was used for the actual measurements.

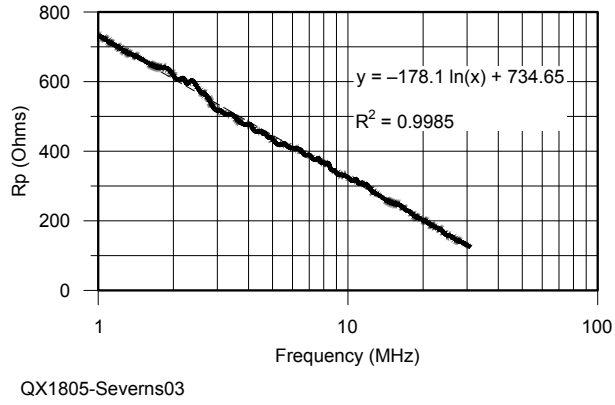

Figure 3 — Fir tree equivalent parallel resistance, *Rp*, second run, 25 Mar. 2007.

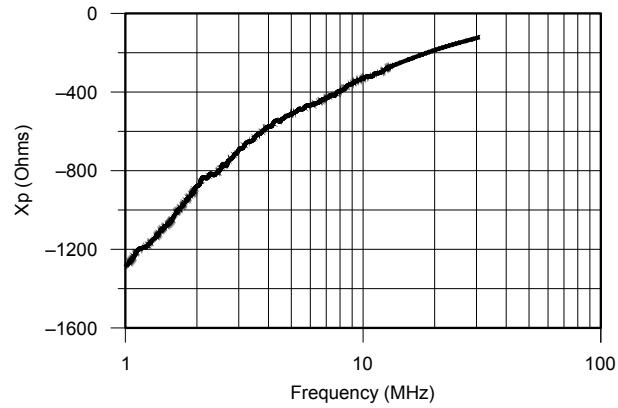

Figure 4 — Equivalent parallel impedance, *Xp*, second run, 25 Mar. 2007.

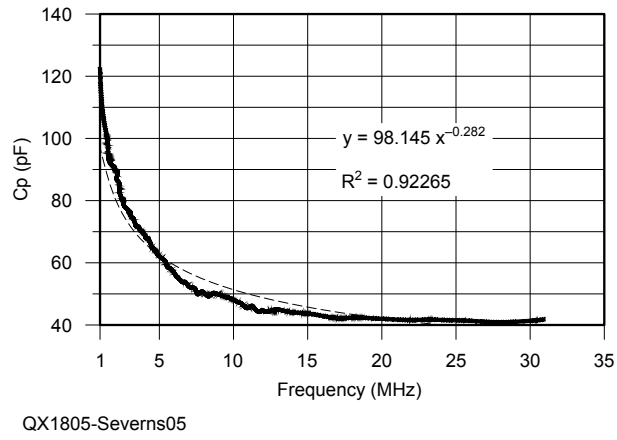

Figure 5 — Equivalent parallel capacitance, *Cp*, second run, 25 Mar. 2007.

connected to the ring. For the load calibration I inserted resistors in series with these wires with a total parallel resistance of 50 ohms.

Test Results

In the first test I connected a dc ohmmeter between the rings. What I noticed immediately was the resistance changing slowly over time much like what you see when checking an electrolytic capacitor for leakage current. The sap of the tree is an electrolyte so that behavior was not a surprise. For the impedance measurements I assumed a parallel *Rp Cp* equivalent circuit. Samples of typical measurements are given in Figures 3, 4, and 5. The general behavior was much the same for both the fir and the maple trees.

The conductivity and permittivity, as a function of frequency, appear to behave very much like soil[3]; conductivity (σ) goes up with increasing frequency — *Rp* goes down — and ε_r goes down with increasing frequency to a point where it flattens out (*Cp* is a function of ε_r).

I made an estimate of σ from the equation for a resistor:

$$\sigma = \frac{L}{(Rp)(A)}$$

where *L* is the 12 inch (0.3048 m) distance between rings; *A* is the effective cross sectional area in square meters.

Determining the cross sectional area, *A*, is a bit tricky. If you assume the conduction is limited to the cambium, a thickness of about 0.125 inches (0.003175 m), and the diameter is 10 inches (0.254 m), then $A = 0.00253$ m^2. From Figure 3, *Rp* is about 325 Ω at 10 MHz. This gives $\sigma = 0.37$ S/m, which seemed pretty high! However, that number is based on a 1/8" conduction layer. Kai, KE4PT, sent me an extract from a book on wood characterization by Bucur[4], which indicates that the characteristics across the entire diameter do not vary greatly, at least for the case of young trees with little or no heartwood. If the wood across the diameter also conducts, then the calculated conductivity is lower. For example, for a diameter *d* of 10 inches (0.254 m), $A = 0.016$ m^2, $\sigma = 0.059$ S/m. This gives a range of conductivity at 10 MHz of about 0.06 to 0.4 S/m. The actual average conductivity is likely somewhere in between.

At this point in my 2007 experiments I found it hard to believe such high values for tree conductivity. Because I did not have any backup from other sources for my measurements I have been reluctant to publish this work. However, in the February 2018 *QST* article the authors assume[5] $\sigma = 0.17$ S/m, which lies within the range of my measurements. Their value was derived from extensive earlier work in the professional literature so I now have some faith in my measurements. The only additional comment I would add is that the values of conductivity used in the NEC model should include the variation with frequency (dispersion) so clearly shown in my measurements.

I think at this point we can use NEC modeling with some confidence to estimate the effect of trees on HF antennas. Unfortunately that effect appears to be substantial and not a good thing!

Rudy Severns, N6LF, was first licensed as WN7AWG in 1954. He is a retired electrical engineer, an IEEE Fellow and ARRL Life Member.

Notes

[1] K. Siwiak, KE4PT, and R. Quick, W4RQ, "Live Trees Affect Antenna Performance", *QST* Feb. 2018, pp. 33-37.
[2] Rudy Severns, N6LF, "A 3-Element 160 Meter Vertical Array", NCJ May/June 2009, pp. 12-13.
[3] Rudy Severns, N6LF, "Measurement of Soil Electrical Characteristics at HF", *QEX* Nov/Dec 2006, pp. 3-9.
[4] Voichita Bucur, **Nondestructive Characterization and Imaging of Wood**, Springer Series in Wood Science, Chapter 7.
[5] Tree data; D. Tomasanis, "Effective Dielectric Constants of Foliage Media," RADC-TR-90-157, Interim Report AD-A226 269, Jul. 1990.

Andrzej (Andy) Przedpelski, KØABP

7260 Terrace Pl., Boulder, CO 80303-4638: **kc0cwk@comcast.net**

Satellite Distance and Velocity

Determine a satellite's distance and velocity using missile miss distance indicator scoring techniques.

Ever since I retired I wondered if it would be possible to determine a satellite's distance and velocity using missile scoring miss distance indicator (MDI) techniques. Radio Amateurs can make the necessary measurements and calculations using the following techniques to provide answers to that question.

The physics and mathematics in both techniques are the same. The main differences are in the magnitudes of distances and velocities involved. The other difference is that the military systems used recording equipment, which provides a continuous curve of Doppler frequency shift versus time. We could have only discrete points, due to equipment limitations. However, this may actually be an advantage.

The technique would involve taking data points as the satellite traverses overhead. The data would involve noting the received frequency versus time. The ideal satellite path would be a direct overhead pass. This would allow the maximum number of data points and maximum observation time.

Theory

The Miss-Distance Indicator (MDI) system relies on the Doppler effect[1, 2] to obtain the desired information and was originally developed by the Naval Ordnance Laboratory.

We are all familiar with the Doppler effect, manifested as the change in the train whistle pitch as it passes us. This phenomenon was used extensively in missile scoring. It was important to know the accuracy of different tested missiles, since they did miss now and then. The system was fairly simple. A fixed stable signal source — usually in the VHF region — was placed in one vehicle, it was received with its associated Doppler shift by the other vehicle. The Doppler shift was then transmitted by telemetry to a ground station. The Doppler shift curve contains the required information:

- The difference in frequency between the two asymptotes — the maximum and the minimum frequency — is a function of the relative velocity between the two vehicles.
- The time at the middle of the curve — the nominal transmitter frequency — is the time of intercept.
- The steepness of the curve at the intercept time is a function of the miss-distance and the velocity.

The above characteristics are demonstrated in Figure 1. Curves (A), (B) and (C) show Doppler shift for the same closing velocity, but increasing miss-distances. Curve (D) is for an intercept at twice the closing velocity.

The Doppler curve was then analyzed on the ground. The data was extracted using graphical methods. A set of curves, calculated using different scenarios, was available and was compared with the received data. While the above is a somewhat simplified system description, it illustrates the basic principles. A better method is to analyze the data and use mathematics to obtain the velocity and distance information. An actual intercept curve obtained at White Sands Missile Range (WSMR) is shown in Figure 2. The velocity can be easily calculated using the maximum frequency shift at the asymptotes by taking the difference between the maximum and minimum received frequency using Eq. (2). Start[3] with:

$$f = \frac{v \cos \theta}{\lambda} \qquad (1)$$

where f is frequency shift, Hz; v speed, m/s; and λ is wavelength, m.

The use of the equation has the advantage that the whole curve can be reconstructed and plotted using only a limited number of points. Also, the maximum slope of the curve can

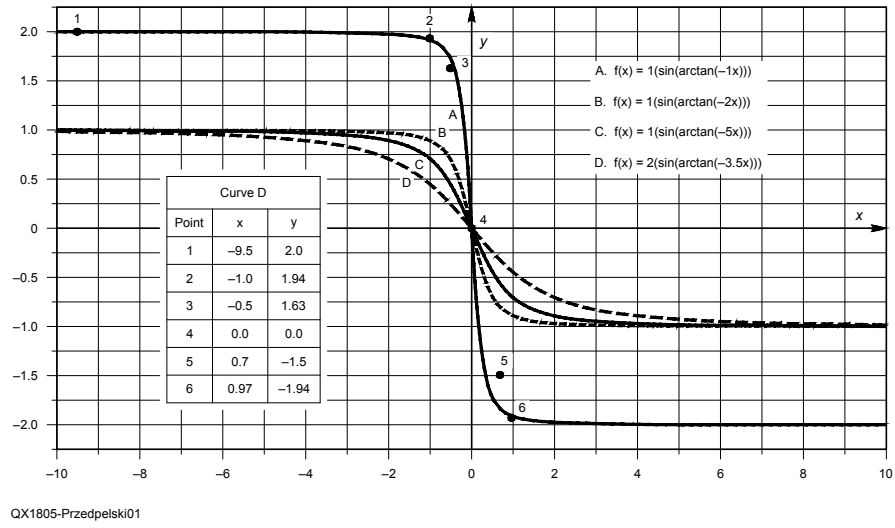

Figure 1 — Intercepts at different velocities and miss distances.

be easily calculated using *Graph* (or similar software) tangent function.

Since $\theta = 0$ degrees, solving for velocity we get:

$$v = f\lambda \,. \qquad (2)$$

In this case the RF frequency was 230 MHz and thus λ = 300/230 = 1.3. Since the two asymptotes were 30.410 kHz and 29.851 kHz — the frequencies determined by the recording equipment used — the maximum Doppler shift was (30.410 - 29.851)/2 or 279.5 Hz. The relative velocity, using Eq. (2), is (279.5) (1.3) = 363.35 m/s or 1192.1 ft/s, not far from the WSMR figure of 1197 ft/s.

To obtain the "miss distance" — the satellite distance at the closest approach in our case — is a little more difficult and less accurate. It is necessary to calculate the closing velocity first, as shown above. Thanks to Descartes it can be shown that the curve of received frequency vs. time is of the shape shown in Eq. (3).

$$f(x) = a\left\{\sin\left[\arctan\left(-bx\right)\right]\right\} \qquad (3)$$

where a is the maximum Doppler shift, b is a function of velocity and miss distance. Two more factors are added, c and d, to shift the curve to match the data points.

$$f(x) = c \pm a\left\{\sin\left[\arctan\left(\left(-b\right)\left(x \pm d\right)\right)\right]\right\} \qquad (4)$$

where c is y-axis offset and d is x-axis offset.

In our case a continuous data curve cannot be obtained due to equipment limitations. Only discrete data points can be recorded. However, Eq. (3) can be used to eliminate erroneous data points. By using different values for factors a and b in a program such as *Graph* a best fitting curve can be drawn.

The procedure is fairly simple. Factor a in Eq. (4) is the maximum Doppler shift. Using Eq. (5) and a graphing program, factor b is selected by trial-and-error to match the slope of the data points. Finally, factors c and d are determined. Then, any points not fitting the curve can be eliminated. This is shown as point (5) in curve (*D*) of Figure 1.

To obtain the distance to the satellite, the velocity has to be calculated first as shown above. Differentiating Eq. (3) — the best curve fitting the obtained discrete points — will give us the slope of the Doppler curve. The maximum value of the slope can be obtained, this time thanks to Newton, by getting the tangent at the point of intercept. This can be done graphically. An easier method is to use *Graph*, which calculates and plots this slope as shown in Figure 3. The distance can then be evaluated[4] using:

$$\left[\frac{df}{dt}\right]_{\max} = \frac{V^2 F}{cD} \qquad (5)$$

or

$$D = \frac{V^2\lambda}{\left[df/dt\right]_{\max}} \,. \qquad (6)$$

An example is shown in Figure 3 using the data from the WSMR intercept of Figure 1.

$$D = \frac{363.35^2 0.75}{614.6} = 165 \text{ m, or } 363 \text{ ft.}$$

This compares to the WSMR figure of 393 ft, which would indicate a difference of less than 10%. The distance calculation is more complicated and more prone to errors.

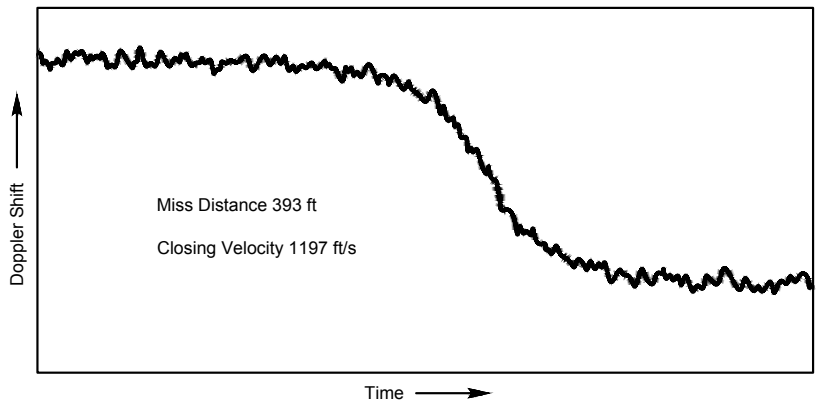

Figure 2 — Measured data for intercept number 1.

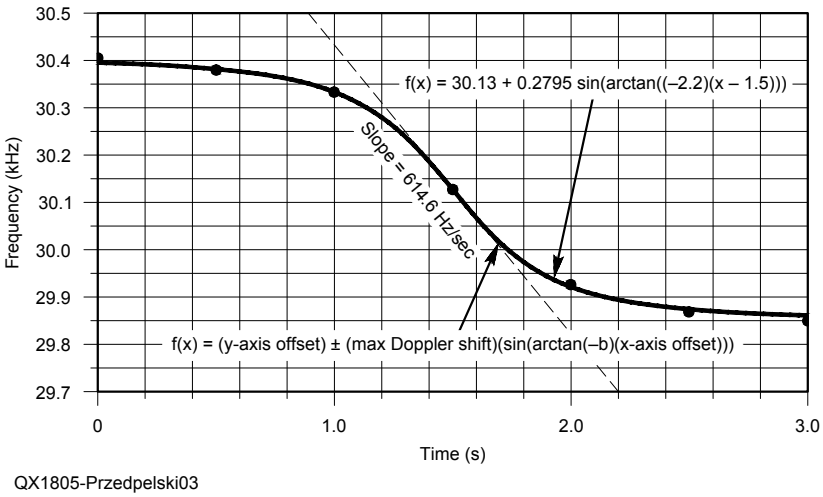

Figure 3 — Reconstruction of Figure 2 using equation (3) showing the maximum slope.

Data

Good satellite Doppler effect data was provided by the Zarya website[5]. It was taken on 8 December 2000 using the GFO satellite. The total transit time was 7 minutes. The data points are shown in Table 1.

Results

The data points of frequency vs. time were then plotted using *Graph* software and then a best fitting curve was drawn as shown in Figure 4. From this figure it is apparent that the transit time was not enough to obtain the asymptotes. This can be corrected, again using *Graph*, by extending the curve until the asymptotes are reached, as shown in Figure 5. Maximum Doppler shift is then easily obtained:

$$\text{DopplerShift} = \frac{(400.04198 - 400.02385)}{2} \text{ MHz}$$
$$= 9.065 \text{ kHz.}$$

From it, the satellite relative velocity can be calculated:

$$v = (9065)(300/400) = 6,799 \text{ m/s.}$$

Table 1.
Satellite Doppler effect data.

Time (min)	*Frequency (MHz)*
0	400.0410
0.5	400.0410
1.0	400.0401
1.5	400.0396
2.0	400.0385
2.5	400.0370
3.0	400.0349
3.5	400.0323
4.0	400.0300
4.5	400.0280
5.0	400.0265
5.5	400.0255
6.0	400.0255
6.5	400.0246
7.0	400.0244

Using the available satellite orbit data we can calculate the velocity:

$$\frac{(6822)(2\pi)}{(95.5)(60)} = 7.480 \text{ km/s}$$

which is within 10% of the Doppler obtained figure of 6.799 km/s. The difference is due to the cosθ factor in Eq. (1). This factor is unity only for a flight directly overhead. Any inclination would decrease the calculated velocity.

There are two ways to get the needed $[df/dt]_{max}$ for the distance calculation. Draw a line at the point of maximum slope, or let *Graph* calculate it using the tangent function. This is shown in Figure 5. Using Figure 5 and Eq.(6) we get:

$$D = \frac{6.799^2}{(0.75)(93.333)} = 660 \text{ m}$$

which is close to the actual value of 500 – 600 m. The larger calculated value may be partially due to the satellite trajectory not being directly overhead.

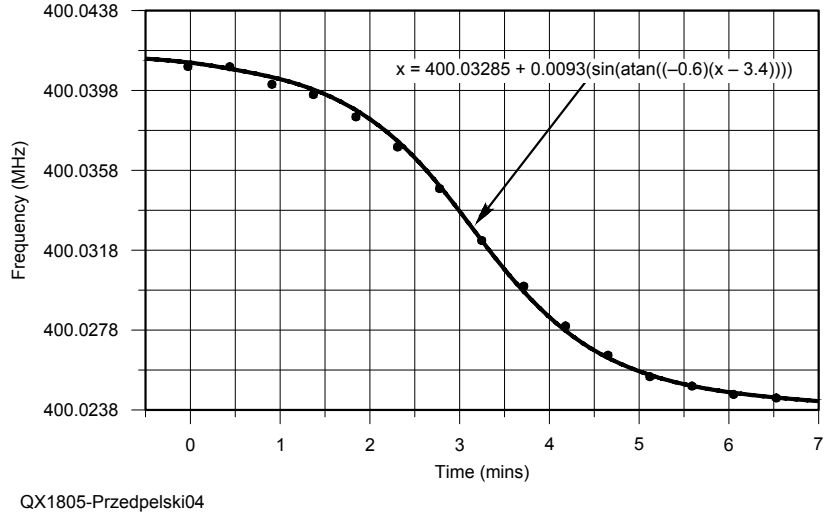

Figure 4 — Zarya data from GFO satellite transit.

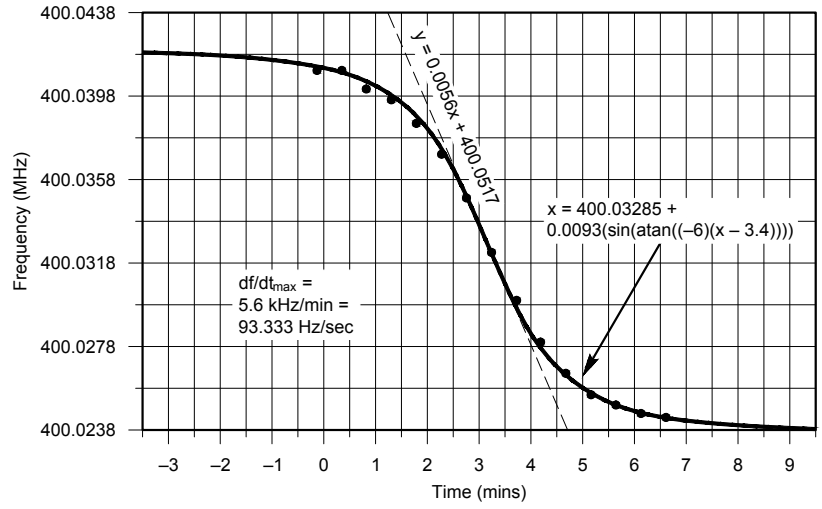

Figure 5 — Extended calculations of Figure 4 to show asymptotes.

Comments

It appears that the MDI techniques can be applied to satellite velocity and distance calculations. However there are certain limitations. For instance, the period of data taking should be as long as possible. While graphing software can artificially extend the curve, as shown in Figure 5, some accuracy may be lost.

To obtain accurate velocity figures, the satellite pass should be directly overhead. Since the distance calculation involves the calculated velocity, any error in velocity is reflected as the square in distance error.

Good graphing software is a big help in performing all the necessary calculations. While the needed graphs can be drawn manually, some accuracy may be lost.

Andrzej "Andy" Przedpelski, KØABP, received his BS degree from the Massachusetts Institute of Technology, and did graduate work at Northwestern University, and DePaul University. He has worked on the development of transmitters, receivers, printed circuit techniques, transistorized frequency meters and direction finders, crystal oscillators, and missile-borne components. Andy received several US patents. During the past few years he has been a Consulting Editor for R.F. Design magazine and was also on its Editorial Review Board. Andy was always interested in radio and built crystal sets while in grammar school. He earned his Technician class amateur license in 1998 and Amateur Extra in 2007. Andy is an active member in ARES and Boulder Amateur Radio Club.

Notes

[1]A. B. Przedpelski, "Doppler Techniques for Miss-Distance Indicating Systems", *Interavia* 1963, No. 3.

[2]J. J. Pakan and A. B. Przedpelski, "Characteristics of a Doppler-type Miss-Distance Indicator for Missile Scoring", *I. R. E. Professional Group on Military Electronics Session*, Jan. 13, 1951.

[3]*Reference Data for Engineers*, *8-th Ed.*, Howard W. Sam & Co., p. 36-13.

[4]B. P. Ficklin, A. H. Maciszewski, J. J. Pakan and K. Ringer, "Equipment Design Trends in Doppler-type Missile Scoring Systems", *I. R. E. Proceedings of the 4-th National Convention on Military Electronics*, Washington, DC, June 27-29, 1960, pp. 605-616.

[5]Zarya website: **www.zarya.info/Tracking/Dopler.php**.

John Stanley, K4ERO
524 White Pine Lane, Rising Fawn, GA 30738; **jnrstanley@alum.mit.edu**

Some Additional Geometries for Loop Antennas

Stacks of rectangular, hour-glass, and diamond shaped loops having one-wavelength perimeter elements are compared.

Ever since the quad antenna was developed in the middle of the 20th century, many different shapes for the loops have been tried with good results. The *ARRL Handbook* and *Antenna Book* include some of this information. Of special interest to me was the 2:1 height-to-width ratio "rectangular" loop that matches directly to 50 Ω, unlike the square loop[1] which has an input resistance of about 120 Ω. I took a look at what happens when various shapes of loops are used.

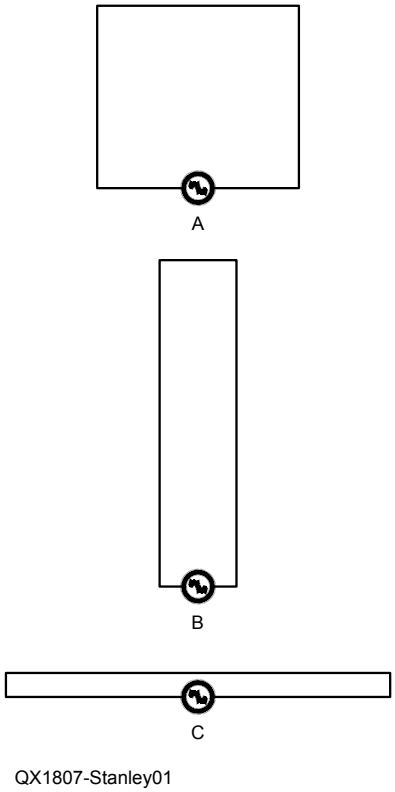

Figure 1 — Antenna A is the familiar square loop, B is a rectangular loop, C is a folded dipole. All use one wavelength of wire.

The Rectangular Loop

My approach was to determine the gain and input impedance of rectangular loop antennas as a function of the height-to-width ratio (Figure 1). An NEC[2] study was initially done with 4 mm diameter copper wires. At 144.2 MHz, this required 2.2 m total wire length to achieve resonance. I opted to run NEC using a total wire length of exactly 2 m, which gave a resonant frequency near 157 MHz. I did this to make the lengths of the sides in meters correspond to the percentage of the wire in each side. Thus, with a side length of 0.5 m, the sides represented 50% of the total wire and, of course, the height would be the remaining 50%. Also, 0.5 m, gives us a square loop. As the height-to-width (H/W) ratio changed, the gain varied as shown in Figure 2. For very small H/W ratios, we have essentially a folded dipole and, as expected, the gain is about 2.15 dBi. As the height is increased with a corresponding decrease in width to keep the total loop length at 2 m, the gain increases as the two current nodes move further apart, concentrating gain towards the horizon. The gain peaks at the point where 80% of the wire is in the vertical wires (H) and 20% in the horizontal wires (W) for a H/W ratio of 4. The calculated gain was about 4.5 dBi. Above that H/W ratio the gain drops off as losses in the wires begin to

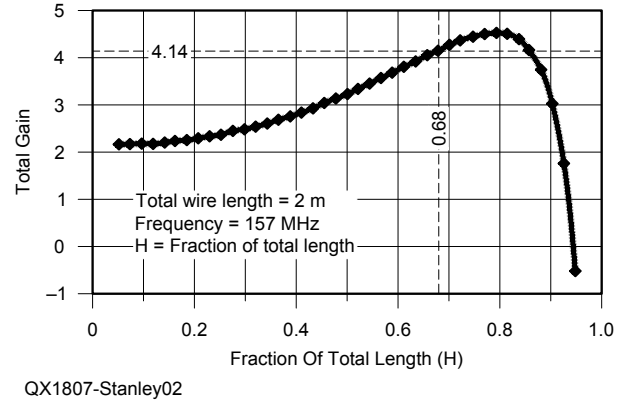

Figure 2 — Gain, dBi, of a full wave loop vs. H (height) as a fraction of one wavelength.

predominate over the radiation resistance.

The feed point resistance R_{in} is about 282 Ω for the folded dipole (H/W nearly 0) and decreases as the H/W increases (taller thinner loop). We would expect the R_{in} to be about 120 Ω for the square loop (H/W = 0.5) as is well known for a "quad" loop. The R_{in} is 50 Ω for H/W = 2 (H = 0.67) as is known from the *ARRL Antenna Book*. These values can be confirmed and the R_{in} for other H/W values can be read from the top curve in Figure 3. The bottom curve shows reactance that can be expected at the feed point as the resonant frequency of the loop changes somewhat with H/W ratio. In developing this graph, the frequency (157 MHz) was chosen to be resonant at H/W = 0.5, that is, for a standard square quad loop. Note that for H/W ratios above and below 0.5 the resonance shifts a bit leading to some inductive reactance that can be tuned out by a slight shortening of the total loop length.

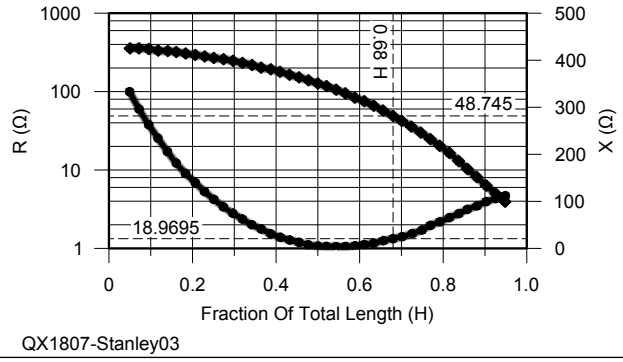

Figure 3 — Real (top) and reactive (bottom) parts of impedance of a full wavelength loop vs. height (H) as a fraction of one wavelength. The loop is resonant at H/W = 0.5.

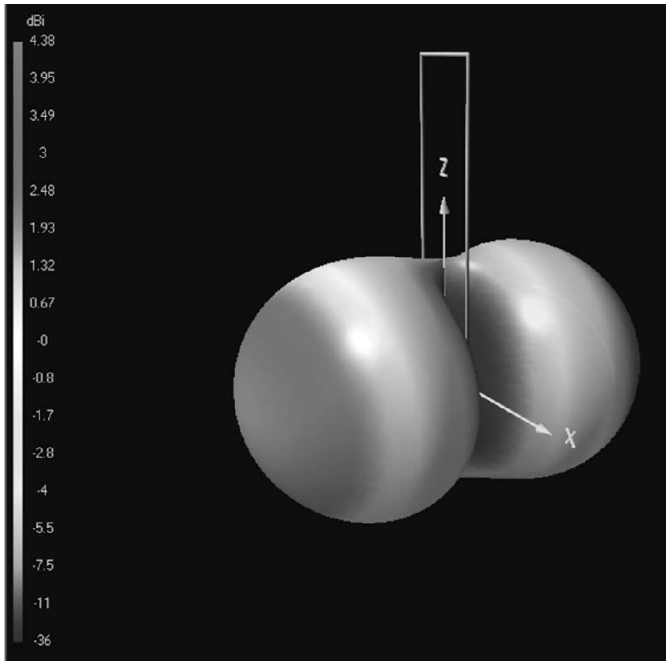

Figure 4 — 3D pattern for a horizontal loop with H/W = 4.

At the point of maximum gain (H/W = 4), R_{in} = 20 Ω. The gain curve at this point is very flat and we could vary the H/W somewhat for ease of matching with insignificant loss of gain. Figure 4 shows an NEC-generated 3D pattern for the H/W = 4 loop. The gain drops off due to loss of efficiency (copper losses) as the currents become large and the radiation resistance drops. A slightly lower H/W ratio could raise the R_{in} to 25 Ω with virtually no gain change. Even at the 50 Ω point (H/W = 2), the gain is only slightly less, thus the *ARRL Antenna Book* design is a good choice both for gain and ease of matching.

NEC-generated patterns confirmed that the straight up and down gain approaches zero as one would expect when H/W is very high. At this point the top and bottom wires, while very short, are a half wave apart and in phase so their contributions to the vertical waves produce cancellation. It is this cancellation of the vertical wave that puts more power towards the horizon up to the point where inefficiency begins to decrease the gain. Of course, with a very tall thin loop, the radiation resistance approaches zero, meaning losses are huge and matching is virtually impossible. The antenna becomes a low resistance dummy load.

Measurements on a real loop showed that a H/W ratio of 3 gave a R_{in} = 26 Ω (77 cm high and 26 cm wide for 144.2 MHz). This is pretty close to the NEC-derived values. This loop was made of insulated stranded wire about 0.75 mm diameter, or close to #20 or #22 AWG. The curves of Figure 3 used thinner wire, therefore the result is somewhat pessimistic about resistive losses at high ratios. It does serve to indicate that using the #22 AWG wire is probably not a serious cause of loss at H/W ratios up to 3:1. Insulation seems to "lengthen" the wires by about 5%, requiring shortening to achieve resonance compared to the NEC-derived lengths calculated using bare wires.

Wire lengths can be determined from Tables 1 through 3. Table 1 can be used for any frequency, but requires some calculations. Values in Table 2 are for 144.2 MHz where many of my tests were done. For convenience, Tables A1 through A3 are provided for 50.1, 222.2, and 432.1 MHz, with dimensions given in meters. Dimensions are calculated for bare wires of a diameter about 0.0005 wavelengths (1 mm at 2 m). If your wire is thicker or insulated, you must adjust these dimensions, but they will serve as a starting point.

The pattern of the single-loop design will vary somewhat with H/W ratio but will be something like the pattern shown in Figure 4. As the H/W decreases, the pattern will flatten as the signal up and down is further canceled. Of course, there will be nulls off the sides as with a quad loop. This graph is for the maximum gain case where the H/W is about 4 to 1.

Table 1.
Dimensions for loops vs. R_{in} and Gain, dBi. Frequency f is in MHz.

R_{in} at f	*Length L, of wire, m*	*Loop height H, m*	*Loop width W, m*	*Gain, dBi*
25	313/*f*	117.0/*f*	39.0/*f*	4.4
50	316/*f*	106.0/*f*	52.0/*f*	4.1
75	317/*f*	96.0/*f*	62.0/*f*	3.8
100	318/*f*	88.5/*f*	70.5/*f*	3.5
112	319/*f*	84.0/*f*	75.0/*f*	3.4
282	286/*f*	1.0/*f*	142.0/*f*	2.2

Table 2.
Calculated dimensions for 144.2 MHz.

R_{in}	*Length L, m*	*Height H, m*	*Width W, m*
25	2.17	0.81	0.27
50	2.19	0.74	0.36
75	2.20	0.67	0.43
100	2.21	0.61	0.49
112	2.21	0.58	0.52
282	1.98	0.01	0.98

Table 3.
Dimensions of the single and double diamond antennas at 144.2 MHz. Width and height of each diamond vs. gain and R_{in}.

Wire length, m	*Width/2, m*	*Height/2, m*	*Ri_n of single, Ω*	*Gain, dBi, of single*	*Ri_n of 2 stack, Ω*	*Gain of 2 stack*
2.22	0.392	0.392	117	3.65	275	5.6
2.21	0.37	0.41	100	3.73	235	5.8
2.21	0.32	0.45	75	3.95	160	6.0
2.23	0.3	0.47	63	4.03	135	6.2
2.23	0.275	0.485	50	4.10	120	6.4
2.24	0.26	0.496	45	4.13	100	6.45
2.24	0.25	0.5	42	4.18	96	6.5
2.24	0.15	0.54	15	4.36	40	6.6

A number of loops were constructed using these dimensions and were found to produce results quite similar to the NEC values provided adjustment was made to account for insulation on the wires, which was not included in the NEC model. Thus, I have confidence that the models are good.

Stacked Loops

Investigations were done to see the effect of stacking loops above the first one. Stacking increases the gain as additional loops are added, and will sharpen the pattern in the vertical plane. The pattern in the horizontal plane is unaffected. Loops can be stacked by cross-connecting the common wires between the two loops as shown in a Figure 5. This feeding/phasing technique is similar to that used for the venerable Sterba curtain antenna. Stacking loops in this manner tends to raise the impedance by approximately the number of loops. For example, the two loops have nearly twice the impedance of a single loop of the same H/W ratio. Narrow loops with about R_{in} = 30 Ω are stacked to get R_{in} close to 50 Ω. The gain with two such stacked loops is about 6.5 dBi or about 2 dB more than a single loop of the same ratio. R_{in} for the two-turn loop is somewhat less than twice that of the one turn loop. Also, some interaction between the crossing wires is evident. They should probably be kept a half inch or so apart at 144 MHz. Offsetting one in the horizontal plane seems to be the way to do this. Adjusting the spacing between them seems to provide some fine-tuning of the resonant frequency.

A plot of antenna current magnitude and phase (Figure 6) shows that the 4 horizontal wires have equal and in-phase currents. The two center wires occupy essentially the same space so they are equivalent to a single wire with double the current. Thus we have three horizontal radiators with unequal currents in a 1:2:1 ratio. Unequal currents in a stack of dipoles are sometimes used to clean up the pattern but, in this case, are simply a result of the feed method.

Double-loop antennas were tested on 144 and 432 MHz, and the R_{in} was confirmed to be close to the NEC-calculated values.

The Hour-glass Antenna

An interesting simpler support geometry, which requires only two cross arms was studied. We can simply cross the vertical wires as they go up, see Figure 7, rather than using a horizontal cross bar. For approximately the same total wire length, we get a bit more gain and simpler construction. The 3D pattern (Figure 8) is not quite as clean, but for gain towards the horizon, this may not matter. This hour-glass may be attractive in place of the two-high stacked square loop option. At 7 dB, its gain is about 3 dB higher than for a square loop, and 5 dB higher than dipole gain. Like the other versions, the H/W ratio determines the input impedance. The one shown here is optimized for direct feed from 50 Ω. This can be thought of as two delta loop antennas

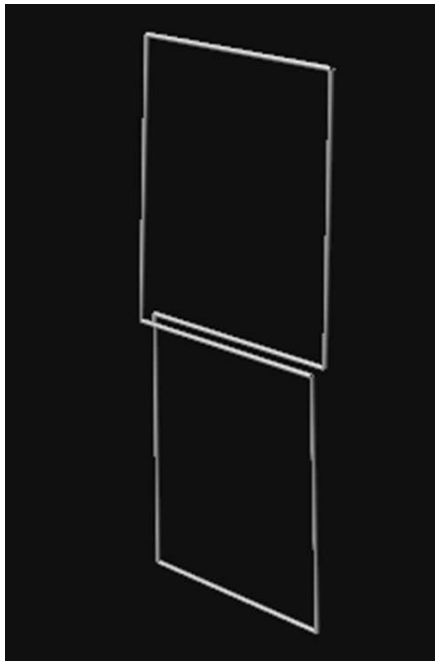

Figure 5 — Stacked loops are fed via cross-connected wires that are displaced slightly in the horizontal plane. The feed point, not shown, is at the mid-point of the bottom horizontal wire.

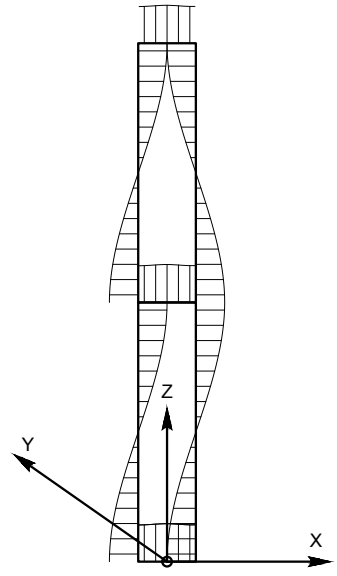

QX1807-Stanley06

Figure 6 — A NEC representation of currents in the various parts of the two-stack loop.

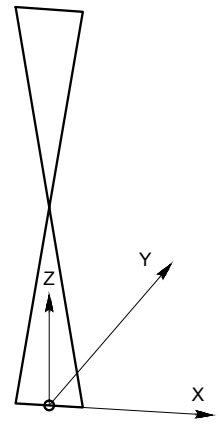

QX1807-Stanley07

Figure 7 — Geometry of the hour-glass antenna. The feed point is at the mid-point of the bottom horizontal wire, and the wires do not touch where they cross.

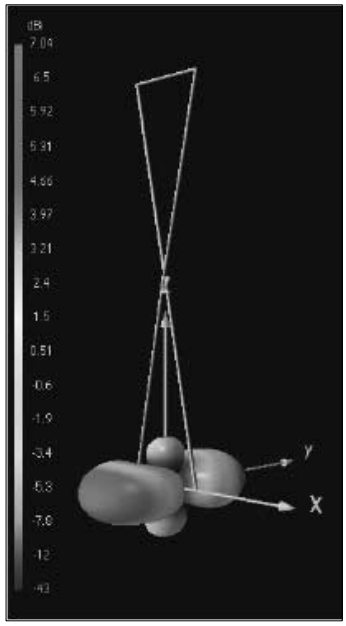

QX1807-Stanley08

Figure 8 — 3D pattern and geometry of the hour-glass antenna.

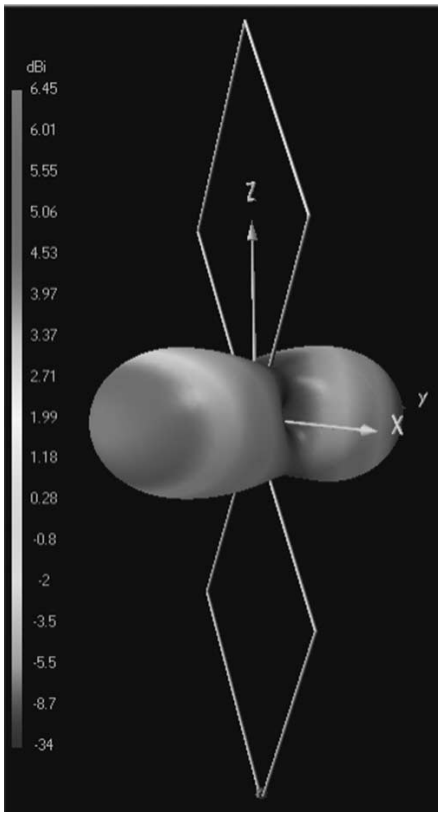

Figure 9 — 3D pattern and geometry of the stacked diamond antenna. The feed is at the bottom corner. The center wires cross but do not connect.

stacked, with the bottom one inverted. The wires cross in the center, but are separated by about 2 mm thick insulation, so that they do not touch. Horizontal radiation occurs from the center as well as the top and bottom of this antenna.

Hour-glass antennas were constructed for 144, 222 and 432 MHz and were found to have R_{in} close to the calculated values. The spacing between the two crossed wires affects the resonant frequency slightly and should be constant. See Appendix A for images of my antennas.

Diamond Loops

The diamond loop is well known. Many builders/users choose to feed the loop at the bottom corner instead of at the center of the bottom side. We examine what happens when we change the shape of, and stack, the diamond loop. Figure 9 shows the pattern and geometry of the stacked diamond loop. The feed is at the bottom corner, and the center wires cross but are not connected.

If flexible wires supported by arms are to be used for the elements, the supports must resist the high voltage that exists at the ends of the arms (corners of the diamonds). Thus, the use of wooden spacers might not be optimum. Self-supporting stiff wire construction might be an option.

Note that unlike the square loops where stacking loops increases the R_{in} by *less* than the sum of the individual R_{in} values, with the diamonds R_{in} increases by somewhat *more* than the sum of the individual R_{in} values. This is related to the mutual impedances between the multiple loops. The square loops have strong coupling via magnetic fields due to the closely spaced horizontal wires. With diamond loops, the wires cross at an angle and the magnetic fields couple somewhat less. Also, the difference in total length varies only slightly as the H/W ratio varies. This variation is well within the limits imposed by NEC accuracy and wire type variations. One could, therefore, use a value of 2.23 m as the starting length for loops of any shape when constructing a single loop antenna. The final value will be determined by adjusting

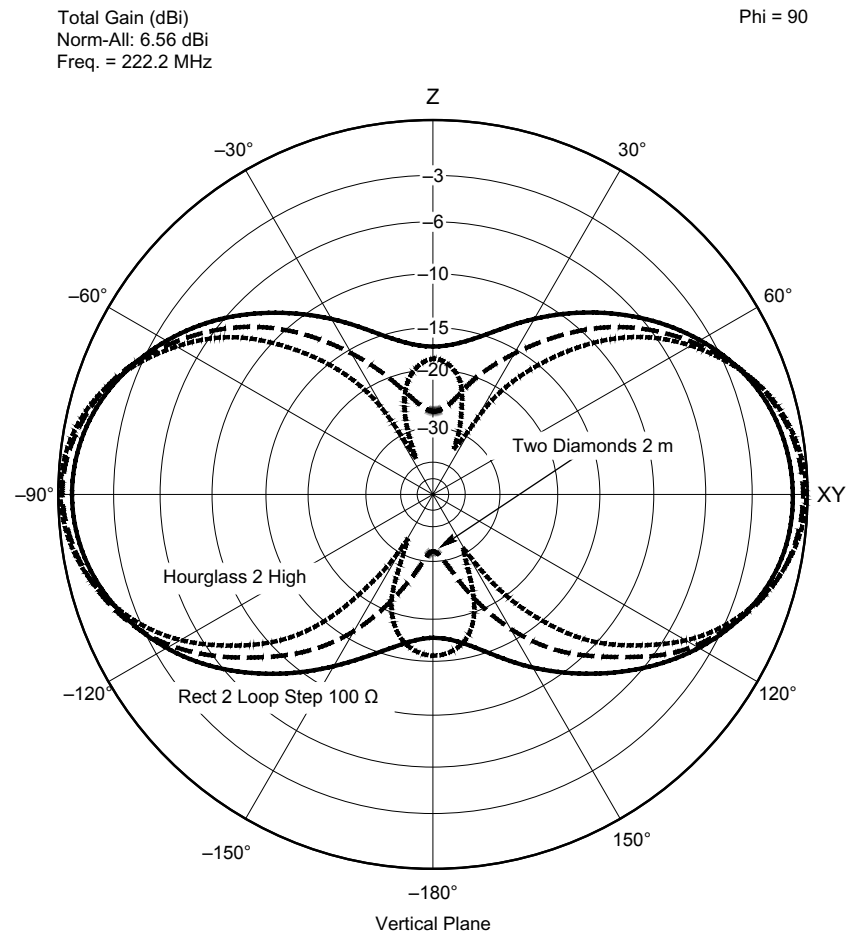

QX1807-Stanley10

Figure 10 — Patterns for the rectangular, hour-glass and diamond two-loop antennas.

for resonance at the desired frequency. I have not built any stacked diamond loops and so cannot confirm that they match the NEC predictions.

Comparison Among Three Stacked-Loop Geometries

I compared three loop options: the square, hour-glass (double delta), and diamond stacks to determine which configuration was best for gain and patterns. In each case R_{in} = 100 Ω, and the stack was two loops high.

The relative patterns are as shown in Figure 10. The rectangular loops are not as tall as the hour-glass or delta loops. This leads to about 0.5 dB less gain on the horizon, and less suppression of radiation towards the zenith. The patterns are similar enough that the choice among them might well be decided by the relative ease of construction. The hour-glass seems to be best on this basis, requiring just two support arms, and having no high voltage at the crossing point. The diamonds seem to take second place. However, any one these designs is usable. When overall height is a limiting factor, the rectangular loops might well be chosen.

Stacks of Three or More Loops

We can also stack three or more loops. For a 100 Ω R_{in} , the three square loops each had about a 2:1 ratio. These add, but also interact so the new R_{in} is 100 rather than 150 Ω. This is a useful value in that one can feed two of these loops in parallel and get 50 Ω without further matching. The two could be fed as sets of loops going up and down from the feed point for narrower vertical pattern and about 3 dB additional gain. Alternatively, they could be mounted at right angles to each other and fed with a 90° phase shift to produce an omni directional pattern (turnstile feed). In that case, we sacrifice about 2 dB of gain from the bi directional pattern of a single set of three. Finally, a set could be tuned as a passive reflector behind the first set and if the tuning is properly chosen, one can get 50 Ω input and nearly 10 dB of unidirectional gain. This, in effect, is similar to a stack of three close-spaced cubical-quad antennas. Of course, the single loop and the double loop can also be fed in these same ways for bidirectional, omnidirectional or unidirectional patterns.

The rectangular and diamond loops lend themselves to stacks of three or more loops simply by extending the geometry upwards. The hour-glass configuration would be more useful for a stack of 4 (2 hour-glasses) but not so much for a stack of three. I have used two stacks of three rectangular loops for an omnidirectional 2-meter gain antenna by feeding in the turnstile method. The matching proved somewhat more complicated than with the pair of single loops that I used on six meters[3] but was not too difficult, with the results as expected.

I look forward to other experimenters using this information to develop various types of antennas based on the single or stacked loops as part of omnidirectional, bidirectional and omnidirectional arrays.

Appendix A

Tables A1, A2 and A3 show calculated dimensions in meters for 50.1 MHz, 222.2 MHz and 432.1 MHz single loops, respectively. Figure A1 shows three-high

Table A1.
Calculated dimensions for 50.1 MHz.

R_{in}	*Length L, m*	*Height H, m*	*Width W, m*
25	6.25	2.34	0.78
50	6.31	2.12	1.04
75	6.33	1.92	1.24
100	6.35	1.77	1.41
112	6.37	1.68	1.50
282	5.71	0.02	2.83

Table A2.
Calculated dimensions for 222.2 MHz.

R_{in}	*Length L, m*	*Height H, m*	*Width W, m*
25	1.409	0.527	0.176
50	1.422	0.477	0.234
75	1.427	0.432	0.279
100	1.431	0.398	0.317
112	1.436	0.378	0.338
282	1.287	0.005	0.639

Table A3.
Calculated dimensions for 432.1 MHz.

R_{in}	*Length L, m*	*Height H, m*	*Width W, m*
25	0.724	0.271	0.090
50	0.731	0.245	0.120
75	0.734	0.222	0.143
100	0.736	0.205	0.163
112	0.738	0.194	0.174
282	0.662	0.002	0.329

Figure A1 — Left to right, a three-high stack rectangular loop for 144 MHz, hour-glass antennas for 144 and 432 MHz.

stack of rectangular loops for 144 MHz, and an hour-glass antennas for 144 and 432 MHz. Figure A2 shows a close-up of the feed system, including a 50 to 200 Ω balun for the 144 MHz three-high stack square loop antenna. Figure A3 shows a close-up view of the 432 MHz hour-glass antenna with its direct 50 Ω feed.

John Stanley, K4ERO, and his wife Ruth,WB4LUA, retired to Rising Fawn, Georgia after 45 years in international broadcasting, where they did engineering, consulting, and training with Christian radio stations in many countries. As an ARRL Technical Adviser for the past 27 years, John has contributed to many ARRL publications.

Notes

[1]Page 9-38, *The ARRL Antenna Book, 23rd Edition*, ARRL Item no. 0444, available from your ARRL dealer, or from the ARRL Store. Telephone toll-free in the US 888-277-5289, or 860-594- 0355, fax 860-594-0303; **www.arrl.org/shop/**; **pubsales@arrl.org**.

[2]The 4nec2 NEC-based antenna modeler and optimizer, by Arie Voors, is available from **www.qsl.net/4nec2**.

[3]John Stanley, K4ERO, "An Omnidirectional 6-Meter Horizontally Polarized Antenna", *QST* Apr. 2017, pp. 38-42.

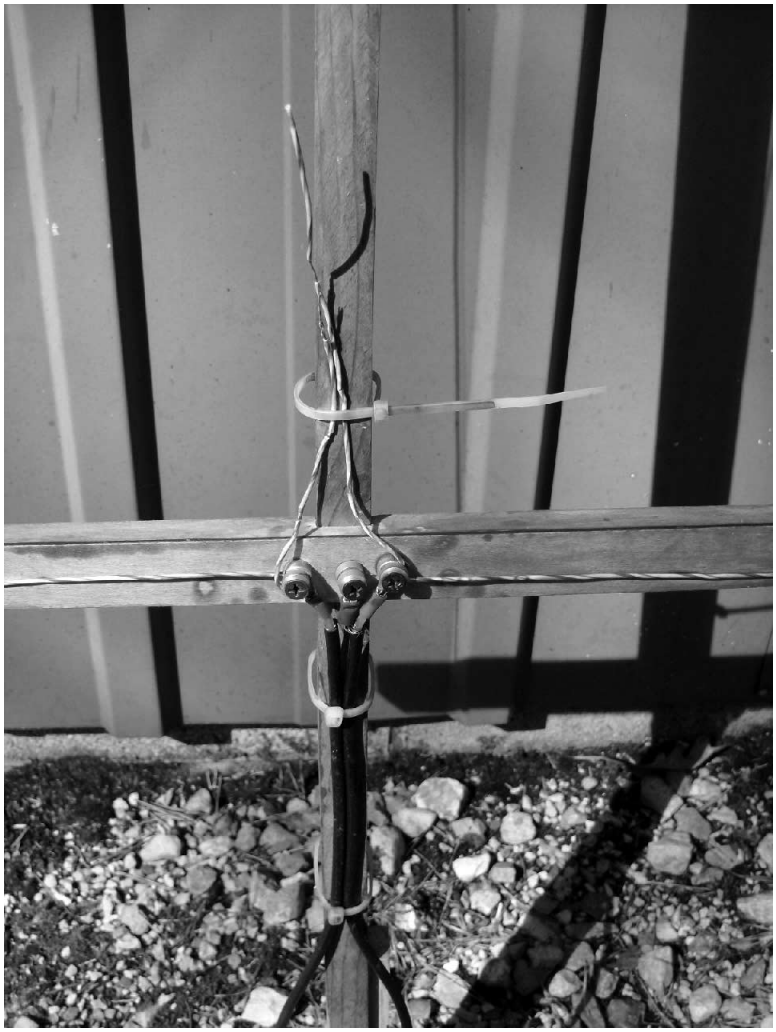

Figure A2 — Feed system via 50 to 200 Ω balun for 144 MHz three-high stack of square loops antenna.

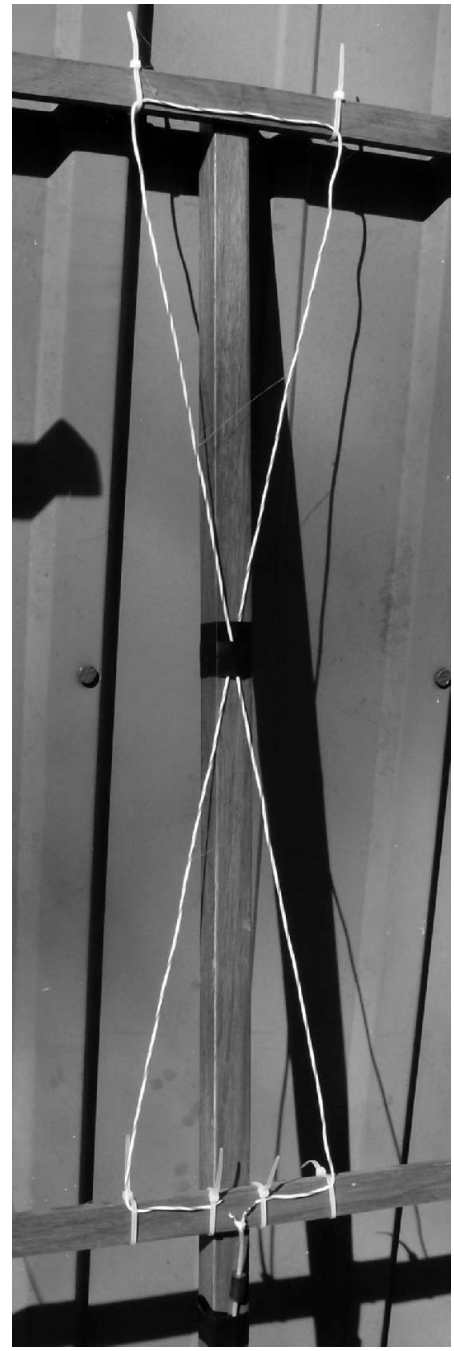

Figure A3 — Close up of a 432 MHz hour-glass test antenna with direct 50 Ω feed.

Mark Griffith, KDØQYN
501 S. Oak St, Union, MO 63084; **mark.griffith@pigate.net**

PiGate Emergency E-mail System

The PiGate system combined with Winlink 2000 global e-mail system can provide a simple, robust platform that can be deployed in nearly any disaster scenario.

A version of this article was presented at the 2016 ARRL/TAPR Digital Communications Conference, Sept 16-18, 2016. St Petersburg, FL.

Imagine an emergency communications system that is very small, self-contained, easily deployed, requires minimal power, and can be managed by anyone with the skills to connect to a web page. Disaster victims can then use their own tablet computer, smartphone, or other device to connect to this system and send e-mail to their family and friends, or any other e-mail address in the world, or even send a text message to a phone.

Introduction

Amateur Radio has a long history of providing communications during disaster situations. Ham operators spend much time and money to be able to help in times of need. In the past, amateur operators have setup portable radio stations in all sorts of environments. They were able to provide a much-needed capability when other forms of emergency communications were unavailable. The annual Amateur Field Day is an exercise hams use to test their abilities to operate under austere conditions.

As communications in our increasingly complex world have evolved, and so have the needs of emergency agencies that are served by the voluntary Amateur Radio force. Digital methods of communications are becoming more necessary for speed and accuracy. The demands that can be placed on a volunteer amateur operator to correctly transmit a list of much needed emergency equipment, or medications, using voice methods are staggering.

People today are more "connected" than they have been at any time in history. Tens of millions of people in the world know about and use e-mail. The vast majority of these people also have smartphones and use them constantly. The notion of instantly being able to communicate with those you wish, no matter where you may be, is no longer a dream. Amateur Radio itself seems to be an archaic or quaint way to talk to people around the country or world when all anyone needs to do is pick up a smartphone and verbally tell it to call anyone they wish. The connection is made in seconds. This type of instant communication is greatly missed during a disaster situation.

The challenge is to try and bridge this gap, using Amateur Radio in a way that will give people an accurate, fast, and easy digital way to communicate using e-mail.

The Winlink 2000 System

As stated on Wikipedia[1], "Winlink, also known as the Winlink 2000 Network, is a worldwide radio messaging system that mixes internet technology and appropriate amateur radio frequency (RF) technologies. The system provides radio interconnection services including: e-mail with attachments, position reporting, graphic and text weather bulletins, emergency relief communications, and message relay. The system is built and administered by volunteers without pecuniary interests. Winlink 2000 is a project of the Amateur Radio Safety Foundation, Inc. (ARSFI), a charitable entity and 501c(3) non-profit organization registered with the US Internal Revenue Service."

The Winlink2000 system is the backbone of the PiGate. In June 2016, Winlink handled over 65,000 e-mail messages. There are currently nearly 1,000 Radio Message Server (RMS) stations[2] around the world that are ready 24/7 to support the Winlink system. The ability of the PiGate to connect to that system, either via local Ethernet (if available in a disaster area), Packet[3] VHF/UHF radio, or PACTOR HF radio gives PiGate the capability to handle emergency communications in any shelter or other site where disaster victims may be gathered.

VHF/UHF RMS Station Network

Many disaster scenarios in the past have been localized enough that the needs of responders would have been greatly enhanced if reliable communications were available just a few miles from the disaster site. Amateur Radio operators using VHF voice communications has been most often used as the method that "always gets through". In many areas, there are so many repeaters that it is difficult to add a new one that can fit into the local repeater frequency allocations. Expanding the Winlink Radio Mail Server (RMS) station list can do a great deal to help emergency communications, and with enough Packet RMS stations throughout the country, any area could have reliable emergency communications.

This expansion was the reason to develop the PiGate RMS. Like the PiGate, this is a completely portable device that acts as a RMS. Used in conjunction with the PiGate, it would be placed outside the disaster area where an internet connection can be made, and using an Ethernet cable or WiFi, link to a public hot spot to provide the connection to the Winlink system.

The Raspberry Pi Mini-computer

The recent development of the Raspberry Pi[4] computer at an extremely low cost allows something like the PiGate and PiGate RMS to be developed cheaply and be within the

purchasing range of nearly all Amateur Radio licensees. This very small, fully functional computer, with very low power requirements, allows virtually unlimited ability due to its programming capabilities and the pre-built software packages that are available freely via download from the internet. In addition, the Raspberry Pi computer is very stable and reliable, two features that are very much needed in disaster scenarios.

The TNC-Pi

John Hansen at Coastal Chipworks[5] developed a companion board for the Raspberry Pi that contains a fully featured KISS TNC. This board, in conjunction with the Winlink2000 Packet RMS station network allows the PiGate and PiGate RMS to work in a majority of potential disaster locations, and provide quick, easy, and reliable e-mail capability.

Pre-packaged Software

Several software products are freely available via the GNU Copyleft license and are integrated into the PiGate system. The integration of these products are what makes the PiGate and PiGate RMS work;

- AX.25 radio communications protocol[6] that uses the KISS TNC.
- Paclink-unix[7] developed by a team of part time programmers. This provides the method of transmitting and receiving e-mail via AX.25 and other protocols.
- Exim4 mail transfer agent for sending and receiving e-mail[8] that are specially formatted for the Winlink2000 system.
- Hostapd (Host access point daemon) to configure and bring up the WiFi hot spot.
- Dovecot to provide WiFi login authentication to the PiGate e-mail server.
- Apache for the web service.
- A customized version of SquirrelMail to provide the e-mail server.
- For the PiGate RMS, the Raspbian operating system provides the WiFi[9] and other capabilities needed and John Wiseman's excellent BPQ32 software the Winlink connection.

Web Based Administration Software

Integrating all these products to work together also required a way to manage it all as there are a number of configuration files that need to be setup correctly for it to work. Even with a complete knowledge of how this was done, making changes can easily lead to misconfiguration and the system failing. Creating a simple web interface that can be used from the web browser of a smart phone or tablet gives the PiGate administrator the ability to make changes needed during a disaster situation without having to resort to logging into the PiGate and edit numerous configuration files. This same interface is used to monitor the status of the PiGate as users (disaster victims) use the system to send e-mail to their family and friends.

The PiGate can be mostly automated, where there is little or no action needed by the station administrator once the initial setup is completed to allow disaster victims to send e-mail. Configuration of some items, like the master RMS station list, are done through the web interface, upon demand and before deploying, while an internet connection is available. The PiGate RMS uses a built-in 3.5 inch touch screen display to setup and start/stop the Radio Mail Server (RMS) software. Once configured and running, it is completely automatic and can continue for an indefinite time.

How it all works

The basic premise of the PiGate is to provide users (disaster victims) with the ability to send e-mail to their family and friends without needing someone to do it for them. This also provides them a measure of privacy. The key components are the WiFi hot spot, web based e-mail server, the paclink-unix software and the AX.25 protocol to do the actual connection to a RMS station.

Once the initial station configuration is done by the amateur radio administrator, users are given the information to login to the WiFi hotspot, connect to the e-mail server (Figure 1), and compose and send their e-mail. Each user is normally given a separate login account to the e-mail server. The users can use a smartphone, tablet, or laptop computer to make the connection via a web browser application, and compose their e-mail. This, of course, assumes that these devices and the batteries are good. If not, the amateur operator can choose to type in the e-mail, or provide users with a device, or provide them the ability to charge their own devices.

To conform to normal message traffic protocols within a disaster area, the PiGate, by default, does not allow return e-mail. Each e-mail sent has the *Reply To* field set to NOCALL so return e-mail will not be accepted. Each message composed is formatted so as to be acceptable to the WinkLink2000 system. Also, each one has a footer attached informing the recipient that this message was transmitted via Amateur Radio as a service to the community. Messages can also be sent as a text message to a recipient's smartphone, and the PiGate will detect these messages and format them differently to better use the SMS text message system. Everything was designed

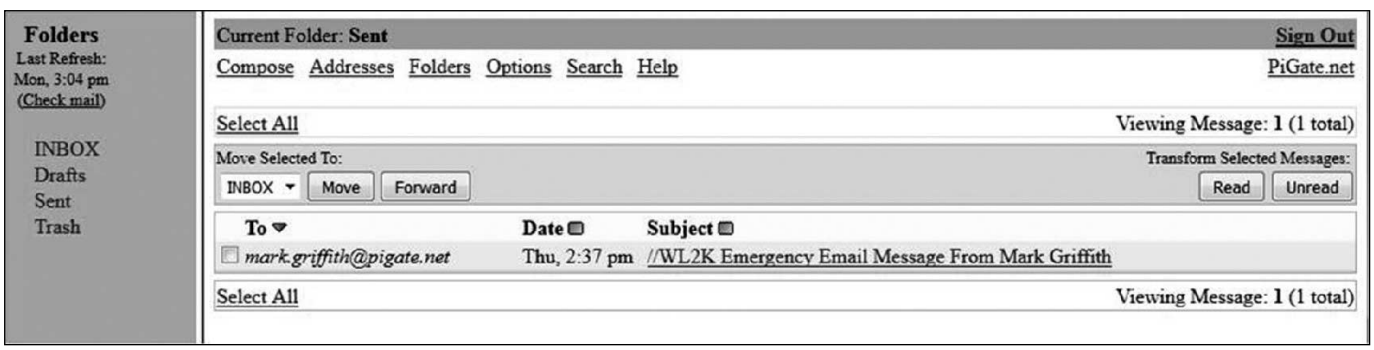

Figure 1 — PiGate e-mail server.

to be used from a smartphone. The touch screen system works well. Once an e-mail is composed, it is placed in the outgoing message queue to be sent during the next radio transfer session.

Radio Transfer

The amateur administrator during the initial setup would have determined the RMS station to connect to for message transfer and tested this connection. This setup is then used for all future message transfers unless changed by the amateur operator. The operator can choose either Packet VHF/UHF RMS stations, or PACTOR HF RMS stations. Connections to PACTOR stations are highly dependent upon many factors, and the PACTOR modems are expensive. Packet connections normally work much better, although the range with a VHF/UHF connection is limited. Even so, a great many locations within the USA have a PACKET RMS station within reasonable range and can be used for emergency e-mail message transfer.

If a PiGate RMS station is used in conjunction with a PiGate, many more options are now opened. For example, since the amateur operator now controls both ends of the radio link, they can choose any frequency allowed by their operating license. Also, increased antenna options are available. A high gain Yagi antenna at the PiGate RMS end can be pointed to the disaster area, and a similar antenna at the PiGate end will help ensure strong steady signals.

Winlink2000 E-mail Transfer

Once the message or messages are transferred to the RMS station (Figure 2), they are processed though the Winlink2000 global e-mail system. Messages are sent either via internet connections between the several Central Messaging Servers (CMS) or via radio links if the internet is not available. This ensures e-mail capability in even the most widespread disasters. E-mail messages appear in the inbox of the user they are addressed to just like any other e-mail. Messages can also be sent as a text to a smartphone. Each cellular service provider has a method of sending an e-mail as a text message, so simply using that method allows text to phone capability. A complete list of worldwide cellular providers and the method of sending to a smartphone is included in the on-line docs available on a PiGate through the web-based management system.

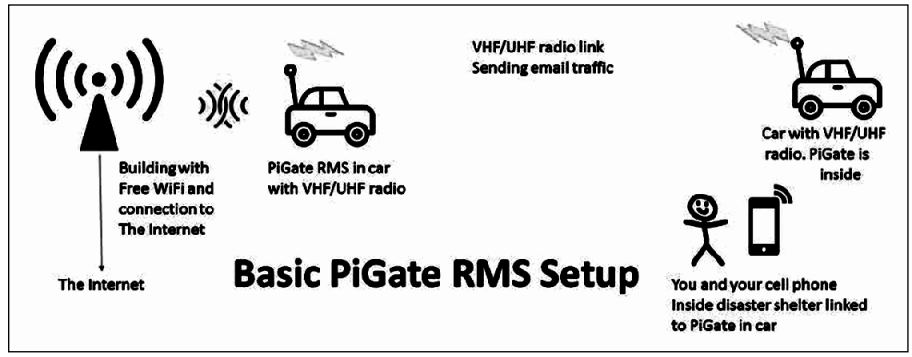

Figure 2 — Basic PiGate RMS setup. [Source: www.pigate.net/pigate-rms.html].

New Features

Since the introduction of the PiGate in 2016, many new features have been added. This includes the ability to request e-mail documents that will be sent to the amateur operators Winlink account and then retrieved using the PiGate. These documents include weather text forecasts as well as charts and graphs, marine weather charts to aid boaters around the world, and the ability to create HTML forms of the most often used documents and attach these to an outbound e-mail. These forms include the standard ARRL Radiogram as well as many ICS forms. Future development will continue as users make requests and new ideas present themselves.

Conclusion

The PiGate system[10] is designed to be portable, require minimum power, and ease of use. Combining these features with the capabilities provided by the Winlink2000 global e-mail system provides a simple, robust platform that can be deployed in nearly any disaster scenario to provide "last mile" communications to emergency responders and disaster victims. People can use the device on their own, with little or no training, using their own smartphone or other device.

The PiGate software is provided free of charge to anyone that would like to download it and build a PiGate system. Regular updates are available from the PiGate web site. A nifty case is a downloadable 3D printer image which can be printed on nearly any 3D printer.

Mark Griffith, KDØQYN, has been an active Amateur Radio operator since 2012. Prior to that, he received his first Technician class license in 1969 at the age of 16, and operated 2 meter AM in the New Jersey area as WA2HHF. After joining the USAF in 1971, he let his license lapse and was re-licensed in 2012 after a 40 year break. Mark spends nearly all of his on-air time using digital modes such as JT65, JT9, and some PSK and RTTY during contests. As a member of the local ARES chapter, Mark developed a desire to help improve the ability of amateur volunteers to use digital modes from disaster areas to improve the speed and quality of service.

Notes

[1]Wikipedia article on Winlink2000: **https://en.wikipedia.org/wiki/Winlink**.
[2]Winklink2000 RMS stations list tab in: **www.winlink.org/RMSChannel**s.
[3]RMS Packet software: **winlink.org/content/rms_packet**.
[4]Raspberry Pi website: **https://www.raspberrypi.org**.
[5]Coastal Chipworks TNC Pi: **tnc-x.com/TNCPi.htm**.
[6]AX.25 software installation and configuration: **k4gbb.no-ip.org/docs/raspberry.html**.
[7]Compiling and installing the paclink-unix software: **bazaudi.com/plu/doku.php?id=plu:install_plu**.
[8]Setting up an e-mail server on a Raspberry PI: **https://samhobbs.co.uk/raspberry-pi-email-server**.
[9]Configuring a Raspberry Pi as a WiFi hot spot: **https://learn.adafruit.com/setting-up-a-raspberry-pi-as-a-wifi-access-point**.
[10]Learn more about the PiGate and PiGate RMS: **pigate.net**.

Technical Notes

Effects of Ground on Compliance Distances of a Small HF Loop Antenna

The RF safety compliance distances for small HF transmitting loops are published in Table 17 of the *FCC OET Bulletin 65b*[A1] and in *QST*[A2]. Kai Siwiak, KE4PT, calculated these distances using an analytic solution for the near fields of a loop in free space. The effect of ground reflections is included by increasing the input power in the calculations by the FCC-recommended factor of 2.56 (see Section 3 of *OET Bulletin 65b*). This conservative assumption corresponds to an increase in the fields by a factor of 1.6.

The *far field* gain and antenna pattern of a small loop are affected by the height of the loop above ground[A3]. For this note I used a computer model of a typical Amateur Radio HF loop to learn how the loop height and ground properties affect compliance distances, which are determined by *near fields*.

NEC Model

My NEC-2 model is for a vertical 0.8 m (2.7 ft) diameter loop of 10 mm (3/8 in) made of copper tubing. A voltage source is at the bottom of the loop, and a lossless tuning capacitor is across a gap at the top. Compliance distances are measured from the center of the loop.

Due to non-uniform current around the loop and high voltage at the tuning capacitor, near fields are skewed with respect to the loop axes[A4]. I used color-contour maps of the fields[A5] and high resolution linear scans[A6] to locate the farthest points where the *E* and *H* fields are at the maximum permitted levels (Table 1, "Power Thresholds for Routine Evaluation of Amateur Radio Stations" of *OET Bulletin 65b*). The compliance distance is the larger of the distances determined by the rms values of the total *E* field and the total *H* field.

The first column in my Table A shows theoretical calculations of controlled area compliance distances when the loop is fed with 150 W average power. They are provided by KE4PT, who used an average power of 384 W (or, 150 W × 2.56) in the calculations to include the effect of ground reflections.

The second column shows distances simulated with my NEC model of the loop in free space with an input power of 384 W. The NEC calculations are in good agreement with theory.

The third column shows NEC calculations when the center of the loop is 2 m above "average" ground (conductivity σ = 0.005 S/m, relative dielectric constant ε_r = 13). The power is 150 W. Comparison with column 1 shows that the theory provides conservative compliance distances for this loop.

Loop Compliance Distance

When the loop height is reduced to 1 m, the NEC compliance distances decrease because of resistive loss in the ground. For a loop height of 6 m the distances are up to 8% greater than at 2 m, but they are less than 90% of the conservative calculations in first column.

When the loop height is 2 m, there are no significant differences in compliance distances with "poor" ground (σ = 0.001 S/m, ε_r = 13) compared to "very good" ground (σ = 0.030 S/m, ε_r = 20). The same is true at a height of 6 m.

In summary, theoretical calculations based on a field reflection factor of 1.6 give conservative 150 W compliance distances for this small HF loop at heights ranging from 1 to 6 m above ground. This result is valid for ground properties ranging from very poor to very good. — *Regards, Peter DeNeef, AE7PD,* ***HamRadioAndVision@gmail.com***.

Q Factor Formulas

The concept of *Q* originated in 1914 (then dubbed *K*)[B1] and first appeared in print in 1923 when Kenneth S. Johnson used it to represent the ratio of reactance to resistance as a "figure of merit" for inductors[B2]. Since Johnson's first use in electrical networks, this ubiquitous factor has been applied to mechanical devices, golf balls, sharpness of resonance in electrical networks, atomic clocks and, somewhat whimsically, to golf balls and the planet Earth[B3].

Q has about as many different uses as there are different (but equivalent) ways of expressing its value. The different ways of expressing *Q* can be derived one from the other. Here are a few, along with some of their uses.

$$Q = \frac{\text{Series Reactance}}{\text{Series Resistance}} = \frac{\text{Parallel Resitance}}{\text{Parallel Reactance}} \quad (1)$$

is the historical definition, and useful for individual inductors, capacitors, dielectrics and ferrites.

The energy formula is,

$$Q = \frac{2\pi \times \text{Stored energy}}{\text{Energy lost in one cycle}} \quad (2)$$

This fundamental definition is useful with small antennas and with mechanical systems. For example, the height *h* of a golf ball above a surface is proportional to "Stored energy" (*mgh*). The difference Δh between *h* and the height after a lossless re-bound from a solid surface gives $mg\Delta h$, the "Energy lost in one cycle", hence the $Q_{golfball} = 2\pi mgh/mg\Delta h = 2\pi h/\Delta h$. A golf ball that loses 30% of its height in a bounce has a *Q* of $2\pi/0.3$ or about 21.

The companion power formula is,

$$Q = \frac{2\pi \times \text{Stored reactive power}}{\text{Power lost}} \quad (3)$$

where power is energy × frequency, and is useful with antenna systems. For antennas, the power lost is dissipated to radiation and to resistive losses.

The classic bandwidth formula is,

$$Q = \frac{\sqrt{F_H F_L}}{F_H - F_L} = \frac{\text{Frequency}}{\text{Bandwidth}} \quad (4)$$

and is useful for simple resonant circuits, including small antennas, when the impedance $Z = R + jX$ then F_H is the frequency where $R = X$, and F_L is where $R = -X$, so that $F_H - F_L$ is the 3 dB bandwidth, or the VSWR = 2.62 point bandwidth in a circuit that is matched at the geometric mean frequency. When measured using a matched transmitter, this the *loaded Q*.

The logarithmic decrement formula is,

$$Q = \frac{\pi}{\delta} \quad (5)$$

where the logarithmic decrement δ is the natural logarithm of the ratio of two non-zero amplitude values exactly one cycle apart of a damped sinusoidal voltage or current waveform.

The incremental impedance formula is,

$$Q = \frac{f}{2}\frac{\left|\Delta Z/\Delta f\right|}{R} \quad (6)$$

where for a small antenna, $|\Delta Z/\Delta f|$ is the magnitude of the incremental change in impedance Z divided by the incremental change in frequency f; and R is the resistance, or Re{Z}, at frequency f. This formula is useful for small antennas were the Im{Z} does not cross zero, but has a minimum value.

In a resonant circuit having an inductor with its Q_{Ind} and a capacitor with its Q_{Cap}, the individual component Qs can be combined as,

$$\frac{1}{Q_{total}} = \frac{1}{Q_{Cap}} + \frac{1}{Q_{Ind}} \quad (7)$$

which is true for all forms of resonant circuits no matter whether the individual component losses are in parallel or series form.

The Q formulas can be applied in combination. For example, the Q of an antenna can be found with the bandwidth formula Eqn. (4), then Eqn. (3) can be applied with "Power lost" set equal to the transmitter-supplied power to find the total "Stored reactive power" in the antenna near field. In some cases, that stored reactive power can be quite impressive!

Eqn.(1) can be used to calculate the ideal unloaded Q of a small loop antenna by considering the inductor impedance and just the radiation resistance. The bandwidth Eqn. (4) can then be used to obtain the total Q including all losses. The ratio of the Eqn. (4) loaded Q result and half the unloaded Eqn. (1) result is the total efficiency of the antenna.

Finally, Eqn. (1) can be used to obtain the Q_{Ind} including radiation and resistive losses for a small loop antenna. The losses of a capacitor with known Q_{Cap} can then be included using the resonant circuit Q combining Eqn. (7) to obtain the total Q. — *Regards, Kai Siwiak, KE4PT,* ***k.siwiak@ieee.org***.

Table A. Controlled Area Compliance Distances.

The 0.8 m diameter loop fed with 150 W are shown from theory, a free-space NEC model, and an NEC model of the loop 2 m above average ground.

Frequency	*Theory*	*NEC model*	*NEC model with ground*
7 MHz	2.1 m	2.1 m	1.8 m
14 MHz	2.4 m	2.5 m	2.0 m
21 MHz	2.6 m	2.7 m	2.1 m
28 MHz	2.6 m	2.7 m	2.1 m

Notes

[A1]"Evaluating Compliance with FCC Guidelines For Human Exposure to Radiofrequency Electromagnetic Fields", *OET Bulletin 65b (1997)*; **https://www.fcc.gov/general/oet-bulletins-line**.

[A2]K. Siwiak, Technical Correspondence: "RF Exposure Compliance Distances for Transmitting Loops, and Transmitting Loop Current," *QST*, May 2017, pp. 64-65.

[A3]P. DeNeef, "Effects Due to Ground for Small Transmitting Loop Antennas," *QEX,* Jul./Aug, 2018.

[A4]K. Siwiak, "Effect of Small HF Loop Near Fields on Direction Finding," *QST*, July 2015, pp. 63-64.

[A5]Arie Voors, 4nec2 NEC based antenna modeler and optimizer, **www.qsl.net/4nec2/**.

[A6]Several versions of EZNEC antenna modeling software are available from developer Roy Lewallen, W7EL, at **www.eznec.com**.

[B1]E. I. Green, "The story of *Q*," American Scientist, vol. 43, pp. 584-594, Oct. 1955.

[B2]K. S. Johnson, Electrical Network, US Patent 1,628,983, Filed July 9, 1923, issued May 17, 1927.

[B3]K. Siwiak, KE4PT, "*Q* and the Energy Stored Around Antennas", *QST*, Feb. 2013, pp 37-38.

Send your short *QEX* Technical Note to the Editor, via e-mail to qex@arrl.org. We reserve the right to edit your Note for clarity, and to fit in the available page space. "*QEX* Technical Notes" may also appear in other ARRL media. The publishers of *QEX* assume no responsibilities for statements made by correspondents.

Letters

An Optimized Grounded Base Oscillator Design for VHF/UHF, (May/June 2018)

Dear Editor,

The article by Dr. Ulrich L. Rohde, N1UL, and Dr. Ajay Poddar, AC2KG, is very interesting, useful and didactic. It makes *QEX* magazine an excellent read, and gives esteem to Amateur Radio. I believe that we radio amateurs need be in the forefront of solutions for the use of the electromagnetic spectrum, and millimeter waves is a new frontier.

I read other articles from Dr. Rohde, including those about DROs (direct resonator oscillators) that operate at 10 GHz, which I enjoyed very much. I asked Dr. Rohde if it is possible and practical to use DROs to generate millimeter wave (above 18 GHz) signals. If so, this type of oscillator would be very useful in many millimeter wave applications.

My article, "Adapt Your Equipment to Operate at Millimeter Waves up to 32 GHz", will be published soon in *QEX*, and therefore an article about DROs at millimeter waves can be useful to continue the topic, and can be incentive to *QEX* readers and experimenters. — *Best regards, Euclides Lourenço Chuma, PY2EAJ*.

Dr. Ulrich L. Rohde, N1UL, replies,

Thanks for your comments. My / our plan was to introduce the much higher accuracy of non-linear mathematics, and yes I think DROs can be build up to 24 GHz. — *73, Ulrich L. Rohde, N1UL.*

Design of a Two-band Loaded Dipole Antenna, (Sept./Oct. 2017)

Dear Editor,

Regarding the David Birnbaum, K2LYV, article, I've seen various definitions of reactance. If you define reactance X as the imaginary part of the impedance Z, then the numerator of Eqn. (1) should be $+\omega L$ and not $-\omega L$. — *73, Gérald Lemay,VA2GLU*.

David Birnbaum, K2LYV, replies,

It does appear that the sign for Eqn. (1) is incorrect, as is the sign for Eqn. (2). However, the solution for ω_0 and X_0 is correct since we use only the ratio of X_2/X_1 and so the sign error cancels out. The two equations near the bottom of column 1 on page 21 are not numbered, but they are the ones used to calculate the component values. — *Best regards, David Birnbaum, K2LYV*.

Measuring Characteristic Impedance of Coax Cable in the Shack (Nov./Dec. 2017)

Dear Editor,

I would like to offer the following alternative to the John Flood, K4DLX, method of measuring the characteristic impedance, Z_0, for any length of two conductor cable. My method requires measuring the inductance L with the far end shorted, and measuring the capacitance C with the far end open. The characteristic impedance is then,

$$Z_0 = \sqrt{\frac{L}{C}}$$

where L is in henry and C is in farad. This formula is fundamental to transmission line behavior and accurate providing losses are negligible. My recent example of a length of twin flex gave 76.44 pF and 0.410 μH to provide the useful value of 73.2 Ω. The units reconcile since inductance in henry is volt seconds per ampere, and capacitance in farad is ampere seconds per volt. The square root of the ratio is volt per ampere, or ohms. The result is independent of frequency, so you can use a low frequency LC meter.

I have used this technique to select balanced twin line needed for phasing two driven elements in a 2-band Yagi antenna. I used the ADE LC meter for this test, but that is not critical — *73, Ron Skelton, W6WO*.

Upcoming Conferences

2018 Central States VHFS Society, Inc. Conference

Wichita, Kansas
July 26-29, 2018
www.2018.CSVHFS.org

The annual Central States VHF Society Conference will be held on July 26-28 at the Doubletree by Hilton Hotel at the Wichita (Eisenhower) Airport. This year is our Society's 52nd Conference, an ARRL-sanctioned operating specialty convention.

This year's event will start with a Meet and Greet Thursday night and end with family entertainer Curtis the Mentalist at the grand-finale banquet. Friday and Saturday feature state-of-the-art technical programs, noise figure measurements, antenna range, Rover Row, Dish Bowl, VHF 101 education seminar for newcomers to weak signal operations, equipment auctions, luncheons, family tours, door prizes, hospitality suites, guest speakers, and a VHF/UHF/Microwave swap fest.

The $99 room rate is available until July 6th or until the group block is sold-out.

ARRL/TAPR Digital Communications Conference (37th)

Albuquerque, New Mexico
September 14-16, 2018
www.tapr.org

The 37th Annual ARRL and TAPR Digital Communications Conference will be held September 14-16, 2018. in Albuquerque, New Mexico, at the Sheraton Albuquerque Airport Hotel. Rocky Mountain Ham Radio will be hosting the event.

The ARRL and TAPR Digital Communications Conference is an international forum for radio amateurs to meet, publish their work, and present new ideas and techniques. Presenters and attendees will have the opportunity to exchange ideas and learn about recent hardware and software advances, theories, experimental results, and practical applications.

Call for Papers: Technical papers are solicited for presentation at the ARRL and TAPR Digital Communications Conference and publication in the Conference Proceedings. Annual conference proceedings are published by the ARRL. Presentation at the conference is not required for publication. Submission of papers are due by **July 31, 2018** and should be submitted to: Maty Weinberg, ARRL, 225 Main St., Newington, CT 06111, or **maty@arrl.org**.

Topics include, but are not limited to: Software Defined Radio (SDR), digital voice (D-Star, P25, WinDRM, FDMDV, DRMDV, G4GUO), digital satellite communications, Global Position System (GPS), precision timing, Automatic Packet Reporting System™ (APRS), short messaging, Digital Signal Processing (DSP), HF digital modes, internet interoperability with Amateur Radio networks, spread spectrum, IEEE 802.11 and other Part 15 license-exempt systems adaptable for Amateur Radio, using TCP/IP networking over Amateur Radio, mesh and peer-to-peer wireless networking, emergency and Homeland Defense backup digital communications, using Linux in Amateur Radio, updates on AX.25 and other wireless networking protocols, and topics that advance the Amateur Radio art.

Call the Sheraton Albuquerque Airport Hotel and mention the group code "ARRL and TAPR Digital" to receive the special DCC room rate of $99.00 single/double plus applicable taxes. This special rate is good until **August 12, 2018**. Reservation can also be made online. See website for full details.

Microwave Update 2018

Dayton, Ohio
October 11-14, 2018
www.microwaveupdate.org

Microwave Update (MUD) is an international conference dedicated to microwave equipment design, construction, and operation. It is focused on Amateur Radio microwave bands. The Midwest VHF-UHF Society (MVUS) is pleased to host this year's event. The conference will be held at the Holiday Inn, 2800 Presidential Drive, Fairborn, Ohio 45324.

Call for Presentations and Papers: The program committee is calling for papers and presentations on the technical and operational aspects of microwave Amateur Radio communications. Tell us about your latest project, design or operating adventures. Please email your proposals, questions, and submissions to John Ackermann, N8UR, at **jra@febo.com**.

Presentations selected may be given in person or by proxy. Please send an abstract and expected duration no later than **August 25, 2018**. Ideally, send your draft presentation by the same date. We encourage presenters to submit a companion paper for publication in the proceedings book. This paper would ideally be text based and expand on the presentation slides, but a simple copy of the slides is also okay. Either way, this material must be received no later than **September 1, 2018** to be included in the book. Additional material (presentation slides, schematics, source code, more text, background info, etc.) to be included on the proceedings CD must arrive no later than **September 25, 2018**. All conference attendees will receive a copy of the book and CD.

Room rate is $110.00 per night, and is available for 3 nights before and after the conference. Reservations must be made directly through the hotel at 937-426-7800. You must name the group you are with: *Microwave Update 2018 Conference* to receive the special rate. Reservations must be made by 12:01am on September 15, 2018. Airport transportation can be arranged through the hotel for a round trip cost of $30.00.

24th Annual Pacific Northwest VHF-UHF-Microwave Conference

Seaside, Oregon
Oct 12-13, 2018
www.pnwvhfs.org

Join other weak-signal VHF, UHF and Microwave operators for the 24th Annual PNW VHF Society Conference to be held at the Best Western Ocean View Resort, 414 North Prom, Seaside, OR. Conference registration is $55 before October 1, or $65 thereafter and at the door.

Call for Speakers and Papers: The Pacific Northwest VHF Society is looking for speakers and papers. Please send your abstract to Jim, K7ND, **secretary@pnwvhfs.org**. Authors will be notified of acceptance by September 14 for inclusion in the program and it will be posted on the website.

Abstracts are solicited on these VHF-UHF-Microwave topics and more: FT8, JT4, JT9, JT65, ISCAT, MSK144 and other digital modes; antenna theory and design; propagation; microwaves; frequency stabilization; EME tools, tips and techniques; hill-topping, roving and portable operation; the world above 1000 MHz; transverters and amplifiers; Software Defined Radio; remote station operation; amateur television; contest equipment, techniques and strategy; lasers and other radiation sources, and other subjects related to VHF and up.

Call the hotel reservation desk at 503-738-3334 to reserve a room. Be sure to ask for the "Pacific Northwest VHF Society" room rates. If a Saturday night reservation is asked for, then a Friday night stay might also be required. Not a big discount this year but a discount nonetheless. You may want to compare rates on-line; there are less expensive places to stay in town.

See website; more details will be posted as they become available.

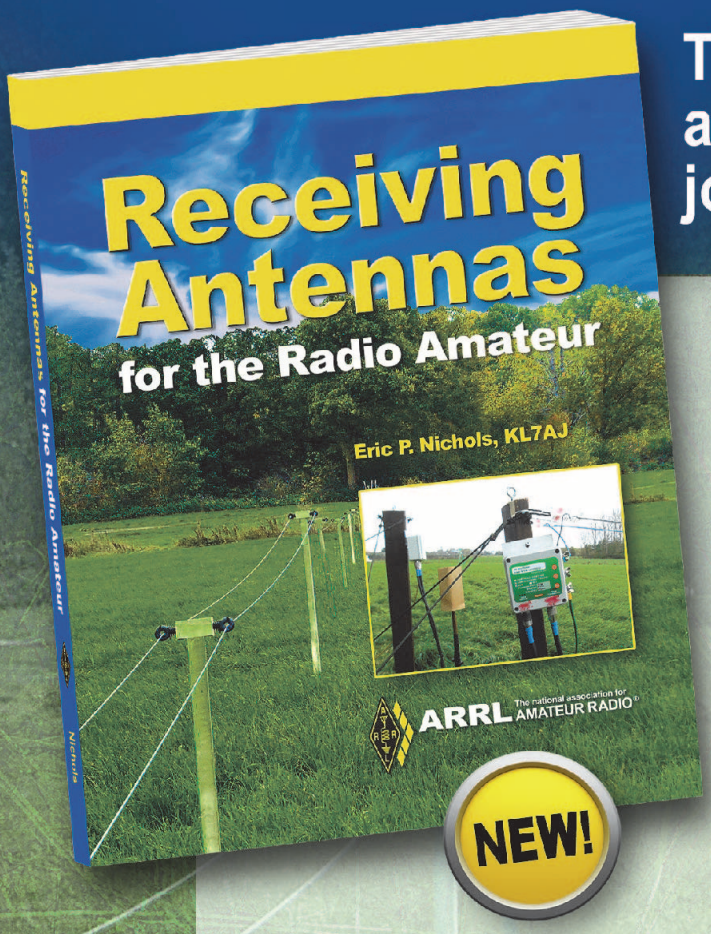

Transmitting and receiving antennas have different jobs to do.

Receiving Antennas
for the Radio Amateur

Eric P. Nichols, KL7AJ

Although the fundamental characteristics of antennas apply to both transmission and reception, the requirements and priorities of receiving antennas can be vastly different from those of transmitting antennas. ***Receiving Antennas for the Radio Amateur*** focuses entirely on active and passive receiving antennas and their associated circuits. There are relatively few cases where a radio amateur cannot benefit from a separate, well-designed receiving antenna or antenna system. On the low bands, including our new allocations at 630 and 2200 meters, heavy emphasis on the receiving end of these radio paths is essential for success.

The *active* antenna holds a prominent position in this book, as it offers good receiving performance while taking up minimal space. Recent developments in radio frequency (RF) semiconductors, especially low-noise RF operational amplifiers, have made a number of previously difficult-to-implement active antenna designs simple to build.

Table of Contents

- Receiving Antennas are Different!
- Your Friend, the Decibel
- The Preamplifier Problem
- The Amazing Disappearing Antenna
- The Receiving Antenna as a Signal Generator
- The Quest for Infinite Power Gain
- The Role of the Resistor in the Receiving Antenna
- The Small Loop Antenna
- Achieving the Perfect Null
- You *Can* Make Accurate Field Strength Measurements
- The Aperiodic Loop
- The Q Factor
- The Beverage: In a Class of Its Own
- Dealing with Non-Reciprocal Propagation
- The Evolution of the eXOgon Antenna
- The Lowdown on LF
- The Random Wire
- Arrays and Beamforming Networks
- Powering Your Active Antenna
- Diversity Methods
- NVIS Receiving Antennas
- Receiving Antenna Projects and Accessories
- Materials and Construction Techniques
- Our Two New Bands

Receiving Antennas For the Radio Amateur
ARRL Item No. 0789
ARRL Member Price! Only $24.95 (retail $27.95)

ARRL The national association for AMATEUR RADIO®

www.arrl.org/shop

Toll-Free US 888-277-5289,
or elsewhere +1-860-594-0355

QEX 7/2018

YAGI URBAN BEAM

The UrbanBeam is excellent for use in high density population areas or properties with small lot sizes, where a full-sized Yagi may not be an option. The distinctive shape and small footprint (15.5 sq ft turning radius) of the UrbanBeam helps make neighbors and spouses happier, while still delivering the exceptional results you would expect of a SteppIR Yagi. The UrbanBeam is a high-performance, two element Yagi on 20m-6m and folded dipole on 40-30m. With features such as 180 degree direction change, bi-directional mode and full element retraction for stormy weather. You can enjoy all the features of a SteppIR Yagi while chasing low-sunspot-cycle DX or rag-chewing with your friends!

YAGI URBAN BEAM

GO SMALL

steppIR
COMMUNICATION SYSTEMS

DETAILS & ORDERING:

www.steppir.com

425-453-1910